The University of Southern Mississippi

The Aquila Digital Community

Spring 5-2017

Formation of Nanostructured Epoxy Networks Containing Polyhedral Oligomeric Silsesquioxane (POSS) and Silica Nanoparticles

Amit K. Sharma
University of Southern Mississippi

Recommended Citation

FORMATION OF NANOSTRUCTURED EPOXY NETWORKS CONTAINING

POLYHEDRAL OLIGOMERIC SILSESQUIOXANE (POSS)

AND SILICA NANOPARTICLES

by

Amit K. Sharma

A Dissertation
Submitted to the Graduate School
and the School of Polymers and High Performance Materials
at The University of Southern Mississippi
in Partial Fulfillment of the Requirements
for the Degree of Doctor of Philosophy

Approved:

_____
Dr. Jeffrey S. Wiggins, Committee Chair
Associate Professor, Polymers and High Performance Materials

_____
Dr. Sarah E. Morgan, Committee Member
Professor, Polymers and High Performance Materials

_____
Dr. Robson F. Storey, Committee Member
Distinguished Professor, Polymers and High Performance Materials

_____
Dr. Sergei I. Nazarenko, Committee Member
Professor, Polymers and High Performance Materials

_____
Dr. Joseph R. Lott, Committee Member
Assistant Professor, Polymers and High Performance Materials

_____
Dr. Jeffrey S. Wiggins
Director, School of Polymers and High Performance Materials

_____
Dr. Karen S. Coats
Dean of the Graduate School

May 2017

COPYRIGHT BY

Amit K. Sharma

2017

Published by the Graduate School

THE UNIVERSITY OF
SOUTHERN
MISSISSIPPI.

ABSTRACT

FORMATION OF NANOSTRUCTURED EPOXY NETWORKS CONTAINING

POLYHEDRAL OLIGOMERIC SILSESQUIOXANE (POSS)

AND SILICA NANOPARTICLES

by Amit K. Sharma

May 2017

This dissertation is focused on structure-property-processing relationship studies based on well-defined polyhedral oligomeric silsesquioxane (POSS) modified epoxy networks to present a comprehensive understanding of hybrid network behavior. In this research, a monoamine functional POSS molecule is incorporated into the epoxy monomer as pendant unit to mimic common epoxy structures and then crosslinked to form well-defined epoxy hybrid networks. The POSS cages behave as nanosized pendant unit in the epoxy matrices, while the mass fraction of POSS cages is varied and the effects on physical properties are examined with respect to changes in network architecture.

Our initial efforts focus on studies of POSS-epoxy precursors prepared by reacting aminopropyl isobutyl POSS and the diglycidyl ether of bisphenol A (DGEBA) monomer in a batch reaction. The precursor architecture can be directly analyzed by nuclear magnetic resonance spectroscopy (^{29}Si NMR) and size exclusion chromatography (SEC). These studies reveal the conversion of aminopropyl isobutyl POSS into POSS-DGEBA precursor during prereaction at varying reaction conditions, such as varying prereaction temperature and varying DGEBA molecular weight. Results also suggest that

the reaction between aminopropyl isobutyl POSS and DGEBA at isothermal conditions follows similar kinetics as that for the neat epoxy-amine systems.

A novel continuous reactor method is developed to synthesize POSS-DGEBA precursor with the aim of improving prereaction efficiency between aminopropyl isobutyl POSS and DGEBA. Studies suggest that by using a continuous reactor, full conversion of aminopropyl isobutyl POSS into the precursor was achieved in less than a minute, compared to several hours in a batch process. Fabricating transparent networks with large mass fractions of pendant POSS by the continuous reactor method demonstrates the concept of network modification by molecular level dispersion of pendant POSS. Physical and thermal properties of hybrid networks demonstrate structure property relationships with respect to POSS content, which appears to be true network behavior, given that a molecular level dispersion of pendant POSS in crosslinked epoxy networks has been achieved.

Studies of nanostructured epoxy networks containing pendant POSS and non-functionalized silica nanoparticles (SNP) prepared using the continuous reactor method suggest that favorable interactions between pendant POSS and SNP surfaces enhance matrix nanoparticle interactions. Results suggest better dispersion of SNP and improved load bearing properties of these networks due to the favorable interaction between pendant POSS cage and SNP.

This research reveals a unique strategy for molecular level dispersion of pendant POSS into epoxy networks with excellent control over nanostructure formation and properties, leading to increased strength through plasticization of glassy polymer networks.

ACKNOWLEDGMENTS

DEDICATION

To My Wonderful Wife Renu

The experience and learning I have during graduate school, my whole

achievement, are all indebted to her. She was always by my side with all the love and

support whenever I need her.

TABLE OF CONTENTS

LIST OF TABLES

LIST OF ILLUSTRATIONS

xiv

CHAPTER I - INTRODUCTION

Scientific Motivation

Epoxy resin has been utilized in wide-ranging fields such as adhesives, coating, electronics encapsulation materials, airplanes and satellites due to its features of mechanical strength, electrical insulation, chemical stability, and corrosion resistance. However, high brittleness, low anti-oxidization performance, and poor heat resistance have hindered its application in many high-end areas (aerospace, for example). Among many ways of modifying epoxy with a variety of fillers (elastomers, plastics particles, and other agents), the modification of epoxy using inorganic nanoparticles has drawn considerable research interest because it provides unusual properties suitable for high-tech applications. Generally, termed as "organic/inorganic hybrid nanocomposites", they are considered good candidates for use in high-end applications like high-temperature resistance,[1,2] barrier[3–5], and electronics applications[6,7] etc., and have been studied intensively. These organic/inorganic hybrid nanocomposites often exceed expectations because of the incorporation of the nanosized inorganic component into polymeric materials, those are otherwise not achieved by traditional composites.[8,9]

The extraordinary properties based on the combination of inorganic nanomaterial with organic building blocks have great potential to improve the shortcoming of epoxy networks for high-end applications such as aerospace. A significant amount of work has been done to study practically all the combinations of epoxy based organic/inorganic hybrid nanocomposites.[10–13] Inorganic nanomaterials including carbon nanotubes, clays, metal oxides (e.g., TiO_2, Al_2O_3), and so forth, among which polyhedral oligomeric silsesquioxanes (POSS®) molecules are viewed as very important building blocks for

1

epoxy hybrid nanomaterials. The research into epoxy incorporating POSS over the last several years has led to unexpected applications, new synthetic routes, and a deep understanding of fundamental polymer physics through epoxy-POSS interactions. The main limitation of POSS is their poor compatibility with the epoxy systems because of inert organic groups, which leads to aggregation and processing problems. This limitation can be mitigated by controlling the appended organic groups, which increases compatibility with epoxy polymers. This procedure, which is usually very effective, adds another processing step to the synthesis of the materials, increasing cost and variation within physical properties.

The core motivation for the present research arises from a need to understand how to tailor important fundamental properties while developing epoxy-POSS nanocomposites for target applications. To create desired properties in nanocomposites, the correct architecture must be designed and processed appropriately, and one must have a detailed understanding of the relationships between nanostructure, processing, and properties. Unfortunately, the majority of POSS-based nanocomposite research has been focused on developing novel properties; and no systematic study of 'nanostructure-processing-property' relationships has been performed. This understanding between processing, structure, and properties can help to develop the ability to design/process the precise nanostructure for desired applications. The best strategy for this purpose is to develop a more systematic methodology for designing nanostructure by selecting desired POSS component of interest and assembling them in an optimal array for desired properties.

A similar objective has been the motivation of the research presented here. The fundamental issues of this research were to develop a novel methodology to incorporate monofunctional POSS as a pendant unit into the epoxy network at a molecular level and study the nanostructure with different variables. Monofunctional POSS with one amine group and seven isobutyl group per molecule has been chosen as a model compound for this research since the structure-property relationships for epoxy networks containing pendant POSS with isobutyl group have not been fully understood because of the difficulty in incorporating pendant POSS at a molecular level in epoxy networks. This research work also aims to gain a fundamental understanding of interactions between pendant POSS and silica nanoparticles and to observe its influence for generating nanostructured morphologies in cured networks and relating these morphologies to macroscopic properties.

Architecture of Organic/Inorganic Hybrid Materials

Organic-inorganic (O/I) hybrid materials offer prospects for many new applications in extremely diverse fields. It is expected that hybrid materials will advance the field of engineering. However, the properties of hybrid materials strongly depend on the aggregation state of the inorganic material, and the characteristic of O/I interphase.[14–16] It has been shown that a small amount of inorganic particle aggregation results in increased strength of polymeric materials.[17], however, large aggregation leads to a micro-composite system. Aggregation is typically driven by polarity differences between the filler surface and the polymer matrix, which is caused by the presence of organic groups on the inorganic surface (e.g., hydroxyl). This result in poor interactions between inorganic surface and polymer compared to inorganic-inorganic interactions. Generally,

compatibilization of the inorganic surface by chemically modifying the nature of the inorganic surface improves the interfacial interactions between the inorganic surface and polymer and help to avoid aggregation. These strong interfacial interactions are the key to the full potential of rigid and inorganic phase within the polymeric system.[18]

A wide array of architectures utilizing O/I hybrid materials has been studied based on various methodologies. The first example of hybrid architecture is based on encapsulation of inorganic nanoparticles by a polymeric layer, which can be prepared by using emulsion polymerization. In this process, monomer is usually adsorbed on the inorganic surface and polymerization initiates at the surface of particles, followed by propagation within the adsorbed monomer layer to prepare polymer encapsulated inorganic particles.[19–21]

Another group of O/I hybrid architecture are based on grafting polymerizable groups on the nanoparticle surface. Generally, a hydroxyl group or a coordination center is required to prepare these architectures. The initiator moieties are usually appended to the surface of particles or particle clusters to allow grafting of polymers 'from' the inorganic surface. Significant amounts of published literature for the preparation of polymer-grafted inorganic particles are based on initiating the polymerization 'from' the initiating groups on the particle surfaces.[22,23] Alternatively, the inorganic surface can have reactive functionality, e.g. hydroxyl, which provides a reactive site for end-functionalized polymer chains in a 'grafting to' technique via a coupling process. An example includes modification of ZnO particle surfaces by anchoring polymethacrylic acid chains.[24] Typical hybrid polymer structures formed by this architecture are a

homopolymer,[25,26] telechelic polymers,[7,27–29] block copolymers,[30–33] star-shaped, and branched polymers[34–36] as shown in Figure 1.
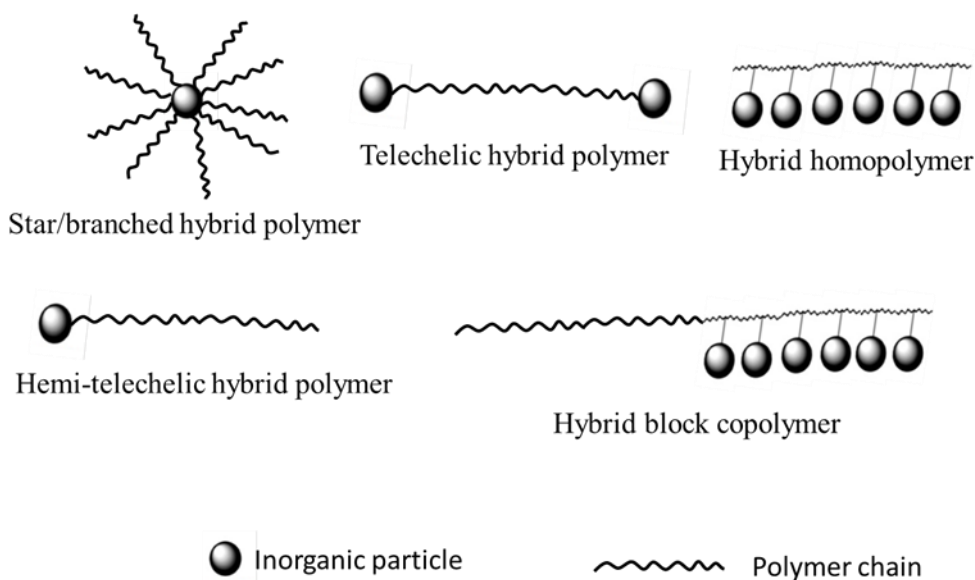
Figure 1. Hybrid polymer structures

    Transition metal oxide clusters modified with organic groups are a more recent hybrid material used in reinforced polymeric systems. However, modification of transition metal oxides clusters with organic groups is challenging due to hydrolytically unstable bonds between transition metal atoms and carbon atoms. This has been accomplished by using bi-or multi-dentate architectures such as sulfonates, carboxylates, phosphonates etc.[37–39] Typically, modified metal oxide can be prepared by two ways: 1. Synthesizing the metal oxide clusters in presence of a functional group; or 2. Post-modification of the surface groups. One example of developing metal oxide cluster by post synthesis method is the development of hetero-tungstate cluster K_4 [$SiW_{11}O_{39}$] derivatives, by reaction with various trichloro- or triethoxysilanes $RSiX_3$ (X = Cl or OEt) containing polymerizable group R (R = allyl, vinyl, styryl, or methacrylate).[40,41] Another example of functionalizing metal oxide clusters during synthesis demonstrates in the

5

formation of modified metal cluster based on titanium or zirconium. When metal alkoxides $M(OR)_4$ (M=Ti, Zr) were allowed to react with excess of acrylic or methacrylic acid, crystalline clusters of the general composition $M_xO_y(OH/OR)_z(OOCR)_w$ of different size and shape were obtained as shown in Figure 2.[42–45]
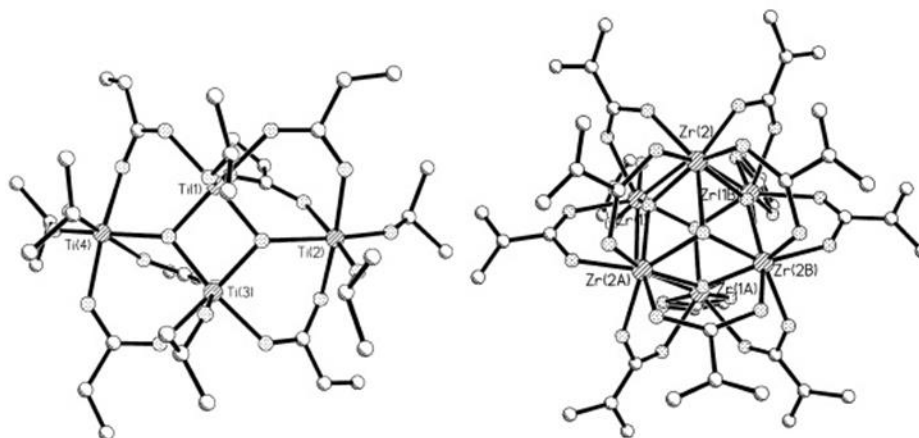
Figure 2. Organically modified metal compound (titanium and zirconium)

Though there are many organically modified transition metal oxide clusters with various functional groups, like acrylonitrile, acrylates, etc., their use in polymerization processes is limited because of the interactions between reactant monomers with ligands, which make the characterization of these materials difficult.[46]

Perhaps the most significant example of cluster-like inorganic components is that of silsesquioxane compounds. Silsesquioxane-based hybrid materials account for the significant amount of the research in literature. A variety of architectures has been developed based on silsesquioxane to prepared well-defined hybrid polymers.[47] An understanding of silsesquioxane based polymeric materials offers important background knowledge for the systematic nanostructure-processing-property studies contained in this dissertation.

Silsesquioxane

Over the last few years, interest in silsesquioxane-based molecules has increased dramatically because of the nanoscale size and hybrid nature of these molecules.[48] The chemical structure of silsesquioxane molecules is comprised of the basic composition $(RSiO_{1.5})_n$, where R is the organic side group on Si-O-Si skeleton structure, including alkyl, aryl, hydrogen, etc.[49] The chemical structure of silsesquioxane molecules can be categorized into two groups: caged and non-caged structures. In addition, the non-caged structures of silsesquioxane molecules can be further categorized into partial cage, ladder, and random structures as shown in Figure 3.[50]

Caged structures are usually known as polyhedral oligomeric silsesquioxanes (POSS), and POSS are discussed separately in next section as they are a very important family of silsesquioxane that accounts for the significant amount of research.

(a) Partial cage structure   (b) Ladder structure   (c) Random structure

(d) T_8 (e) T_{10} (f) T_{12}
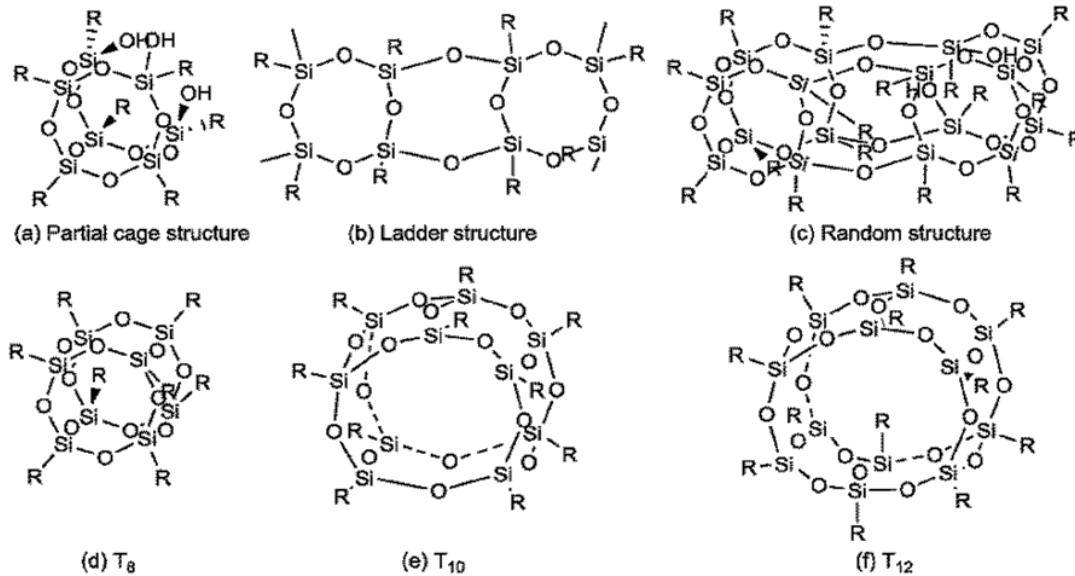
Figure 3. Chemical structures of silsesquioxanes; Non-caged- a-c, Caged- d-f

Polyhedral Oligomeric Silsesquioxanes (POSS) as Building Blocks

The structure of POSS can be represented as $(RSiO_{1.5})_n$; where n is 4, 6, 8 …and 12.[51] Most of the literature reported about POSS is actually based on T_8 type structure, where n= 8; it is generally referred to as 'octa silsesquioxane' or 'cage'. The T_8 type structure can be prepared easily in bulk quantities, has been considered a model POSS molecule, and studied extensively. In addition to the number of silicon atoms, the most significant factor to characterize POSS compounds is the functionalities of the organic groups, R, attached to the cage. Figure 4 presents the most general chemical structure of a T_8 type POSS structure, with a basic composition of $(SiO_{1.5})_8R_7X$.[52]

Nonreactive organic (R) groups for solubilization and compatibilization

Nanoscopic in size with an Si-Si distance of 0.5 nm and a R-R distance of 1.5 nm

May possess one or more reactive groups suitable for polymerization or grafting

Thermally and chemically robust hybrid (organic-inorganic) framework

Precise three-dimensional structure for molecular level reinforcement of polymer segments and coils

Figure 4. Schematic structure of a POSS with the general formula $(SiO_{1.5})_8 R_7X$

Easy manipulation of the organic functionalities, highly symmetric molecules of nanoscale size (1-3 nm), and simple manufacturing process makes POSS potentially useful as nano building blocks for polymer nanocomposites.[53–56] Here onwards in this dissertation, 'POSS' will refer only to the T_8 structure.

8

Based on structure flexibility, POSS can be separated into three categories: 1. Molecular silica, where all organic side groups are non-reactive [57] 2. Monofunctional POSS, where only one of organic side group is reactive. 3. Multifunctional POSS, where more than one organic group is reactive, the most common molecule in this category is the octafunctional POSS, where all the organic groups are reactive.

Considering the structural tunability of POSS, as described above, the importance of POSS as a nano-object can be further elucidated by considering other factors like size, monodispersity, and hybrid character.

The size of POSS molecule is intermediate between that of typical organic monomers (1-10Å) and macromolecules (20~100 nm).[58] When compared to silica nanoparticles, POSS is typically one order smaller than the smallest silica nanoparticles available.[59] The monodisperse size allows precise modeling of the behavior of POSS molecules in polymers, but only in the case of molecular level dispersion of POSS in the polymer matrix. Another important factor to consider is the true hybrid character of POSS. The inorganic Si-O-Si skeleton ensures good thermal properties; Organic groups on POSS could be selected to be well-suited with organic surroundings, such as solvents and polymers. Choice of these organic groups allows tailoring of POSS compatibility with different organic surroundings, ranging from full miscibility to partial segregation to full immiscibility (micron scale phase separation).[51]

POSS-Reinforced Epoxy Nanocomposites

The selective modification of organic side groups makes POSS molecules useful to prepare hybrid polymers with well-defined structures. A variety of POSS-based architectures have been developed by using advanced synthesis protocols.[60–64] Several

reviews have been published on POSS related nanocomposites,[47,51,65] but the focus of this research is POSS-based epoxy polymers. A large body of literature exists utilizing POSS in epoxy polymers and is focused on the incorporation of multifunctional and monofunctional POSS. In these systems, efforts have been focused on monitoring the miscibility-dispersion of the POSS as particulate fillers and studying the structure-property relationships. In this section, we focus on the various POSS architectures; those are used to incorporate POSS into epoxy networks and to see how these architectures affect the network properties.

Multifunctional POSS-DGEBA Polymers

The existence of multiple reactive groups on the POSS cage typically improves the solubility of the POSS in epoxies. A significant amount of research on multifunctional POSS incorporation into epoxy networks has focused on Octakis (dimethylsiloxypropylglycidyl ether) silsesquioxane (OG-POSS). Laine et al. prepared OG-POSS by reacting 4 or 8 equivalent of allyl glycidyl ether with Q_8M_8H (shown in Figure 5) using a Karstedt's catalyst and prepared nanocomposites through reacting OG-POSS with 4, 4' diamino diphenyl methane (DDM). Nanocomposites were analyzed for cross-linking density and tensile properties. Network architecture was proposed based on amine: epoxide ratio. It was successfully demonstrated that a well-defined nanocomposite with controlled variation of the organic tether architecture can be made, and their properties can be assessed.[66]
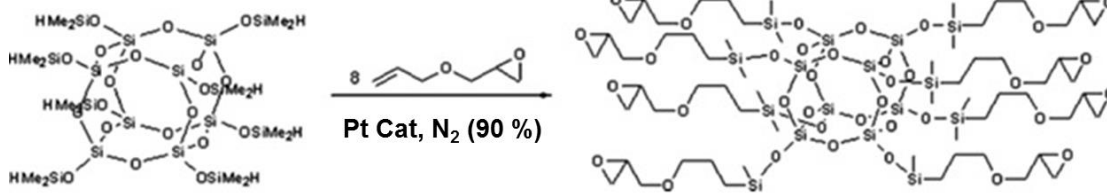
Figure 5. Synthesis of OG-POSS

In a similar example, Kim et al.[67] have used OG-POSS as co-monomer along with diamino diphenyl sulfone (DDS) to synthesize hybrid epoxy-amine network and studied deformation processes to understand toughening behavior with respect to curative concentration. Results showed an increase in both glassy and rubbery state modulus with DDS concentration, indicating an increase in crosslink density by using OG-POSS. The toughening mechanism was identified as a plastic deformation process caused by the formation of nanoscale voids in the network, possibly templated by limited POSS aggregation. Figure 6 schematically represents the deformation process of the epoxy-POSS networks.
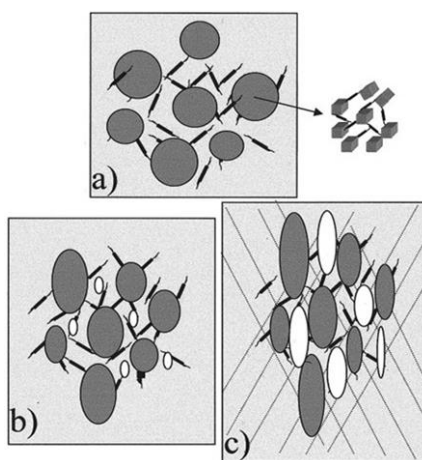
Figure 6. Schematic representation of deformation process in epoxy-POSS networks a- Un-deformed; b- Initial deformation; c- Plastic deformation

11

Lee et al. reacted OG-POSS with a fluorine-based curative, 5-trifluoromethyl-1, 3-phenylenediamine (FPA), and aromatic amine curative, DDM to prepare epoxy-POSS nanocomposites. Results indicated that high rigidity of FPA and possible interactions between fluorine and silicon led to superior thermal/mechanical properties of OG-POSS/FPA network compared to OG-POSS/DDDM. Results also indicated superior dielectric characteristics with a low coefficient of thermal expansion, which makes OG-POSS/FPA a potential candidate for high-end applications such as electronic packaging.[68]

OG-POSS macromonomer can be used as a reactive additive to epoxy networks. In one example, Teo et al. copolymerized OG-POSS with a hexahydrophthalic anhydride (HHPA) in presence of tetraglycidyl-4, 4'-diamino diphenyl methane (TGDDM) to study the cure kinetics of hybrid networks. It was revealed that reaction kinetics is higher for OG/HHPA compared to TGDDM/HHPA. The addition of 5 mol % of OG-POSS in the networks resulted in a 20°C increase in T_g and significant improvement in storage modulus, with respect to TGDDM/HHPA network. Figure 7 shows SEM micrographs of networks containing 5 % OG-POSS with premix time.[69]
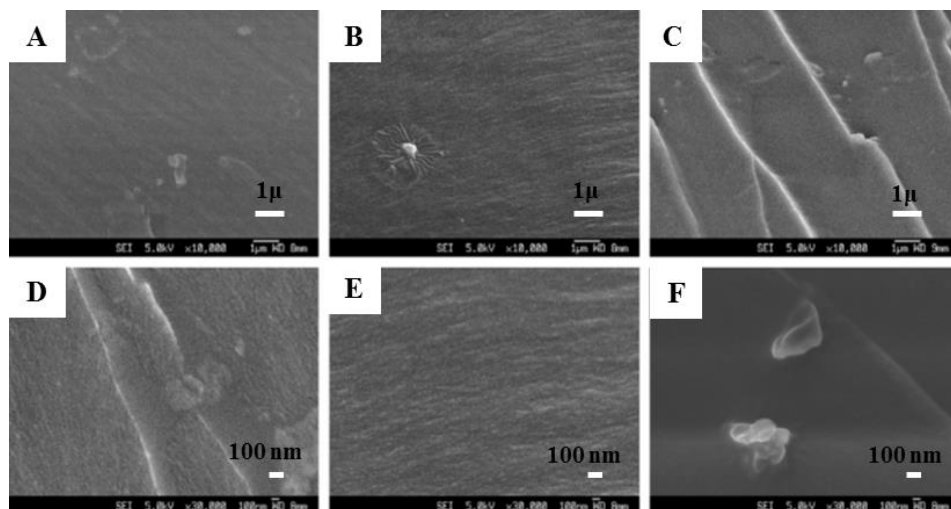
Figure 7. SEM of 5 mol. % OG hybrid materials at premixing times (A and D) 0 min, (B and E) 10 min, (C and F) 20 min.

Chen and coworkers[70] copolymerized OG-POSS with diglycidyl ether of bisphenol A (DGEBA) monomer to observe POSS dispersion in the hybrid networks. They observed the formation of 30–50nm particles during photopolymerization process. The resultant nanocomposites showed improvement in rubbery state modulus, which confirms the reinforcement effect by additional crosslinking within the network. Ni et al.[71] compare epoxy-POSS networks based on POSS reactive functionality. A non-reactive POSS-based on nitrophenyl groups (ONP-POSS) and a reactive POSS-based on aminophenyl groups (OAP-POSS), were introduced in DGEBA-DDM networks. SEM studies reveal that OAP-POSS/epoxy networks exhibit homogenous morphologies compared to ONP-POSS/epoxy network, which displays phase separated morphology. However, phase separated POSS-rich phases dispersed uniformly into the network (spherical particles of less than 0.5mm size), as can be seen in Figure 8
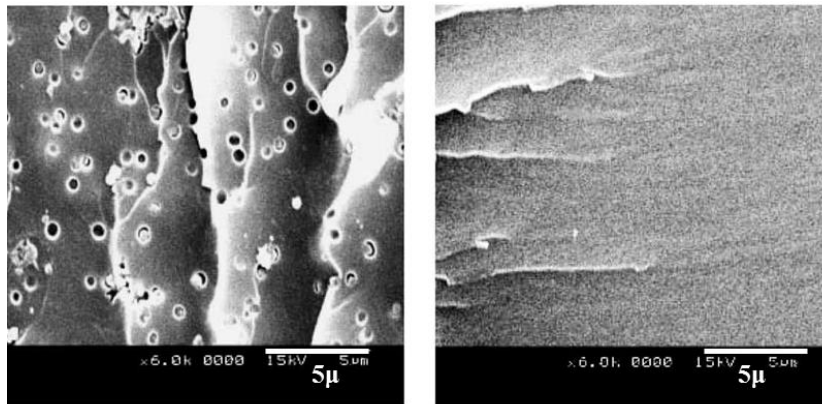
Figure 8. SEM of hybrid networks with (a) 10 % ONP-POSS; (b) 10 % OAP-POSS

Reproduced with permission from reference no. 71

In all these systems, octafunctional POSS served as a junction point in the network architectures and reinforced the network by increased crosslinking density and hindered segmental motions in the rigid regions surrounding the POSS units. However, at higher loadings of multifunctional POSS, nanocomposites exhibited low T_g's compared to conventional epoxy networks.[66,67,72,73] This is due to the conversion during cure, which is likely the result of steric hindrance and the soft linkage between the epoxy and POSS.[74]

Monofunctional POSS-DGEBA Polymers

Monofunctional POSS in epoxy networks as pendant unit can display entirely different properties when compared with multifunctional POSS-based epoxy networks. The true potential of pendant POSS on network properties requires a molecular level dispersion. Given the reduced solubility of monofunctional POSS in epoxy resins, it has presented a considerable synthetic challenge to prepare epoxy-POSS networks with POSS as a pendant unit. Lee et al. prepared an amine terminated POSS macromers by reacting monoepoxy POSS with polyether-diamine (Jeffamine® D230) in presence of 1, 4-butanediol diglycidyl ether (BDGE). These macromers were then used to prepare

14

epoxy-POSS nanocomposites containing less than 10 wt. % pendant POSS according to the reaction scheme shown in Figure 9. The increase in T_g without affecting crosslink density was explained by considering the bulk of the POSS cage's capability to restrict polymer chains motions. However, a microphase separation was observed in the resulting networks, which indicated incompatibility of POSS molecules with the epoxy network.[75]

$R = c\text{-}C_6H_{12}$ (Cyclohexyl),
$c\text{-}C_5H_9$ (Cyclopentyl)

BDGE

JEFFAMINE D-230

60°C
3hrs

POSS-epoxy prepolymer

+

DGEBPA
n~0-0.5

100°C
24hrs

POSS-reinforced epoxy resin
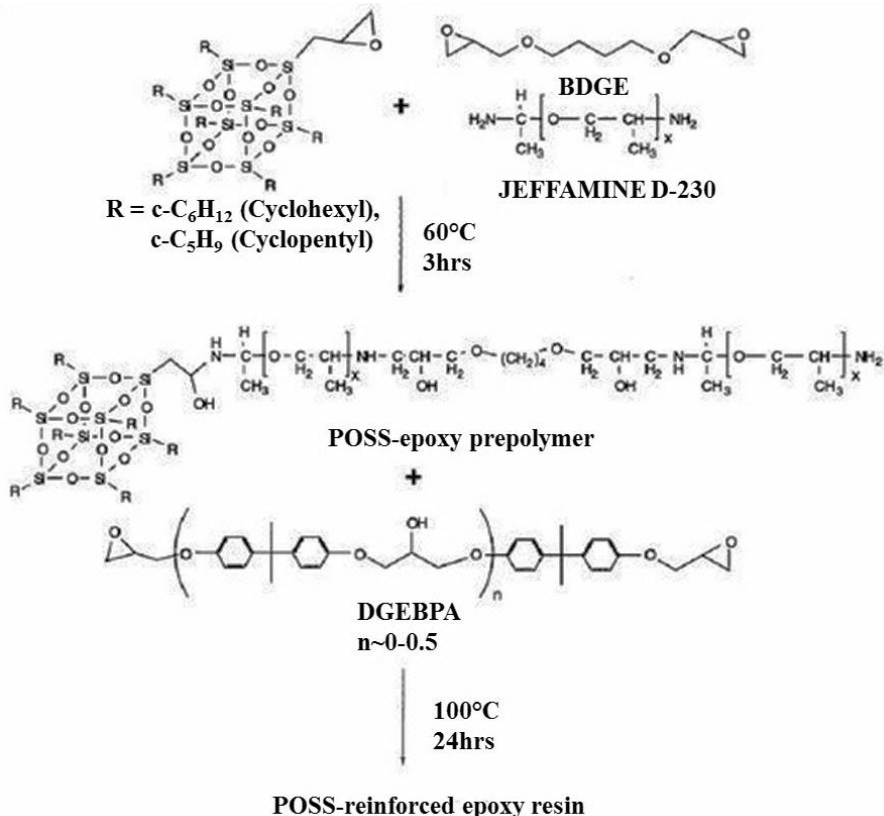
Figure 9. Formation of POSS reinforce epoxy network

To prepare epoxy hybrid networks containing high weight fractions of monofunctional POSS, Abad et al.[76] reacted monoepoxy POSS with 4,'4-[1, 3 phenylene bis-(1-methylethylidene)] bis (aniline) to prepare an amine terminated precursor. This precursor was then used to cure DGEBA to obtain epoxy–POSS hybrid materials containing 52 wt. % of POSS. Phase separation was observed at the time of mixing

DGEBA and amine terminated POSS precursor, which led to a macro-phase separation in the network. In addition, a secondary phase separation occurred during polymerization, producing spherical POSS domains as shown in Figure 10. This phase separation was explained by the incompatibility between isobutyl groups and DGEBA.
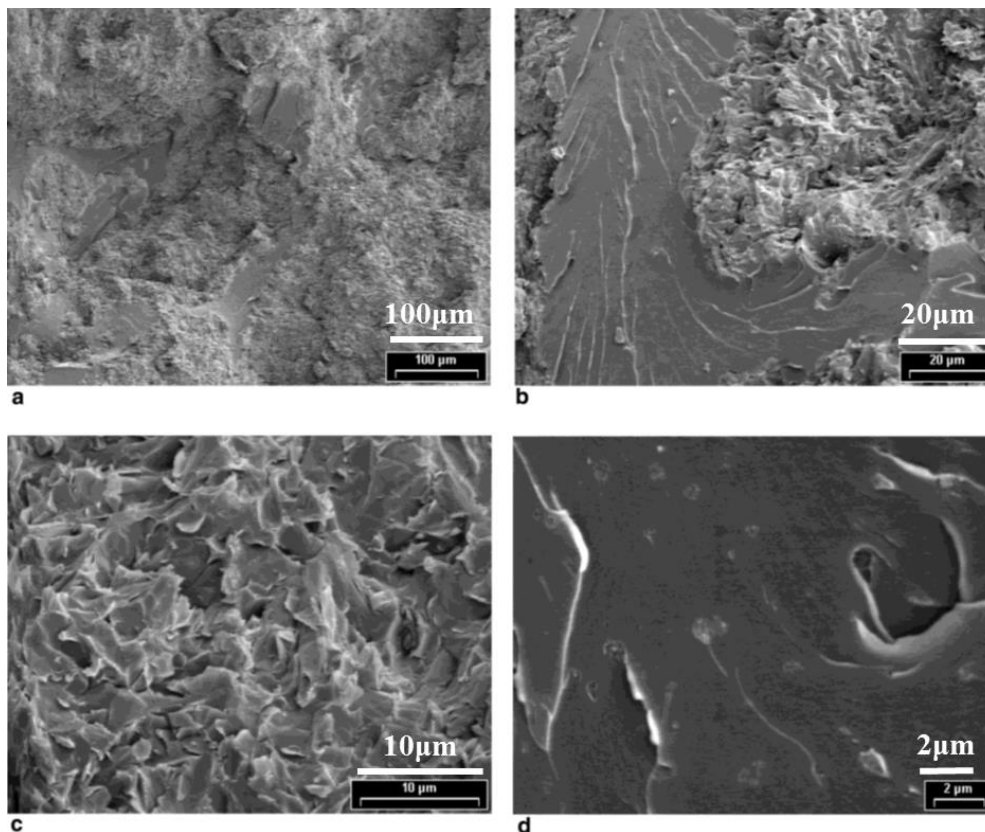
Figure 10. SEM of epoxy network containing 52 wt. % of POSS at various scale

Liu et al.[74] reported a two-step process to incorporate monoamine POSS in epoxy networks. In the first step, POSS-DGEBA precursor was prepared; unlike POSS monomer, the precursor was more compatible with epoxy monomers. Figure 11 shows a schematic representation of the two-step process used to fabricate epoxy-POSS networks containing high weight fraction of pendant POSS. An additional peak corresponding to higher molecular weight product was observed in precursor's gel permeation

chromatography (GPC) spectrum, as shown in Figure 12, which indicated the reaction

between monoamine POSS and DGEBA.
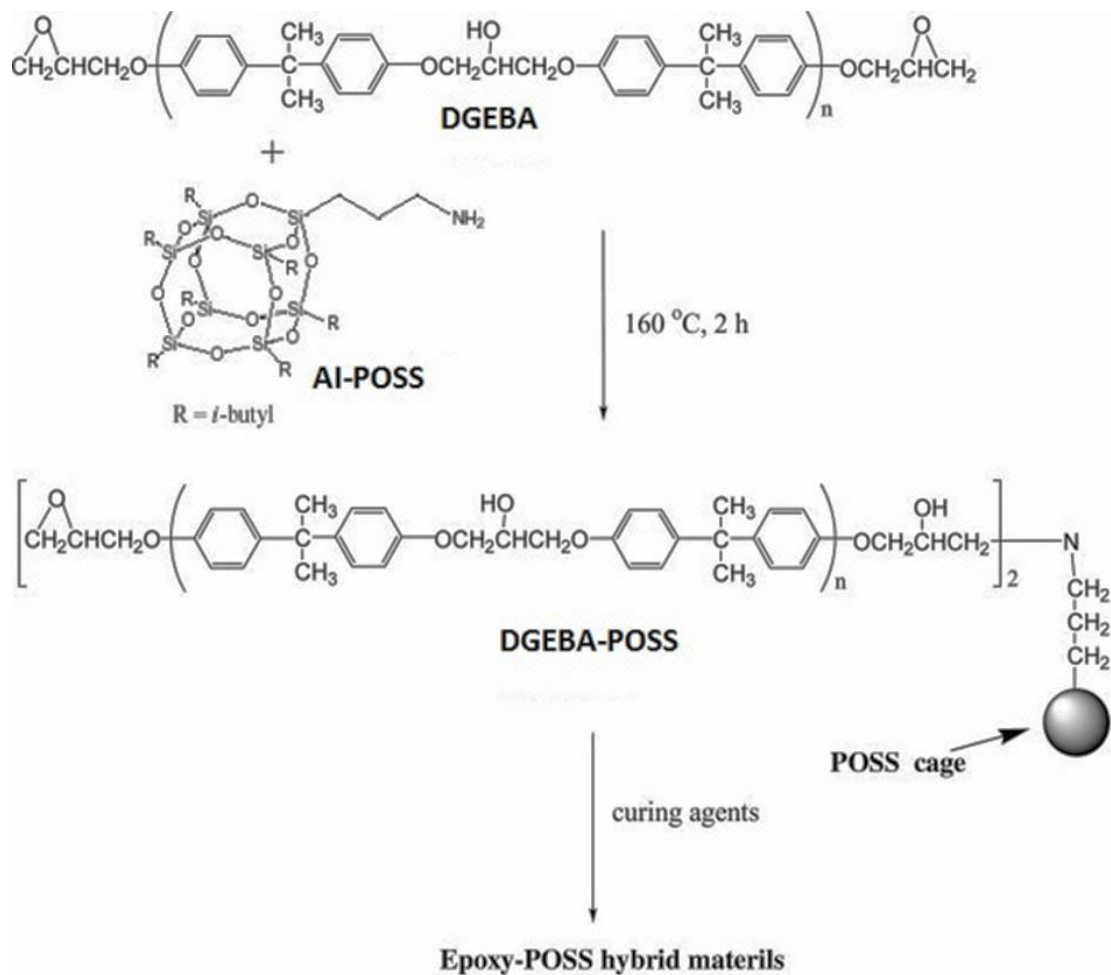
Figure 11. Epoxy hybrid networks containing pendant POSS- Two-step process
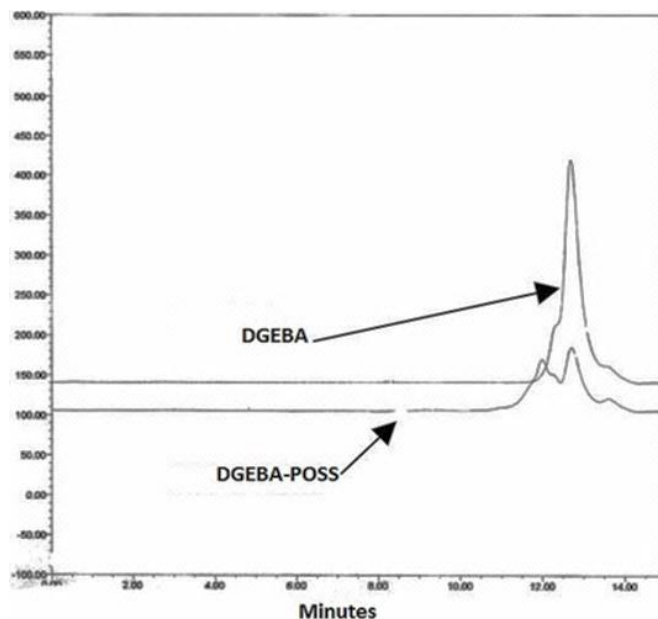
Figure 12. GPC chromatograms of DGEBA and DGEBA-POSS precursor

The precursors were cured with DDM, dicyandiamide (DICY), and diethyl phosphite (DEP) curing agents in the second step to synthesize epoxy hybrid materials containing POSS. Interestingly, DICY and DEP curative efficiently avoided microphase separation, however, macrophase separation was still observed in aromatic amine cured network.[74] Further modification of this process by Matejka et al.[77] performed the prereaction at lower temperature (100°C) and excess DGEBA (1:3 molar ratio) compared to Lui's process (1:2 mol ratio and 160°C) to eliminate the epoxy homopolymerization at higher temperature[78] and the formation of POSS–epoxy precursors terminated by the low reactive-NH group. They have analyzed a wide array of epoxy-POSS networks containing POSS as dangling units and as blended objects in the organic medium. The schematic structures along with the names of the POSS used are reported in Figure 13.

18

Epoxy or amine functionalized POSS were used to partially replace the respective amine curative or epoxy monomer in the system to synthesize epoxy hybrids networks.

Based on the results of studying various organic side groups (Octyl, Butyl, Methyl, and Phenyl), and covalently binding POSS into the network and polymerization process, it was observed that the network morphology of the hybrid networks is controlled by regulating POSS–POSS and POSS-polymer interactions. As observed, POSS molecules with octyl groups show good compatibility with the epoxy matrix; however, reaction induced phase separation occurred during polymerization, resulting nanosized (~100 nm) amorphous aggregates. Other substituents showed strong POSS–POSS interactions, which led to the formation of large crystalline domains (up to 500 nm) as observed by SAXS.
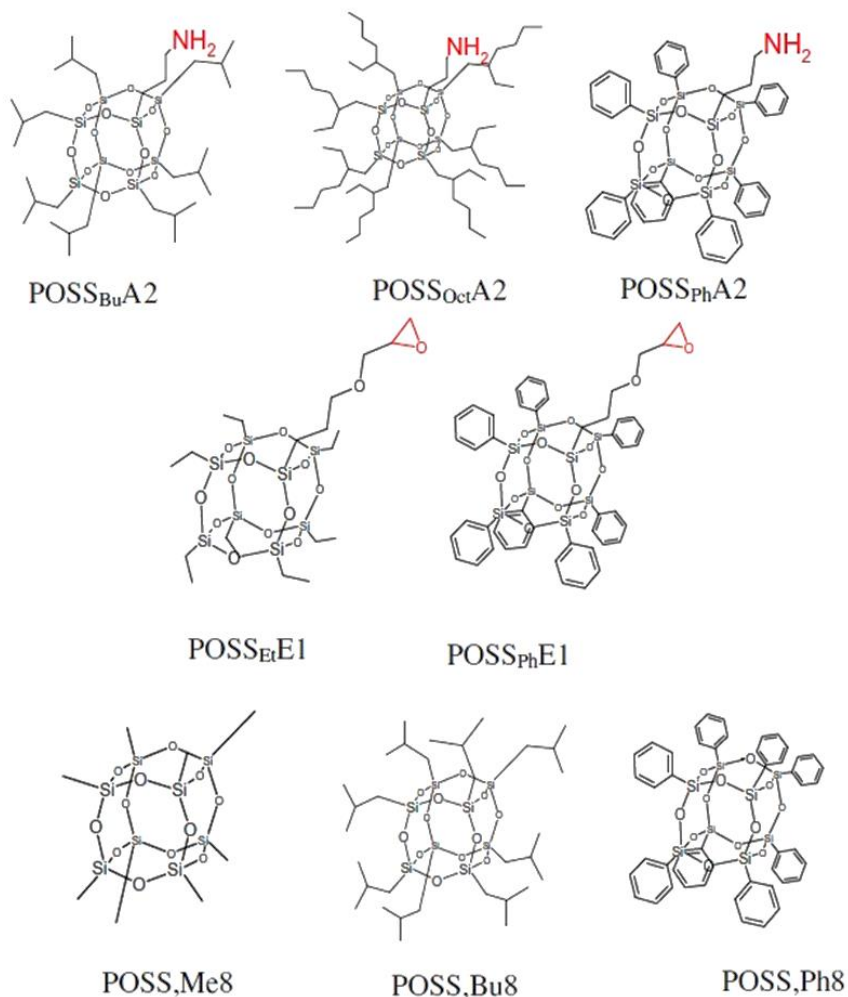
Figure 13. The functionalized and nonfunctionalized POSS units

The ordering of the resultant hybrid structure was more obvious in the case of the hybrid network with octyl substituted POSS, while a less ordered structure was observed with POSSPhA$_2$ or POSSBuA$_2$ (Figure 14). Surprisingly, monoepoxy POSS did not show any sign of structural ordering. This was due to network chains being disturbed by the presence of the monoepoxy POSS, which led to network defects. The use of a two-step synthesis procedure significantly improved homogenization of pendant POSS in epoxy networks as shown in Figure 15.[77]
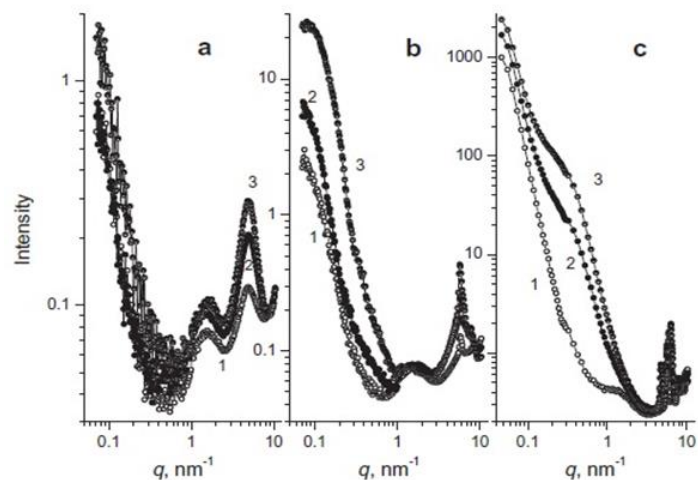
Figure 14. SAXS profiles of the hybrid networks DGEBA–D2000–POSS, A2 containing various amount of POSS units with different substituents (a) POSSOctA2, 1– 15 wt.% POSS, 2–30 wt.%, 3–43 wt.%, (b) POSSBuA2, 1–11 wt.% POSS, 2–22 wt.%, 3–34 wt.%, (c) POSSPhA2, 1–13 wt.% POSS, 2–25 wt.%, 3–38 wt.%.
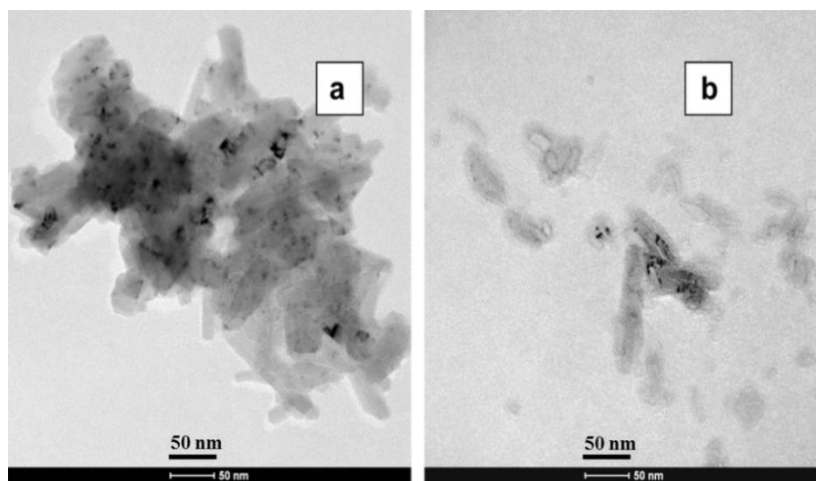
Figure 15. TEM of hybrid DGEBA–D2000–POSSBuA2 (38 wt. %) prepared by (a) one step and (b) two-step procedure

Polymerization-induced phase separation was also observed in the work of Dai and coworkers, where mono-anhydride POSS (AH-POSS) was pre-reacted with DGEBA and hybrid network were prepared using hexahydrophthalic anhydride (HHPA) as curing agent. Morphology studies indicate that for POSS loading less than 30wt %, a 'vesicle'

structure formed in epoxy-POSS networks.[79] Higher POSS loading resulted in macro-phase separation during liquid phase mixing as well as during the polymerization. Phase separation and incompatibility of POSS with the epoxy matrix led to a decrease in network thermal and viscoelastic properties. A similar POSS precursor was synthesized by Chiu et al. by reacting isocyanate-propyldinethylsily-isobutyl-POSS (IPI-POSS) with an excess of DGEBA (Figure 16).[80] SEM and TEM micrographs of DDM cured networks demonstrated evenly dispersed POSS particles with a size scale of 20-30nm. A significant increase in T_g, char yield, and flame resistance was reported by introducing a small quantity of IPI-POSS-modified epoxy (<12 wt. %).

POSS dispersion for low loading levels (<10wt%) was improved by using a prereaction was observed by Frank et al.[81] An aromatic diamine, DDS was used to cure POSS-DGEBA precursor reported by Lui.[74] Given the slow reactivity of DDS and immiscibility of POSS into the epoxy, a cure induced phase separation was observed. However, dispersion of POSS in epoxy-POSS networks is significantly improved by curing these networks at high temperature. Figure 17 shows the SEM micrographs of epoxy-POSS networks cured at 125°C and 180°C.

Figure 16. Synthesis of the IPI-POSS-modified epoxy (IPEP)

Figure 17. SEM of 2.5POSS-prereacted, (A) 5 hrs at 125°C; (B) 3 hrs at 180°C

For the systems studied for monofunctional POSS incorporation in epoxy

networks, a complex relationship between POSS loading level and material properties has

23

been observed. At low concentration, pendant POSS acts as a plasticizer. At higher concentrations, the aggregation and physical crosslinking act as microscale filler and reinforce the material. The nature of POSS interaction with the polymer matrix is a function of both the loading level and the nature of inert organic side groups.

Other POSS-DGEBA Nanocomposites

One example of POSS-containing hybrid architecture is reported by Zheng et.al, where POSS capped PCL macromolecule was synthesized, followed by hybrid network synthesis incorporating the macromolecule into epoxy resin.[82] The cured epoxy networks displayed a variety of nanostructured morphologies with respect to POSS-PCL macromolecule concentration. Formation of nanostructures in hybrid networks describes the miscibility and phase behaviors of the subcomponents (POSS and PCL chains) of the amphiphile compounds in epoxy before and after cure and are reported to form via self-assembly mechanisms.

In an extension of this work, Zheng et al. reported a hemi-telechelic hybrid PEO by reacting hepta (3, 3, 3-trifluoropropyl) propyl hydro silsesquioxane with allyl-terminated PEO. Self-assembled nanostructured morphology was observed in hybrid networks containing hybrid PEO precursor.[83] A novel organic-inorganic architecture based on POSS and mesoporous silica was reported by Jiao et al. by reacting modified silica particles (NH$_2$-MPS) with octafunctional glycidyl POSS.[84] POSS modified silica nanoparticles enhanced the interaction between the polymer and inorganic phases which deflect crack propagation and increase the absorbed energy.[85]

Each of the above-designated examples demonstrated a variety of techniques applied within epoxy networks which have established nanostructured morphologies as a reasonable approach for enhancing network properties.

High Shear Continuous Chemical Reactor

In recent years, industrial interest in the use of twin screw extruder (TSE) as a high shear continuous reactor has significantly increased. Generally, batch reactors, or plug flow reactors have disadvantages when handling high viscosities or mixing reactants; heat and mass transfer are not efficient especially in viscous systems. Sometimes, a solvent is added to reduce viscosity; however, longer reaction times, environmental concerns, and the requirement of extra purification make this process unattractive to industry. Twin screw extruders offer better handling of high viscosity systems and excellent heat and mass transfer during the reaction. Numerous reports revealed the benefits of using TSE as a continuous reactor for bulk polymerization[86], grafting[87], and compatibilization[88]. A detailed and exhaustive review highlighting advantages and disadvantages of using TSE as a continuous reactor was published by Brown and Xanthos,[89] and another one by Orlando.[90]

A fully intermeshing, co-rotating twin screw set shown in Figure 18 is often the preferred choice for reactive extrusion, because of the self-wiping action and transport efficiency of the material irrespective of viscosity. This ability to efficiently transport material without concern for viscosity is an advantage for reactive systems, since viscosity increases along the reaction path. In addition, the high shear rate promotes better mixing of reactant materials, and the variability in screw design makes TSE a multipurpose reactor, which can be customized based on its application.[91,92]

Figure 18. TSE co-rotating intermeshing screw set

Intermeshing co-rotating twin screw based continuous reactors offer great flexibility in screw design. However, three basic types of screw elements dominate screw designs: conveying, mixing, and zoning elements.[93] Figure 19 illustrated typical screw elements used for screw design in intermeshing co-rotating continuous reactors. [94]
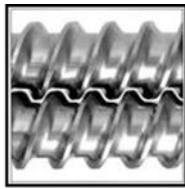
- Conveying Elements
  Feeding
  Pumping, Pressurization
  Blending
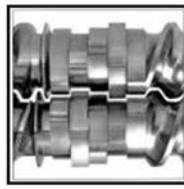
- Mixing Elements
  Blending
  Dispersive Mixing
  Distributive Mixing
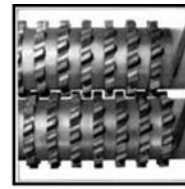
- Zoning Elements
  Restrictive Elements
  Increase Residence Time

Figure 19. Types of screw elements for co-rotating twin screw reactor

In co-rotating TSE, generally mixing is regarded as dispersive and distributive mixing. In dispersive mixing, mechanical stress through co-rotating screws was used to reduce the size of aggregates or liquid droplets; applied shear overcomes cohesive forces or interfacial tension of the phase and reduces the size of aggregates or droplets. The extensional and planar flow characteristics, generated by the screw elements are important to achieve dispersive mixing. In contrast, product homogeneity increases with distributive mixing, which is facilitated by recurring reordering of the minor components without size reduction. Compared to batch mixers, intense mixing in TSE along the screw elements results in highly effective mixing and uniform product. Moreover, the short

residence time (τ) in TSE (typically 5s< τ <2min) is highly beneficial for heat sensitive reactions.[94]

TSE has also been used to prepare POSS-based nanocomposites through melt blending and grafting, however, aggregation occurred in the physical blending of POSS in polymeric systems during melt mixing.[95,96] In an example of blending by reactive extrusion, Butola et al reported allyl-heptaisobutyl-POSS (AHO-POSS) grafted polypropylene (PP) through TSE and investigate the thermal properties of resulting materials. Results revealed the thermal stability of POSS grafted PP is higher compared to neat PP and higher than physically blended AHO-POSS/PP composite. A high melting temperature was observed for POSS grafted PP in comparison with simple blend of POSS and [97]

Within a TSE, intimate interactions of small quantities at each stage of the extrusion process make this a more efficient process compared to traditional batch and flow reactors. More efficient high shear continuous reactors based on TSE will give manufacturers a unique advantage in the production of advanced hybrid materials or the reactive modification of commercially available polymers. In this dissertation, we develop a novel method based on the continuous high shear reactor, which will provide a cost-effect, environmentally favorable, and scalable option to synthesize POSS-based prepolymers with increased reaction efficiency and elimination of post-processing operations.

Research Overview

Because there are still many design variables in processing epoxy hybrid nanocomposites from pendant POSS, initial efforts are devoted to the development of

simple systems wherein selected variables can be altered one at a time in a constant system. Then, the findings in an early study can help to develop a model process to fabricate epoxy hybrid nanocomposites containing a high mass fraction of pendant POSS. POSS-DGEBA precursors were synthesized with the aim to promote incorporation of pendant POSS at a molecular level into epoxy networks. A monofunctional POSS with one amine group and seven isobutyl group has been chosen for use with DGEBA due to its low solubility in epoxy systems, which allows comparison of the prereaction variables (temperature and epoxy equivalent weight) influence on the POSS-DGEBA precursor structure. Thereafter, a novel synthesis technique based on the high shear continuous reactor was developed for this synthesis, in order to make more viable an industrial application of these POSS-based compounds. The effects of prereaction temperature, epoxy molecular weight and continuous reactor processing on the structure of epoxy-POSS precursor were determined via a combination of spectroscopic and chromatographic techniques. Network structure-properties relationships have been proposed as well, with respect to prereaction temperature, epoxy molecular weight and pendant POSS concentration in networks.

In Chapter III, the effects of temperature and epoxy monomer molecular weight on POSS-DGEBA precursor synthesis were studied with the aim of increasing POSS reaction rates to increase incorporation of POSS into the network and avoid phase segregation. The bulk properties are analyzed and structure-property relationships are proposed. Chapter IV presents a novel and efficient method for POSS-DGEBA precursor synthesis based on the high shear continuous reactor. Change in the structure of these precursors with POSS concentration was studied and the nanostructures of POSS in the

epoxy hybrid networks are analyzed. Correlation of the structure morphology with the POSS loading is determined. Chapter V studies the properties of the POSS-DGEBA network containing high mass fraction pendant POSS incorporated at a molecular level. The physical structure of networks was proposed based on thermomechanical, thermal and mechanical properties. Chapter VI explores silica nanoparticle- POSS-DGEBA networks. In-situ dispersion of silica nanoparticles during synthesis of POSS-DGEBA precursor via high shear continuous reactor and network synthesis are presented. The network nanostructure was studied as well and explored the relation of the networks nanostructures with POSS/silica nanoparticles interactions.

CHAPTER II - EXPERIMENTAL

Materials

This research focuses on investigating (I) Synthesis of POSS-DGEBA precursors by reacting aminopropyl isobutyl POSS® (POSS) acquired from Hybrid Plastics Inc. with DGEBA monomers based on varying epoxy equivalent weight (EEW) [EEW=177.5, EEW=245, and EEW=540] acquired from Momentive Inc., (II) Epoxy POSS hybrid nanocomposites consisting of high mass fractions of pendant POSS, and (III) Nanostructured epoxy network containing pendant POSS and silica nanoparticles (SNP) obtained from US Research Nanomaterials, Inc. The SNP used in this research are 99.5% pure and 20-30 nm in diameter with a bulk density of $<0.10g/cm^3$. For this research, POSS modified epoxy resins were cured with aromatic based amine curatives. The two primary curatives were that of 4, 4'-diaminodiphenyl sulfone (DDS) supplied by Royce Chemical Corp., >99% pure and 4, 4'-diaminodiphenyl methane (DDM) supplied by Sigma-Aldrich co., 99% pure. The molecular weight of DDS and DDM are 248.3 and 198 g/mol respectively.

The reason behind selecting these epoxy-amine systems was their superior mechanical properties, chemical resistance, and ease of fabrication. The densely crosslinked glassy polymer network produced by these low molecular weight monomers meet all the requirement of a matrix material for structural composites applications, such as an increase in strength, stiffness, and Tg. Also, these systems have been very well studied in the literature.[98] Another important monomer in this research is POSS, which was selected for its interaction with the epoxy resins. This aspect has been already analyzed in Chapter 1, where it has been shown that most of the literature on POSS-

polymer systems is focused on the POSS dispersion in the final systems. The structures, trade names, abbreviations and molecular weights for these monomers can be found in Table 1. Reagent grade organic solvents, toluene, supplied by Sigma Aldrich, and tetrahydrofuran, supplied by Fisher scientific were used as received. De-ionized water was used for water uptake studies.

<center>Synthesis of POSS-DGEBA Precursor in Batch Reactor</center>
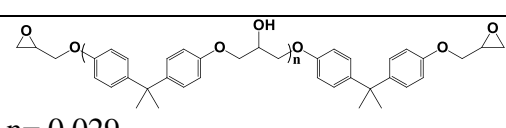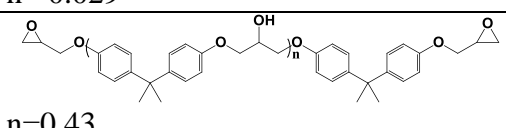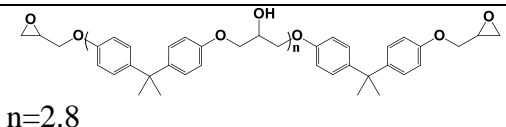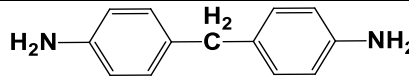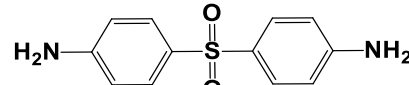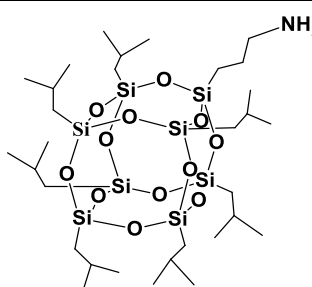
Prereaction of POSS-DGEBA at Varying Temperatures

DGEBA refers to EW177.5 monomer throughout this dissertation, unless otherwise a different EW monomer is specified. The prereacted precursor of POSS and DGEBA was prepared in an analogous way to that described by Matejka et al.[77] At first, POSS and DGEBA at a 1:3 molar ratio were dissolved in THF. After homogenization, the solvent was evaporated and the reaction proceeded in a bulk mixture at different temperatures (100°C, 120°C, 135°C and 150°C). The POSS-DGEBA prereaction is shown in Figure 20. In a typical reaction, 10 grams (11.434 mmol) POSS and 12.177 grams (34.30 mmol) DGEBA were charged to a 150ml round bottom flask. This reactant mixture was then dissolved in 25 grams of THF solvent at room temperature under stirring for 30 minutes. At this point, a clear solution was obtained. The THF solvent was then removed using B.U.CHI Rotavapor® R215 at 40°C and 175 mbar reduced pressure for 2-hrs and 30 mins. The prereaction was performed under continuous stirring at 200 rpm in a bulk mixture at different temperatures (100°C, 120°C, 135°C and 150°C) for 18 hours reaction time. The prereaction between POSS and DGEBA at a 1:3 molar ratio and 100°C reaction temperature for 18 hours were considered as a benchmark conditions in

<center>31</center>

this research. The reason behind selecting these prereaction conditions as a benchmark is their acceptance in existing literature for optimum performance [77,81]

Table 1

Reactant Monomers

Trade name	Structure	DGEBA-ID	Mol.wt (g/mol)
EPON™825	n= 0.029	EW177.5	355
EPON™834	n=0.43	EW245	490
EPON™1001F	n=2.8	EW540	1080
4, 4'-diaminodiphenyl methane		DDM	198
4, 4'-diaminodiphenyl sulfone		DDS	248.3
Aminopropylisobutyl POSS®		POSS	874.58

A dielectric sensor was submerged into the reaction mixture surface from the top in order to measure ion viscosity (discussed in Chapter III) of the reaction mixture during prereaction. The kinetics of the prereaction was also studied by tracking oligomeric molar mass distribution using SEC, and the conversion of POSS into POSS-DGEBA precursor

with time was determined via ^{29}Si NMR. The samples from reaction mixtures were drawn at regular time intervals and were stored at freezing temperature instantly. Just before the SEC or NMR experiment, they were dissolved in THF and CDCl$_3$ respectively, in order to follow the kinetics of the reaction.
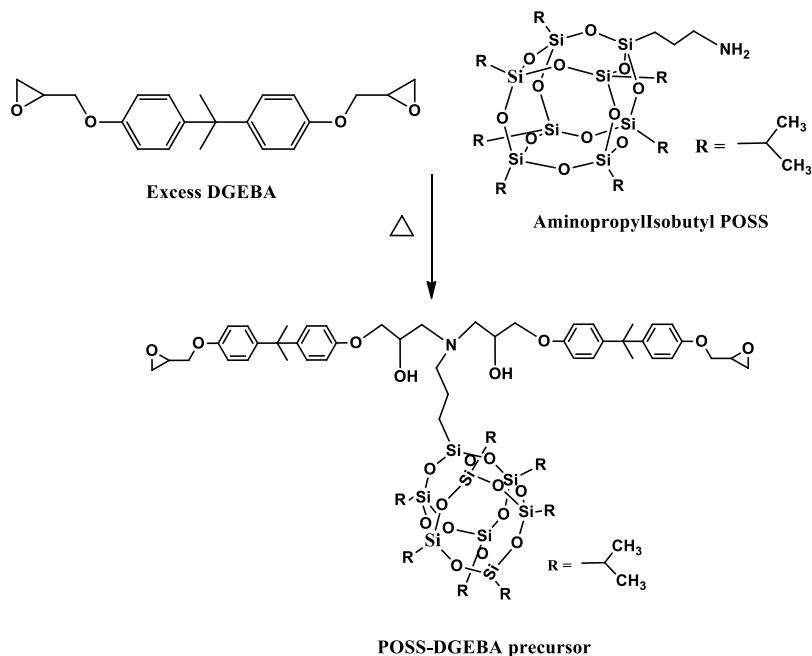
Figure 20. POSS-DGEBA Prereaction

Prereaction of POSS-DGEBA at Varying EEW

The three DGEBA monomers used in this research have different physical states at room temperature. EW175 is medium viscosity liquid, EW245 is high viscosity liquid and EW540 is solid at room temperature. The viscosities of these monomers at 100°C are very different and to ensure a homogenous mixing, or to avoid POSS aggregation in the reaction mixture, the prereaction between different DGEBA monomers and POSS was carried out in a solvent at 100°C. POSS and DGEBA monomers (varying EEW) in 1:3-mol ratio were dissolved in toluene at room temperature in a 500 ml round bottom flask

equipped with a condenser to obtain a clear solution. Table 2 shows the quantities

charged in a reaction flask in order to prepare 15 wt. % reaction solutions.

Table 2

Prereaction Compositions with Varying EW Epoxies using Batch Process

DGEBA	Epoxy, g (mol)	POSS, g (mol)	Toluene, g
EW=177.5	6.13(0.034 mol)	4.94(0.0113 mol)	62.73
EW=245	8.43(0.034 mol)	4.94(0.0113 mol)	75.76
EW=540	18.34(0.0339 mol)	4.89(0.0112 mol)	131.64

Each mixture was stirred until reactants fully dissolved in the solvent. The flask

containing transparent reaction mixture was then heated at 100°C for 18 hours under

constant stirring in an oil bath. After 18 hours, the solution was removed from heat and

brought back to room temperature. The solvent was removed via rotary evaporation at

60°C temperature and reduced pressure to 76 mbar for 4 hours. The product mixture,

which contains unreacted reactants and POSS-DGEBA adducts, was dried under vacuum

at 50°C for 24 hrs. The molecular weight evolution and amine conversion of POSS in

final product mixture was determined by SEC and ^{29}Si NMR

Synthesis of POSS-DGEBA Precursor in Continuous Reactor

POSS-DGEBA precursor (Figure 20) was synthesized by reacting POSS and

DGEBA (EW 177.5) in a twin screw extruder equipped with co-rotating, intermeshing

screws with a barrel length to diameter ratio of 25:1 (PRISM TSE 16TC). The reactor

consisted of five electrically heated zones, an electrically heated and liquid cooled feed

zone, and an electrically heated die. Figure 21 shows the configuration of the screw, the

design was considered to balance the reaction time and shear mixing by using different

screw elements, the screw design is discussed in Chapter 1. A continuous loss to weight

feeder, equipped with a rotatable screw for material transport was used to feed POSS.

The rotatable screws advanced POSS powder through a passage communicating with the

feeding zone in continuous reactor barrel and the discharge feed rate of the POSS was

controlled by means of a variable speed motor. Similarly, a peristaltic pump capable of

transporting liquid feed was used to feed preheated epoxy monomer with a controlled

feed rate at 60°C.
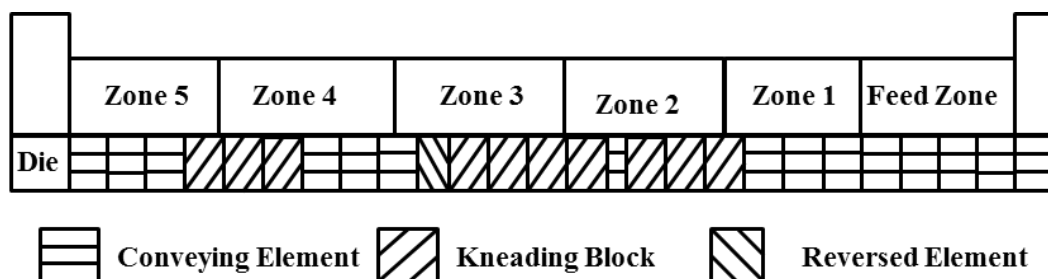
Figure 21. Screw configuration of the continuous reactor

In typical prereaction in a continuous reactor, 1 L of DGEBA was charged in a

flask and placed inside a heat insulating compartment. A hot air dryer coupled with a

thermocouple was used to maintain the temperature of heat insulating compartment at

60°C. A peristaltic pump was used to transport preheated epoxy into the continuous

reactor POSS was charged into the solid feeder to deliver into a continuous reactor. The

calibration of liquid pump and the solid feeder was conducted each time before running a

reaction in order to ensure the right composition of the product mixture.

The continuous reaction was carried out at various processing temperatures,

150°C, 180°C, 200°C, 220°C, and 240°C across all five zones and with a variable screw

speed of 100, 200, 300, and 400 rpm in order to study the effect of processing variables on precursor structure (discussed in Chapter IV). For this purpose, the pump was calibrated to transport 12.6 g/min epoxy, and the solid feeder calibrated to deliver 10.5 g/min POSS into the continuous reactor (1:3-mol ratio of POSS: DGEBA). To prevent further reaction during storage, the product mixture was kept at freezing temperature.

Further, a wide array of molar compositions of POSS and DGEBA was reacted in the continuous reactor to synthesize POSS-DGEBA precursor in order to demonstrate the effectiveness of the process. Table 3 shows the reactant compositions for prereaction in a continuous reactor. Molecular weight distribution of precursor and conversion of POSS into POSS-DGEBA precursor were studied by SEC and ^{29}Si NMR respectively.

Dispersion of Silica Nanoparticles in POSS-DGEBA Precursor Using Continuous Reactor

A key issue of this research has been the dispersion of the pendant POSS and SNP in order to study the nanostructure formation by POSS and SNP in the epoxy network. The favorable interactions between pendant POSS and SNP could lead to increase hybrid networks strength due to the presence of flexible bonding into the network. Similar to the POSS-containing hybrid network, nanostructured containing POSS and SNP were formulated in two steps process. In the first step, SNP were dispersed into POSS modified DGEBA during the continuous reactive processing (CPR). SNP dispersed, and POSS modified DGEBA was then reacted with an aromatic amine curative in a second step to fabricate nanostructured epoxy networks containing POSS and SNP.

Table 3

Reactants Composition for Prereaction using Continuous Process

Sample ID	Mol. ratio POSS: epoxy	EEW 177.5 rate (g/min)	POSS rate (g/min)	Throughput (g/min)
0POSS	-	25.24	0	25.24
1.75POSS	1:140	25.24	0.53	25.77
2.9POSS	1:80	25.24	0.8	26.04
4.9POSS	1:50	21.08	1.1	22.18
7.2POSS	1:30	21.08	1.67	22.75
10.6POSS	1:20	21.08	2.39	23.47
21.8POSS	1:10	17.4	4.85	22.25
45POSS	1:3	13.7	11.2	24.9
54POSS	1:2	9.63	11.2	20.83
70POSS	1:1.05	9.63	21.7	31.33

A series of POSS/SNP/DGEBA prepolymer-dispersion were produced under the evaluated best prereaction condition in a continuous reactor (220°C across all the five zones and a constant screw speed of 350 rpm). Compositions of all POSS/SNP/DGEBA prepolymer-dispersions are listed in Table 4.

Table 4

Composition of SNP POSS-DGEBA Precursor using Continuous Process

Sample	POSS g/min	SNP g/min	EEW 177.5 g/min	Throughput g/min
0POSS-0SNP	0	0	23.26	23.26
10POSS-0SNP	2.43	0	21.87	24.3
20POSS-0SNP	5.046	0	20.184	25.23
40POSS-0SNP	7.16	0	10.74	17.9
0POSS-4SNP	0	1.057	25.3632	26.42
10POSS-4SNP	2.788	1.115	23.9768	27.88
20POSS-4SNP	5.478	1.096	20.8164	27.39
40POSS-4SNP	11.916	1.192	16.6824	29.79
0POSS-12SNP	0	2.838	20.812	23.65
10POSS-12SNP	1.866	2.239	14.5548	18.66
20POSS-12SNP	2.98	1.788	10.132	14.9
40POSS-12SNP	9.976	2.993	11.9712	24.94

DGEBA was at 60°C, this preheated epoxy monomer was then delivered into the continuous reactor by using peristaltic pump calibrated to the desired rate. POSS was feed into the continuous reactor through a solid feeder calibrated at desired feed rate as shown in Table 4. SNP loadings (4% and 12%) were fed by using a separate vibratory feeder with desired feed rates. All the ingredients fed to the continuous reactor were

added through the feed zone. The prepolymer-dispersion was collected and store at a
freezing temperature to avoid further curing

Hybrid Network Preparation

All the hybrid networks prepared throughout this dissertation were formulated
with a stoichiometric balance between equivalents of epoxide groups and equivalents of
active hydrogen (equivalent ratio = 1:1). Two different aromatic amine curatives were
used in this dissertation to formulated epoxy hybrid networks.

Hybrid Network Preparation with DDS Curative

For network preparation from POSS-DGEBA precursors synthesized at different
prereaction temperatures, the POSS-DGEBA precursors were first dissolved in DGEBA
(EW 177.5) to maintain desired POSS content in the final network. A 250 ml Erlenmeyer
flask equipped with a vacuum fitting and magnetic stirring device was used to dissolve
precursor in DGEBA. The reactant mixture was slowly heated to 110°C-120°C while
degassing under vacuum until a transparent and bubble free solution was obtained.
Necessary quantities of DDS curative were then mixed with POSS modified DGEBA
resin. The total epoxy/amine composition is kept stoichiometric (1:1) to obtain
crosslinked networks. The compositions of POSS-DGEBA precursor, DGEBA, and DDS
were calculated based on the targeted POSS content (5wt. %) in the final hybrid network.
Table 5 shows the composition of epoxy hybrid networks prepared from POSS-DGEBA
precursor synthesized at different prereaction temperatures.

Table 5

Networks Composition with Precursor at Temperatures using Batch Process

Sample ID	Precursor, g	EEW=177.5, g	DDS, g	Total, g
Control	0	25.5	8.92	34.42
5POSS@PR100°C	3.88	22.8	8.47	35.15
5POSS@PR120°C	3.55	20.51	7.62	31.67
5POSS@PR150°C	3.99	23.2	8.62	35.81

The reactive mixtures were stirred under vacuum at 120° C for 45 min or until the amine fully dissolve. The reaction mixture was then transferred into pre-heated silicone molds for sample preparation. The system underwent curing at 1°C/min to 180°C, followed by 3-hrs isotherm at 180°C. A post cure for 2 hrs at 200°C was performed for all samples.

The hybrid network containing 5wt % POSS from POSS-DGEBA precursors synthesized with varying EW DGEBA monomers (EW 177.5, EW 245, and EW 540) were prepared using the similar protocol as describe above. The composition of hybrid networks with POSS-DGEBA precursor at varying EW DGEBA monomers are shown in Table 6

Table 6

Networks Composition with Precursor at Epoxy EW using Batch Process

Sample ID	Precursor, g	EEW=177.5, g	DDS, g	Total, g
5POSS@EW177.5	4.5	25.92	9.72	40.14
5POSS@EW245	4.95	23.10	8.59	36.53
5POSS@EW540	7.59	25.95	7.11	33.54

POSS-DGEBA precursor corresponding to 5POSS@EW540 was further used to prepare epoxy hybrid networks containing 5 wt. % of POSS and varying wt. % of SNP. SNP were first dispersed in a mixture of precursor and DGEBA in an Erlenmeyer flask under stirring at 100°C. The dispersion was degassed under vacuum for 1 hour at 100°C. A stoichiometric amount of DDS was then added to the mixture to formulate epoxy hybrid network containing 5wt. % POSS and 0.5, 1.0, 1.5, 2.0, 3.0, and 5.0 wt. % SNP. Weight compositions to prepare hybrid networks containing POSS and SNP are given in Table 7.

Epoxy hybrid networks containing various POSS content were prepared from POSS-DGEBA precursors synthesized in a continuous reactor through polymerization of precursors in the presence of DDS as a curing agent. At first, the POSS-DGEBA precursor was charged to a flask as described before and heated to 100-120°C under vacuum until a bubble free transparent solution was obtained. Thereafter, a stoichiometric amount of DDS was added with respect to epoxide groups into the POSS-DGEBA precursor under stirring, the resultant mixture was then heated to 120°C for 45 minutes or

until amine fully dissolved. Table 8 shows the compositions of epoxy hybrid network prepared from POSS-DGEBA precursors synthesized in a continuous reactor. The reactive mixture was then transferred to preheated silicone molds for curing. A similar cure profile used to cure these networks as described above; 1°C/min till 180°C followed by 3-hrs isotherm at 180°C. All samples were subjected to post cure for 2-hrs at 200°C.

Table 7

Networks Composition with POSS and SNP using Batch Process

Sample	Precursor (@EW540), g	SNP, g	EW177.5, g	DDS, g	Total, g
5POSS-0.5SNP	8	0.17	18.55	7.0	33.72
5POSS-1SNP	8	0.34	18.41	6.93	33.68
5POSS-1.5SNP	8	0.51	18.3	6.88	33.69
5POSS-2SNP	8	0.67	18.16	6.85	33.68
5POSS-3SNP	8	1.01	17.92	6.75	33.68
5POSS-5SNP	8	1.7	17.46	6.54	33.7

Table 8

Network Composition with Precursor (Continuous Process) and DDS

Network ID	precursor, g	DDS, g	Total, g	POSS, wt.%
0POSS-DDS	31.29	10.94	42.23	0
1.75POSS-DDS	35.05	11.96	47.01	1.31
2.9POSS-DDS	35.08	11.77	46.85	2.2
4.9POSS-DDS	30.06	9.79	39.85	3.7
7.2POSS-DDS	29.99	9.43	39.42	5.5
10.6POSS-DDS	29.99	8.92	38.91	8.2
21.8POSS-DDS	29.92	7.26	37.18	17.3
45POSS-DDS	30.58	3.93	34.51	39.8
54POSS-DDS	30.03	2.53	32.56	49.3

Hybrid Network Preparation with DDM Curative

Epoxy hybrid networks containing pendant POSS were prepared through polymerization of POSS-DGEBA precursor in presence of DDM as a curing agent. At first, the POSS-DGEBA precursor was heated between 100-120°C under stirring and degassed under vacuum until a bubble free transparent system was obtained. Subsequently, a stoichiometric amount of DDM was added to POSS-DGEBA precursor based on epoxide groups under stirring for 5 minutes. The resultant mixture was transferred to preheated silicone molds. Table 9 shows the composition of the epoxy hybrid network containing POSS using DDM as curing agent.

Table 9

Network Composition with Precursor (Continuous Process) and DDM

Network ID	Precursor, g	DDM, g	Total, g	POSS, wt.%
0POSS	25.775	7.18	32.956	0
1.75POSS	25.685	6.93	32.62	1.58
4.9POSS	23.340	6.06	29.4	3.94
7.2POSS	23.867	5.97	29.837	5.89
21.8POSS	25.058	4.86	29.918	18.26
45POSS	23.7	2.44	26.14	40.8
54POSS	24.668	1.68	26.35	50.37

Hybrid networks containing POSS and SNP were prepared similarly using DDM. Weight compositions of the hybrid network are presented in Table 10. The similar cure profile was followed to prepare these hybrid networks as discussed earlier. The samples were heated at 1°C/min to 180°C, followed by 3-hrs isotherm at 180°C, and post cure at 200°C for 2 hrs.

Table 10

Network Composition with SNP/Precursors (Continuous Process) and DDM.

Sample ID	Precursor-Dispersion, g	DDM, g	Total, g	POSS, wt.%	SNP, wt.%
0POSS-0SNP	25.12	7.01	32.13	0	0
10POSS-0SNP	24.8	5.94	30.74	8.07	0
20POSS-0SNP	25.31	5.07	30.38	16.66	0
40POSS-0SNP	23.57	2.88	26.45	35.65	0
0POSS-4SNP	26.45	7.08	33.53	0	3.16
10POSS-4SNP	25.65	5.86	31.51	8.14	3.26
20POSS-4SNP	25.81	4.89	30.7	16.82	3.36
40POSS-4SNP	26.42	2.93	29.35	36.01	3.6
0POSS-12SNP	24.95	6.12	31.07	0	9.64
10POSS-12SNP	23.58	4.86	28.44	8.29	9.95
20POSS-12SNP	26.1	4.36	30.46	17.14	10.28
40POSS-12SNP	26.63	2.27	27.9	36.75	11.02

Characterization

Dielectric Spectroscopy

Dielectric spectroscopy measurements were performed using a single-channel DEA 230/1 Epsilon (NETZSCH) system operating at applied frequencies from 0.35Hz and 90 kHz. A 1" tool mount interdigitated electrode sensor (TMS) was used to monitor the in situ frequency dependent ion viscosity (discussed in Chapter III) as it evolved

during the epoxy–monofunctional POSS reaction. The sensor was first calibrated in air

for specific values of gain and phase provided by the Netzsch Co. Experiments were run

in the mid-conductivity mode to accurately monitor the shift in the dielectric signature of

molecular dynamics during the reaction. The reactions were performed at different

temperatures (100° C, 120° C, 135° C and 150° C) for 12-18 hrs. The TMS sensor allows

for near subsurface measurements between the two interdigitated electrodes, the specific

geometry of which is illustrated in Figure 22.[99] The electric field geometry applied during

measurement is of a fringing rather than uniform geometry. With this sensor localized

measurements of the dielectric properties were conducted near the sensor/sample

interface. With this geometry is not necessary to have a fixed sample thickness as long as

the active sensor area is in total contact with the surface and the penetration depth of the

electric field lines into is of approximately the same magnitude as the electrode spacing.

Figure 22. Top Views of the 1" tool mount interdigitated electrode sensor

Reproduced from reference no. 99

Size-Exclusion Chromatography (SEC)

Evolution of molecular weights of POSS-DGEBA precursors were determined

using a SEC system consisting of a Waters Alliance 2695 separations module fitted with

online multiangle laser light scattering (MALLS) detector (MiniDAWN, Wyatt

Technology, Inc.), interferometric refractometer (Optilab rEX, Wyatt Technology Inc.),

and online differential viscometer (ViscoStar, Wyatt Technology, Inc.), all operating at

35° C, and two mixed E (3μm bead size) PL gel (Polymer Laboratories Inc.) GPC

columns connected in series. Freshly distilled THF served as the mobile phase and was

delivered at a flow rate of 1.0 mL/min. Samples were prepared by dissolving 10 mg

oligomer into 1.5 g of freshly distilled THF, and the injection volume was 100 μL. The

detector signals were recorded using ASTRA software (Wyatt Technology Inc.), and

oligomers molecular weights were determined from the refractive index detector response

and assuming 100% mass recovery from the column.

Nuclear Magnetic Resonance (^{29}Si NMR)

Solution state ^{29}Si NMR spectra was obtained using a Bruker Ascend ^{TM} 600MHz

spectrometer operating at 30° C, using 5 mm outer diameter tubes with sample

concentrations of 25-30% (w/w) in deuterated chloroform (CDCl$_3$) (Aldrich Chemical

Co. Acquisition parameters included: A pre-scan delay of 29.34 s and 0.66 s acquisition

time, to yield 30 s intervals between transients, were used to acquire NMR spectra for

reagent and products. Additionally, 14 μs - 90° pulse width and 384 scans were used to

conduct NMR experiment. The monomer conversion was followed throughout the

reaction by tracking the NH$_2$-CH$_2$-CH$_2$-CH$_2$-Si- signal (aminopropyl group on one Si

atom) with respect to 'outer' silicon atom signals of isobutyl-POSS. The relative

concentration of amino-POSS was determined by following the intensity ratio = (signal-

integral/integral of standard signal) of the Si signal bounded with propyl amine. This

signal (located between -67.0 ppm to -67.5 ppm in the case investigated) was always

separated from all the other signals of starting compound and product. All NMR spectra

were analyzed by MestReNova software

47

Differential Scanning Calorimetry (DSC)

Melting and crystallization temperatures of POSS-DGEBA precursors were examined by DSC (Q200 TA Instrument). To obtain melting and crystallization temperatures, samples were prepared by placing 10 mg of POSS-DGEBA precursor within a hermetically sealed TZero® aluminum pan. The samples were then exposed to a heat/cool cycle between 20–220°C, unless otherwise specified, at the rate of 10 °C/min to determine the melting and crystallization peaks. DSC was further used to determine network's glass transition temperatures (T_g's). 5-6 mg samples of cured epoxy hybrid networks containing POSS were prepared as described above and exposed to a heat/cool/heat cycle between 35-300°C, unless otherwise specified, at the rate of 5 °C/min. T_g's were determined by the midpoint of a stepwise enthalpy increase during the second heating.

Dynamic Mechanical Analysis (DMA)

Thermomechanical properties were determined with DMA instrument (Q800) using tension clamps holding cured rectangular samples of dimensions 30 x 5 x 1.5 mm. The temperature dependence of the storage modulus and loss factor tan δ, of rectangular samples (40 x 5 x 1.5mm) was determined with strain amplitude of 0.05% using oscillatory shear deformation at the 1Hz frequency. The temperature was increased from 35° C to 220° C, unless otherwise specified, at a rate of 3° C/min.

Thermogravimetric Analysis (TGA)

A TA Instruments Q50 Thermogravimetric Analyzer with a platinum sample pan was utilized to investigate the possible chemical degradation of samples upon heating.

Samples were heated from 10°C to 600°C at a heating rate of 10°C/min under a nitrogen atmosphere.

Fourier Transform Infrared (FTIR)

FTIR spectroscopy in the near infrared range (4000-8000 cm^{-1}) was used in transmission mode to monitor the presence of relevant functional groups for this chemistry. Experimental runs were performed using a Nicolet 6700 FT-IR from Thermo Fisher Scientific with a white light source and a CaF$_2$ beam splitter. The samples studied were already cured, optically transparent, and with no curvature on the entry or exit surface. Due to inconsistent sample thickness, the results reported are qualitative. A spectrum made of 32 averaged scans (4 cm^{-1} resolution) was collected for each sample. The spectra for neat DGEBA was collected by placing a drop of the liquid epoxy between two glass cover slides (invisible in the near infrared region) which were spaced by a steel washer to maintain constant path length.

Positron Annihilation Lifetime Spectroscopy (PALS)

Average free volume hole size and the relative intensity of o-Ps was determined by positron annihilation lifetime spectroscopy (PALS) on a fast-fast coincidence system, based on a system described by Olson et al., [100] with an average resolution FWHM of 290 ps. Samples for PALS analysis were prepared by direct curing of 1cm diameter and 1 mm thick disks using *WorkSmart* 0.397 inch inside diameter- 0.509 inches outside diameter and 0.7-inch thick silicone o-rings supplied by MSC Industrial Supply Co. NY, USA. A foil wrapped Na-22 source was sandwiched between two sample disks, wrapped in PTFE tape, and placed between two photomultiplier assemblies equipped with BF$_3$ scintillation crystals, aligned coincident to the sample stack. Twelve spectra were collected for each

sample at ambient conditions (23 °C, 45% RH) using a system based on an Ortec

Positron Lifetime System (Advanced Measurement Technology, Oak Ridge, TN) over

one hour to collect greater than 10^6 incidences. Coincidences were compiled using a

multichannel analyzer. Spectra were analyzed for three lifetimes and intensities using the

PATFIT-88 software.[101] The average radius of spherical free volume holes was calculated

by the following relation[102]

$$\tau_{o-Ps} = 0.5 \left[1 - \frac{R}{R_0} + \frac{1}{2\pi} \sin\left(\frac{2\pi R}{R_0} \right) \right] \quad \text{(Eq 1)}$$

Where $\tau_{o\text{-}Ps}$ is the lifetime of the long-lived o-Ps, R is the radius of the cavity, and

R_0 is a constant 1.66 Å. The volume of the spherical hole is calculated as: $<vh> = 4/3\, \pi R^3$.

Density Measurement

Densities of cured hybrid networks were determined by XS104 Mettler-toledo

microbalance at ambient conditions with an accuracy of $\pm$ 0.002 cm^3/g. The density

measurement carried out based on Archimedes' principle, at room temperature using

deionized water. Particular care was taken in selecting samples as internal voids or

bubbles will drastically affect the density values. Density was calculated using the

following equation:

$$\rho = \frac{m_{dry}}{m_{dry} - m_{immersed}} * \rho_{water} \quad \text{(Eq 2)}$$

Where m_{dry} is the mass of the specimen prior to immersion, $m_{immersed}$ is the weight

of the specimen in water, and ρ_{water} is the density of water. The average of 3 density

values is reported.

Cone Calorimetry

Cone calorimeter measurements were performed with the 'Govmark' cone instrument according to ASTM E 1354 using a cone shaped heater with an incident flux $50kW/m^2$.(100) Samples for cone calorimetry analysis was prepared by direct curing of 100 mm x 100 mm x 3mm specimen using a state of art metal mold with aluminum interior. The exhaust flow was set at 24L/s and the spark was turned on continuously until the sample was ignited. Typically the data generated by a cone are quite reproducible with an uncertainty which doesn't exceed +/- 10%. A set of fire-relevant parameters can be obtained using the cone calorimeter including the peak heat release rate (PHRR), average mass loss rate (AMLR), time to ignition (t_{ig}) and specific heat of combustion.[103] The samples were wrapped in aluminum foil without frame or grid and for each sample, three replicates were performed.

Compression Testing

Compression testing procedure followed ASTM 695-02A. Cylinders of 2:1 length to diameter ratio were compressed at a displacement controlled test rate of 1.3 mm/min on an MTS systems corporation Model 810 servo-hydraulic universal test frame equipped with a low friction compression sub-press (Wyoming Test Fixtures Model CU-SP). Displacement was measured by a linear variable differential transformer (LVDT) and the load was measured using an MTS 15kN load cell. Data was recorded at a sampling rate of 10 Hz using Testworks® software.

Scanning Electron microscopy-Energy Dispersive X-ray (SEM-EDX)

Scanning electron microscopy (SEM) was performed using an FEI Quanta 200 SEM coupled with a Thermo scientific energy dispersive X-ray (EDX) to determine the

elemental composition of both the bulk and other microstructural features. EDX software, Noran System Six, was used to analyze the fractured and air-exposed surfaces in high vacuum mode by use of conventional secondary electron imaging with an accelerating voltage of 20 kV, the spot size of 4.5, and a working distance of 10 mm. The samples were sputtered coated with silver with a sputter time of 3 min and 25mA current before being inserted into the specimen chamber.

Transmission Electron microscopy (TEM)

The morphologies of epoxy matrices modified with POSS and/or silica nanoparticles were investigated using a Zeiss EM900 transmission electron microscope using an accelerating voltage of 50 kV. Samples were cut into ultrathin (~100 nm), trapezoidal shaped sections with a Porter-Blum MT-2B microtome (Ivan Sorvall, Inc.), using a diamond knife (DiATOME-U.S., Hatfield, PA) at room temperature. Sections were collected on 200 mesh copper TEM grids (Electron Microscopy Sciences) and imaged without staining.

Water Absorption

Water absorption study was conducted using deionized water. Rectangular epoxy hybrid networks containing POSS samples having a mass of approximately 200 mg and thickness of 1.5 mm were conditioned in a vacuum oven for 12 hours at 100°C prior to measuring initial weights. Dry polymer samples were placed in 20 mL scintillation vials containing ~15-18 mL of fluid. The vials were sealed and stored at 25°C in a Fisher Scientific Model 146E incubator. To measure fluid uptake, samples were periodically removed from the solution, patted dry, and weighed to the nearest 0.1 mg. Percent change in mass for each sample was calculated as follows [104]

$$\% \: Change \: in \: Mass = \frac{m_w - m_i}{m_i} \times 10 \quad \text{(Eq 3)}$$

Where m_w is the wet mass and m_i is the initial mass. Three samples were averaged to give each data point.

CHAPTER III - POSS-DGEBA PRECURSOR SYNTHESIS: - EFFECT OF

TEMPERATURE AND EPOXY EQUIVALENT WEIGHT, NETWORK

MORPHOLOGY, AND PROPERTIES

Abstract

In this Chapter, we focus on investigating the relationships between reaction kinetics and mechanism for the formation of POSS-DGEBA precursors with respect to prereaction temperature and DGEBA equivalent weight. ^{29}Si NMR and SEC were used to determine the influence of prereaction temperature and DGEBA equivalent weight on the reactivity of POSS with DGEBA. Temperature dependent kinetics parameters for POSS-DGEBA prereaction were determined by fitting ^{29}Si NMR data to the kinetic model of Kamal that was extended to include diffusion effect. Fitting of this model to experimental data showed very good agreement over the entire conversion range for prereaction between monoamine POSS and DGEBA. An autocatalytic mechanism, the same as that for the neat epoxy-amine systems, was indicated. In addition, a dynamic dielectric method was used to track prereaction kinetics by monitoring intrinsic viscosity (IV) with reaction time for various prereaction temperatures. SEM-EDX and TEM were employed to investigate phase structure of the final networks cured by DDS using POSS-DGEBA precursors. POSS aggregate size decreased with increased prereaction temperature and DGEBA equivalent weight. Structure-property relationships were established by analyzing thermomechanical properties of epoxy hybrid networks produced from POSS-DGEBA precursors.

Results and Discussion

POSS-epoxy precursor dramatically improves the dispersion of pendant POSS in epoxy systems.[74,77,81] This chapter provides a systematic effort to control the structure and morphology of the epoxy hybrid networks containing pendant POSS in order to prepare relatively well-defined hybrid networks. The effects of prereaction temperature and DGEBA equivalent weight on POSS conversion during prereaction were studied with the aim of increasing reaction efficiency to make POSS incorporation more competitive than phase separation. Additionally, an attempt was made to correlate the experimental data with the kinetic behavior of POSS- DGEBA prereaction. Influence of POSS-POSS and POSS-DGEBA interactions on morphology and thermomechanical properties is explained. POSS and DGEBA at a 1:3 molar ratio was used to conduct prereaction in a batch process as described in Chapter II.

POSS-DGEBA Precursor Synthesis

Reactivity of POSS with Epoxy at Varying Prereaction Temperatures: The relative reactivity of POSS at varying prereaction temperatures was at first monitored by dielectric analysis (DEA) to study the induction time before the reaction starts and the time required to reach maximum conversion. The distribution of POSS-DGEBA precursor's molecular weight was determined by SEC, followed by ^{29}Si NMR analysis to determine the conversion of amino POSS during the reaction.

Prereaction kinetics was tracked by using a newly developed *in-situ* reaction monitoring technique based on dynamic dielectric sensing using an appropriate electrode sensor, as described in Chapter II. The salient parameter is the IV which is monitored as a function of time. IV is a measure of ion mobility, which, in turn, is coupled to polymer

chain segmental mobility. The ions, which are the detectable quantity, are mobile charges which can be a natural product of reactions, or in other cases, existing impurity charges. IV is derived from the dielectric loss permittivity, ε'', through the following relation which holds at low frequencies, f:

$$\text{Ion viscosity (IV)} = 1/\sigma; \ \sigma = 2\pi f \varepsilon'' \varepsilon_{o\ldots} \ \text{(Eq 4)}$$

σ is an electrical conductivity reflective of long range charge migration and ε_o is the vacuum permittivity. σ is related to the average viscosity of the medium in an inverse fashion. Hence its variation is linked to the evolution of structure, and dynamics during the reaction. As the monomers increasingly react and form adducts, the viscosity naturally increases and conductivity diminishes.

The specific temperature effect on reaction kinetics was determined by comparing the reaction data for different temperatures (100, 120, 135 and 150° C) at the low frequency of 1.5 Hz. In Figure 23, it is seen that the induction times (defined as the time up to which IV increases at a considerably greater rate, the point being indicated on the graphs) at these temperatures are 500, 200, 40 and 20 min, respectively. In short, lower temperatures cause longer induction times after which there is an increase in IV indicative of a percolation threshold.

At the earliest times, charges migrating amongst oligomer chains do not experience great differences in the local liquid-like interactive environment but as the number of oligomers increases in number and size in the reaction mixture, greater impediments to mobility are posed and IV rises at a greater rate.
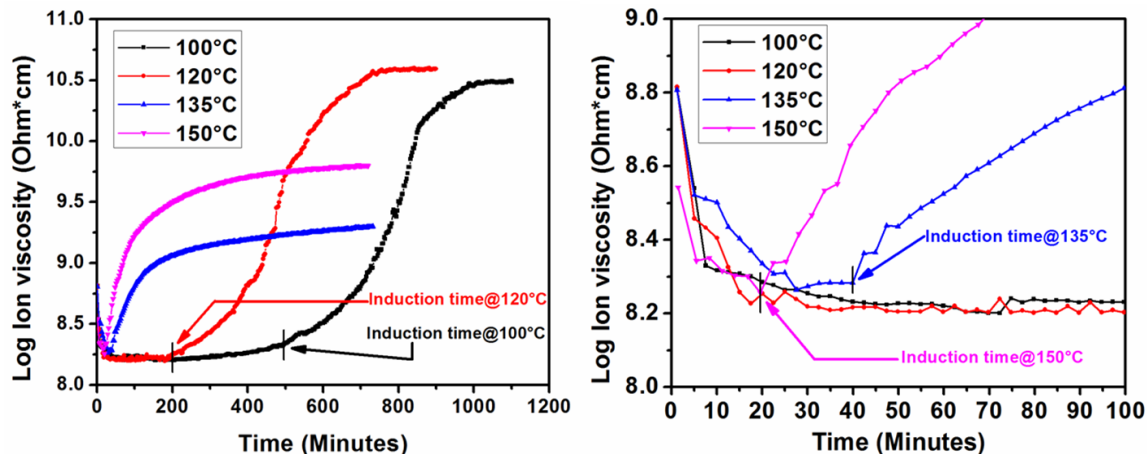
Figure 23. [A] In situ monitoring of the ion conductivity by dielectric sensing at 1.5 Hz with different reaction temperatures. [B] Zoom-in region between 0 to 100 minutes.

In general, IV at a given time should decrease with increasing reaction temperature, which is seen in Figure 23 up to around 500 min, after which there are curve intersections. The nature of the curves changes between 120°C and 135°C such that the two curves at higher temperatures lie beneath the two curves at lower temperatures at the longer times. As mentioned by Hakme et al.,[105] conductivity decreases with the increase of molecular weight during the polymerization reaction. An increase in IV could result from the formation of higher molecular weight epoxy molecules during the reaction at a higher temperature, which is in good agreement with SEC analysis in this study (Figure 24). A plateau in IV over time in all cases can be explained in terms of formation of increasingly more epoxy-POSS adduct causing diffusion and mobility to be more difficult.

In a more detailed analysis, consider the height of the late-stage asymptotic or near-asymptotic behavior in Figure 23. IV is inversely proportional to σ as in equation (4). σ, in turn, is a compound quantity that is the product of the charge mobility μ and charge density ρ $(\sigma = \rho\,\mu)$. Thus, the response of IV may be due not only to the mobility

of charges at a given time in their evolving environment but to their number per unit volume, which itself could evolve in time.

Evolution of oligomer molar mass distribution during prereaction at different temperatures was followed by SEC. The SEC chromatogram in Figure 24(A) characterizes prereaction of POSS and DGEBA at 100°C. The monomers POSS and epoxy and the POSS-DGEBA adduct are distinguished at 15.5, 17.5, and 13-15 minutes respectively. As seen, the formation of higher molar mass oligomers continues up to 8 hours, after which no change is observed in molecular weight distribution in the reaction mixture.
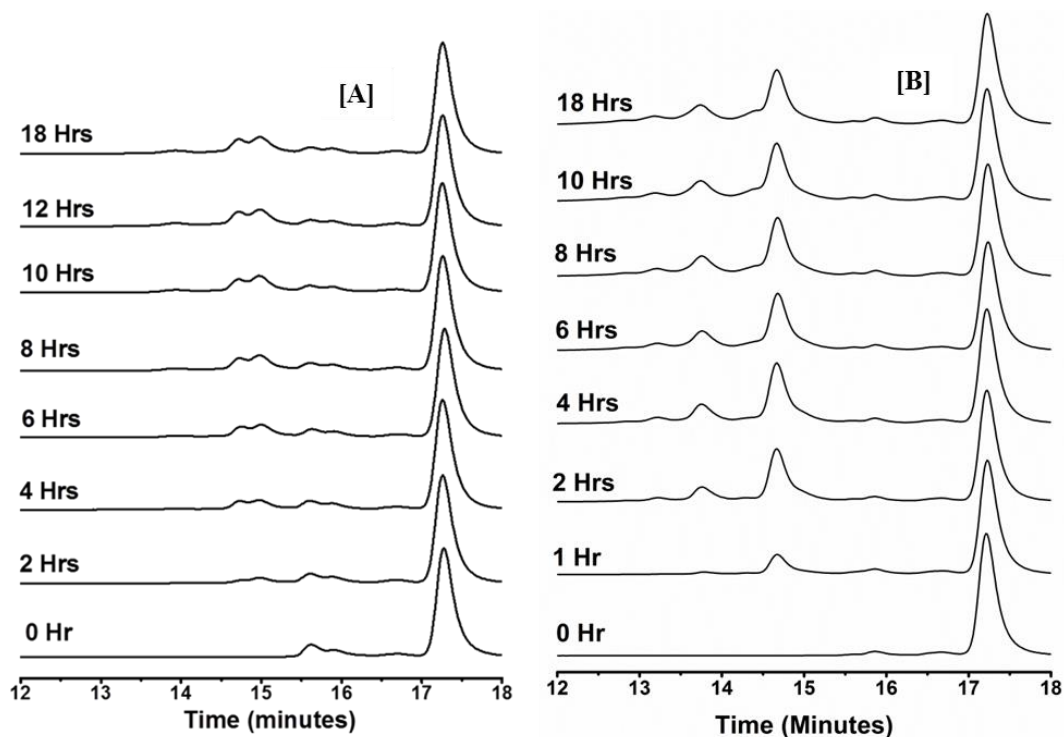
Figure 24. SEC data of the reaction mixture with time at (A) 100°C and (B) 150°C

In Figure 24(B), which shows the SEC chromatogram at 150° C, molecular weight building is observed until 4 hours of reaction after which there is no significant change in molar mass distribution. One important observation is two different peaks at

58

12.7 min and 13.2 min in the 150°C chromatogram which is not observed in the 100° C

chromatogram. Since the reaction is at high temperature, a possible self-polymerization

happen for DGEBA monomer at high temperature and those peaks could be results of

higher molecular weight DGEBA molecules. Formation of extended epoxy monomers

via self-polymerization at high temperature was also observed by Innocenzi and

coworkers.[106]

    Silicon (^{29}Si) NMR spectra were acquired as described in chapter II. Three peaks

were observed in the spectra generated of POSS corresponding to Si atoms in POSS as

numbered (Figure 25).
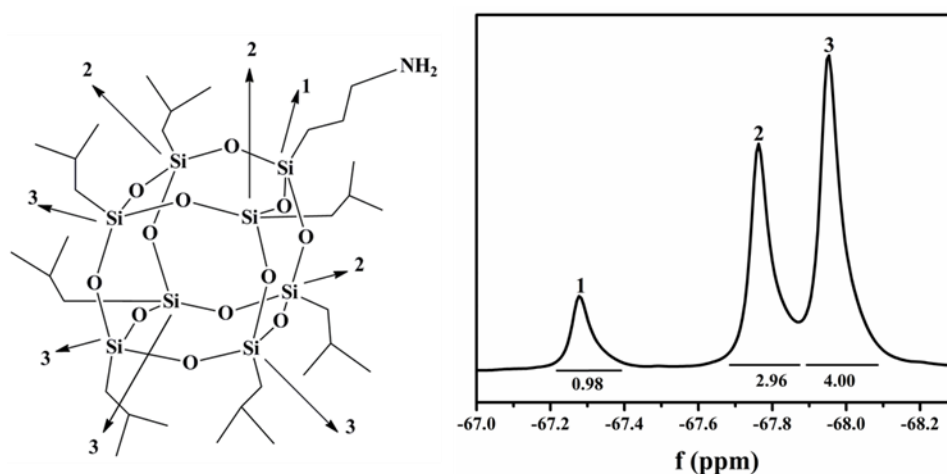
Figure 25. ^{29}Si NMR spectra of POSS with indicated Si atoms chemical shifts.

    The chemical environment around these Si atoms is different as seen in Figure 25.

During the reaction, the peak corresponding to Si atom 1 changes because of the amine-

epoxide reaction which results in a change of chemical environment around atom 1.

Figure 26, shows the ^{29}Si NMR spectra of the reaction mixture at 100°C where the peak

corresponding to atom 1 (-67.1 ppm) splits into three peaks. The two new peaks

appearing at -67.28 ppm and -67.42 ppm during reaction correspond to Si atom '1'

bonded with a secondary and tertiary amine. As the bond polarity of the N-C bond is lower than that of N-H, there was an upfield chemical shift in peaks corresponding to Si atom 1 bonded with secondary peak and tertiary amine. These peak regions were integrated and the integral values were converted to moles in order to see the conversion of POSS. Figure 27 depicts the change in amine concentration with respect to time during the reaction. It was observed that there is a significant amount of unreacted POSS in the product mixture even after 18 hrs reaction time at 100°C. As seen in Figure 27[A], initially the reaction proceeds rapidly and the rate of reaction appeared to be chemically controlled. After 6 hrs the reaction rate was very slow and it does not proceed to 100% conversion due to the slow rate of diffusion of the reacting species. At 150°C prereaction temperature, the reaction initiated at a much higher rate but the conversion stopped much sooner due to the slow rate of diffusion of reacting species caused by increased viscosity due to greater molecular weight. Figures 29 and 30 show that the rate of reaction at 150° C initially was faster than at 100°C and the conversion reaches a plateau at a much earlier time, after 3 hr. The rate of reaction is controlled by the rate of diffusion and rate of collision, which leads to the formation of epoxy-POSS adducts. As the reaction proceeded, the increasing size and the complexities of the epoxy-POSS adduct restricted diffusion and effectively ceased the reaction. One important observation was that the net conversion of primary amines during the reaction at higher temperature was higher as seen in Figure 30. This could be explained by the formation of higher molecular weight epoxies at high temperature as also observed in SEC chromatograms. The presence of hydroxyl groups in the extended epoxy molecules catalyzed the reaction by forming hydrogen bonding between –OH groups and oxygen atom in epoxide ring, which make

60

epoxide group more reactive, and therefore, greater amine conversion before reaction effectively cease because of diffusion effect.
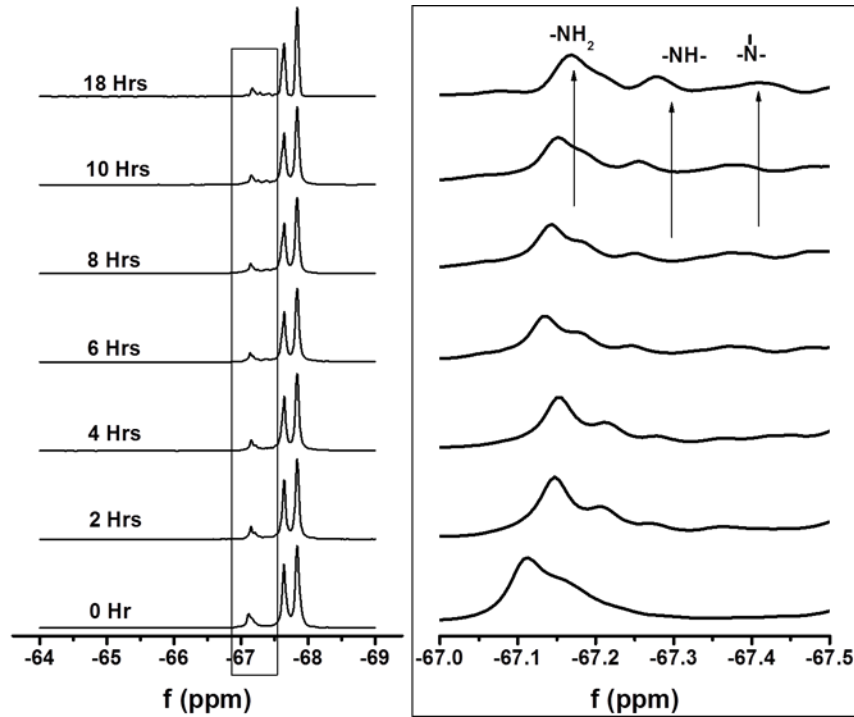
Figure 26. ^{29}Si NMR record of the reaction mixture at 100°C. Zoom in between -67.0 ppm and -67.5 ppm

In order to determine reaction kinetics, the empirical model suggested by Kamal & Sourour[107] for the epoxy-amine reaction was chosen for this system. The model accounts for an autocatalytic and non-autocatalytic reaction in which the initial reaction rate is not zero.

$$\frac{d\alpha}{dt} = (K_1 + K_2\alpha^m)(1 - \alpha)^n \qquad (5)$$

α is the degree of cure corresponding to the rate $d\alpha/dt$ and denotes the conversion of epoxy groups at a given time t. K_1 describes the rate constant of the reaction of partial order n catalyzed by an accelerator, K_2 is the rate constant of the autocatalytic reaction of partial order m. As suggested, Eq. (5) is not correct in comparison with the final level of

degree of curing obtained experimentally since it hardly tends to unity. As reaction

proceeds, the chemical degree of conversion rate is less and less important, and the

reaction becomes diffusion controlled.[108–110] Fournier[108] proposed a semi-empirical

relationship (Eq. 6) based on free volume consideration to extend the Kamal and Sourour

model by a diffusion factor $f_d(\alpha)$ such as:

$$\frac{d\alpha}{dt} = (K_1 + K_2\alpha^m)(1 - \alpha)^n f_d(\alpha) \quad (6)$$

$$\text{With} \quad f_d(\alpha) = \left[\frac{2}{\left(1 + \exp\left[\frac{\alpha - \alpha f}{b}\right]\right)} - 1 \right] \quad (7)$$

Where αf is the final degree of conversion obtained at the end of a given isothermal

curing and hence could be directly obtained from experiment; b is an empirical diffusion

parameter of the material. The Fournier et al. diffusion factor appears to be the most

common relation for diffusion terms to expand the Kamal and Sourour model to enable

conversion rate prediction also in the diffusion-controlled regime.[108] Thus, to identify the

epoxy/amine reaction kinetics, following parameters have to be identified; The total

epoxy/amine conversion corresponding degree of conversion, four parameters of the

Kamal and Sourour model; m, n, K_1 and K_2 and the two parameters of the Fournier et al.

diffusion factor model: b and αf.[111]

Diffusion Effect Analysis

As seen in Figure 27[A], the initial rate of the epoxy/amine reaction was

dominated by molecular collisions before being controlled by diffusion and the

conversion stop after a certain time. As indicated by the model of the cure (Eq. 6), the

analysis of diffusion control can be better seen by rearranging the cure kinetic equation

as:

$$\frac{\frac{d\alpha}{dt}}{(1-\alpha)^n} = (K_1 + K_2\alpha^m) f_d(\alpha) \quad (8)$$

The parameters to determine are n and m where $m + n$ denote reaction order. m and n are

reaction orders for the autocatalytic and catalytic parts of the chemical reaction,

respectively. It appears more coherent and logical to search for fixed values of m and n.

Assuming that the order of the autocatalytic reaction is $m = 1$, a value in agreement for

epoxies in the literature[107,112,113] the correct value for n should lead to a plot of *(dα/dt) /*

(1-α)ⁿ vs. experimental conversion data in a straight line, with K_1 as the intercept and K_2

as the slope for conversion levels before diffusion control *(fd (α) =1)*. Figure 27[B]

consists of plots of *(dα/dt) / (1-α)ⁿ* vs. experimental conversion with various n values. As

a linear curve could be obtained for a value of $n = 2.5$. This indicates that the reaction

order is 3.5, which is fairly close to the literature values for epoxies.[110,111]
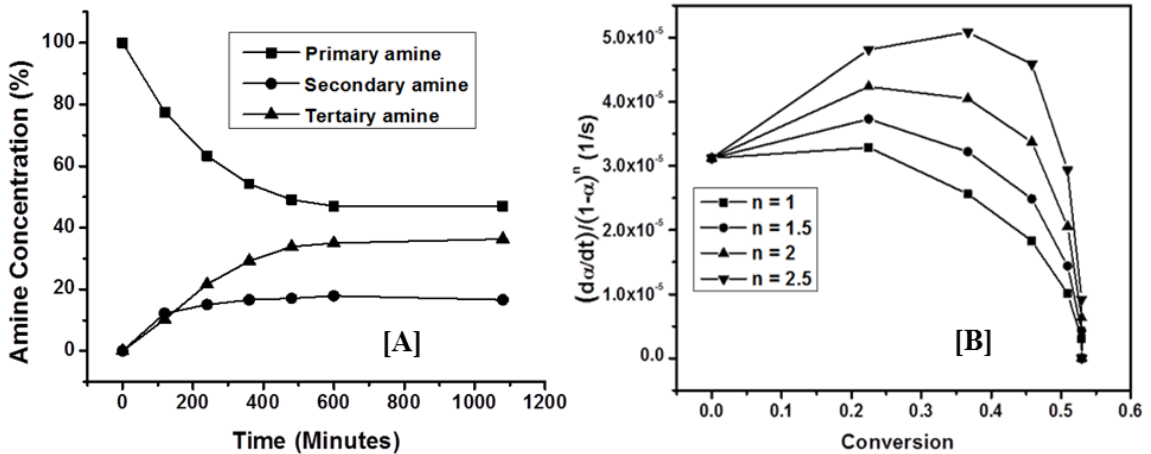
Figure 27. [A] Amine conversion with time for the 100° C isothermal reaction. [B] Plot
of $(d\alpha/dt) / (1-\alpha)^n$ vs. conversion
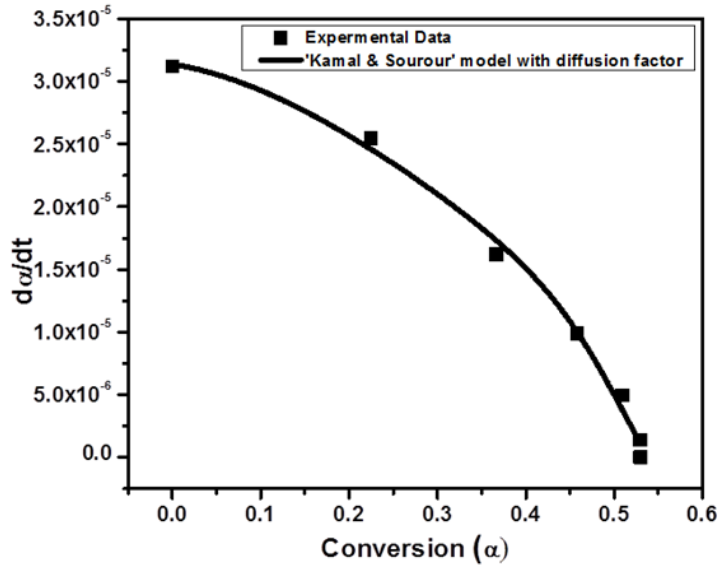
Figure 28. Data fitting according to the Kamal & Sourour model with diffusion factor

Table 11

Reaction Parameters Obtained by Model Fitting

Model	Kamal model with diffusion factor		
Equation	$d\alpha/dt=(1-\alpha)^{2.5} * (K_1+K_2\alpha) * \{2/[(1+\exp(\alpha-\alpha_f)/b)-1]\}$		
Reduced Chi-Sqr	1.57758E-12		
Adj. R^2	0.98918		
Parameters		Value	Standard Error
	K_1	3.13726E-5	1.24951E-6
	K_2	6.74595E-5	1.04308E-5
	α_f	0.53949	0.00848
	B	0.0424	0.01297

Other kinetic parameters, K_1, K_2, and diffusion factor parameters b and α_f, can be identified by fitting the model with diffusion factor to the experimental data, as shown in Figure 28. A similar fit was tried for the data at a higher temperature (150° C) but the reaction proceeded much faster and data point collection after an interval of 1 or 2 hrs was insufficient to monitor the reaction kinetics from ^{29}Si NMR (data fitting; $R^2 = 0.78$). The reaction kinetics parameter at 100°C is shown in Table 11.
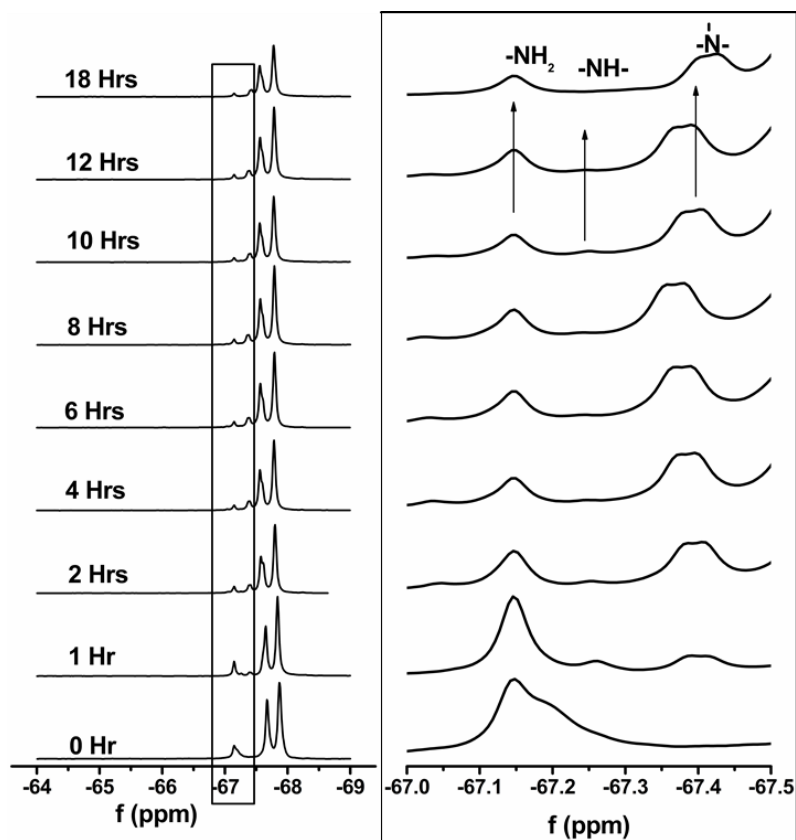
Figure 29. ^{29}Si NMR record of the reaction mixture at 150°C. Zoom in between -67.0 ppm and -67.5 ppm
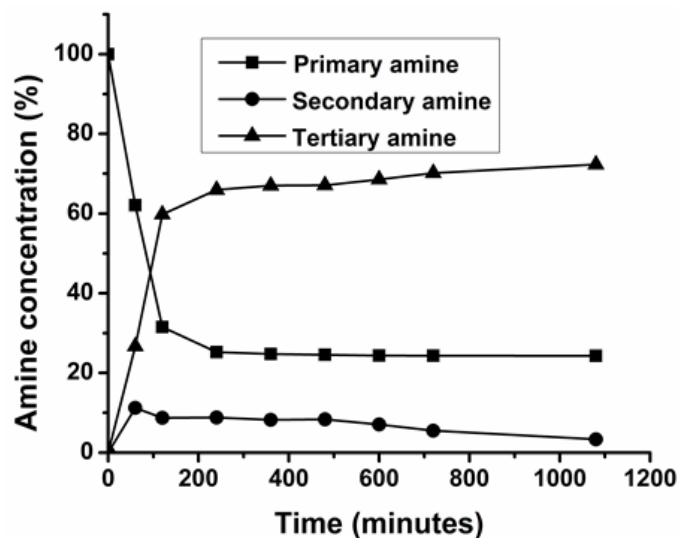
Figure 30. Amine conversion with time at 150°C.

Reactivity of the POSS with Varying EW DGEBA Monomers: ^{29}Si NMR spectrum

confirmed that the POSS cages were intact after the prereaction. The relative

concentrations of the DGEBA-POSS adducts were determined by following the relative

intensity (= ratio (signal integral/ integral-of-standard-signal). Figure 31 proves that there

is only one Peak, corresponding to primary amine peak as described earlier (Figure 25)

that was changing during the course of the reaction. As confirmed by the silicon spectra,

the DGEBA monomers (EW 245 and EW 540) reaction with POSS results in more

adduct formation and less unreacted POSS monomer in the product mixture. In Figure

31, there is a shift in secondary and tertiary amine peaks corresponding to EW 245 and

EW 540 precursors, which would be a result of electronics on the experimental sample

due to different chain length. The disappearance of the peak corresponding to primary

amine in the case of EW245 and EW540 epoxy confirmed that by increasing DGEBA

EW the conversion of POSS increased. As mentioned earlier, it is because of the two

effects, first is the presence of hydroxyl groups in the DGEBA molecules backbone

66

catalyzed the reaction by forming hydrogen bonding between –OH group and oxygen atom in epoxide ring, which make the epoxide ring weaker and more susceptible to attack by amine, another reason of increase conversion is longer epoxy molecules chains reduce the diffusion effect and provide more mobility to POSS cage to react with DGEBA molecules.
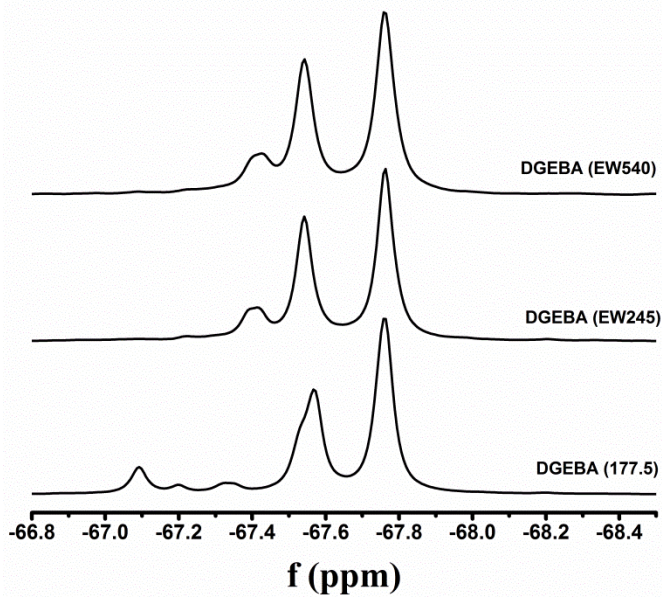
Figure 31. ^{29}Si NMR record of product mixtures with different epoxy equivalent weight

As the product yield a mixture of POSS-DGEBA adducts and unreacted DGEBA. The kinetics of the prereaction was also followed by SEC as an evolution of the oligomer molar mass distribution. The SEC chromatograms, given in Figure 32, depict the evolution of molecular weight after reaction at 100°C. The reaction mixture of DGEBA with POSS showed three distinguished peaks before reaction, where the peak at 17.5 min indicated the population of lower molecular weight epoxy and the peak close to 16 min corresponded to POSS. There was a peak at 15.5 minutes indicating that there was some chain extension in the DGEBA monomer. Similarly, for reaction mixture of EW 245/EW

67

540 and POSS, other than peaks at 17.5 and 16 minutes, there were peaks corresponding to the extended chains in the epoxy. Figure 32 proves formation of higher molecular weight adducts after the reaction, also the rate of disappearance of monomer peaks for EW 540 and POSS reaction is more than DGEBA or EW245 monomers and POSS reaction. This trend indicates that more POSS-DGEBA adducts form in the case of EW540, which is also evident in Figure 32, where we can see a large population of higher molecular weight component after the reaction. These results support the claims made from NMR results.
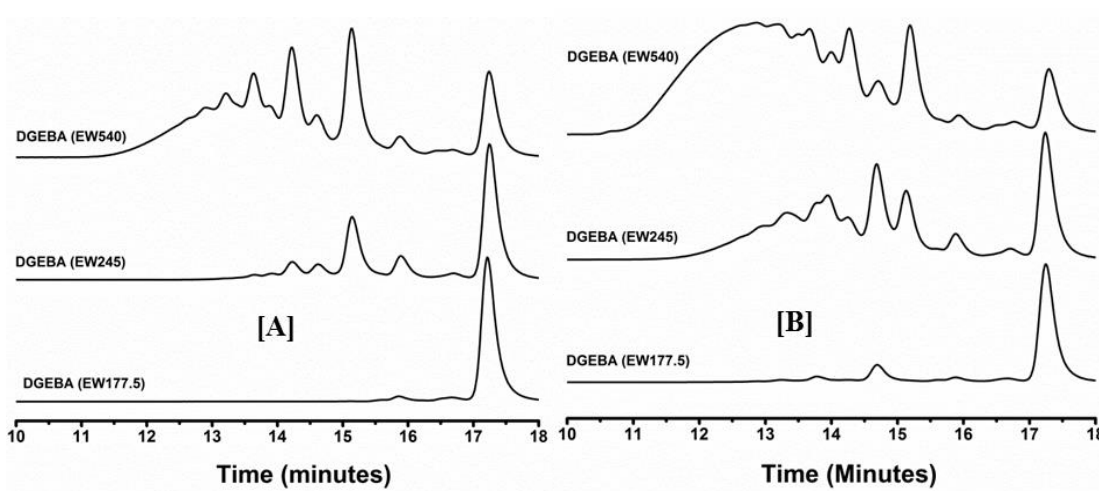
Figure 32. SEC record of reactant mixture; [A] before reaction, [B] after reaction

Morphology of Hybrid Networks Containing POSS

   Hybrid Networks with POSS-DGEBA Precursor at Varying Prereaction Temperature: A stoichiometric amount of an aromatic diamine, DDS was dissolved in POSS-DGEBA precursor and cured at an industrially accepted cure profile to generate a hybrid network containing 5wt. % of POSS as described in chapter II. A primary liquid-liquid phase separation process occurred at the time of adding DDS to the POSS-DGEBA precursor. This led to a macrophase separation into epoxy-rich and POSS-rich regions,

possibly derived from the incompatibility of the isobutyl groups attached to the POSS with the aromatic epoxy-amine network. A secondary phase separation occurred in the epoxy-rich phase in the course of polymerization, producing a dispersion of small POSS domains.

The samples for SEM observations were silver coated by diode sputtering to obtain/display elemental data as mappings of the distribution and relative intensity of previously defined elements over the scanned area (image area). The SEM-EDX analysis provides evidence of POSS migration on the surface. Silver coated samples were used to map the distribution and relative (intensity) of previously defined elements over the scanned area. The migration phenomenon was explained by thermodynamic consideration.[114] According to the Gibbs adsorption isotherm, the lower surface free energy components in a multicomponent system migrates to the surface, thus decreasing the free energy of the surface.[115] Another important thermodynamic cause of the migration of POSS to the surface is the restraining effect of the POSS particles on the mobility of the matrix chains, which causes a decrease in the entropy of the system. In order to increase the entropy, the POSS particles have to migrate to the surfaces. The entropy of the surfaces is much higher due to the higher degree of freedom of surface molecules. Typical SEM micrographs over a large area of hybrid networks are shown in Figures 33-36. Figure 33 shows the image of POSS aggregates in bulk which contains around 13% silicon by weight. Figures 34-36 show images of the samples prepared with different prereaction temperatures. The images of the bulk, seen in Figures 34B and 35D exhibit un-smooth features due to material pull-out that occurs during fracture. There is a

distribution of POSS particle aggregate sizes on the surface for 100° C prereaction

temperature as seen in Figure 34.
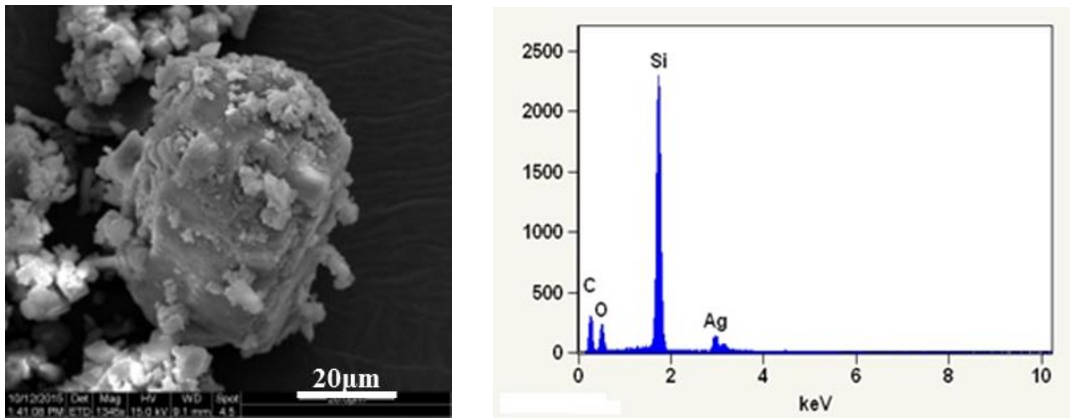
Figure 33. SEM-EDX of POSS aggregate in the bulk
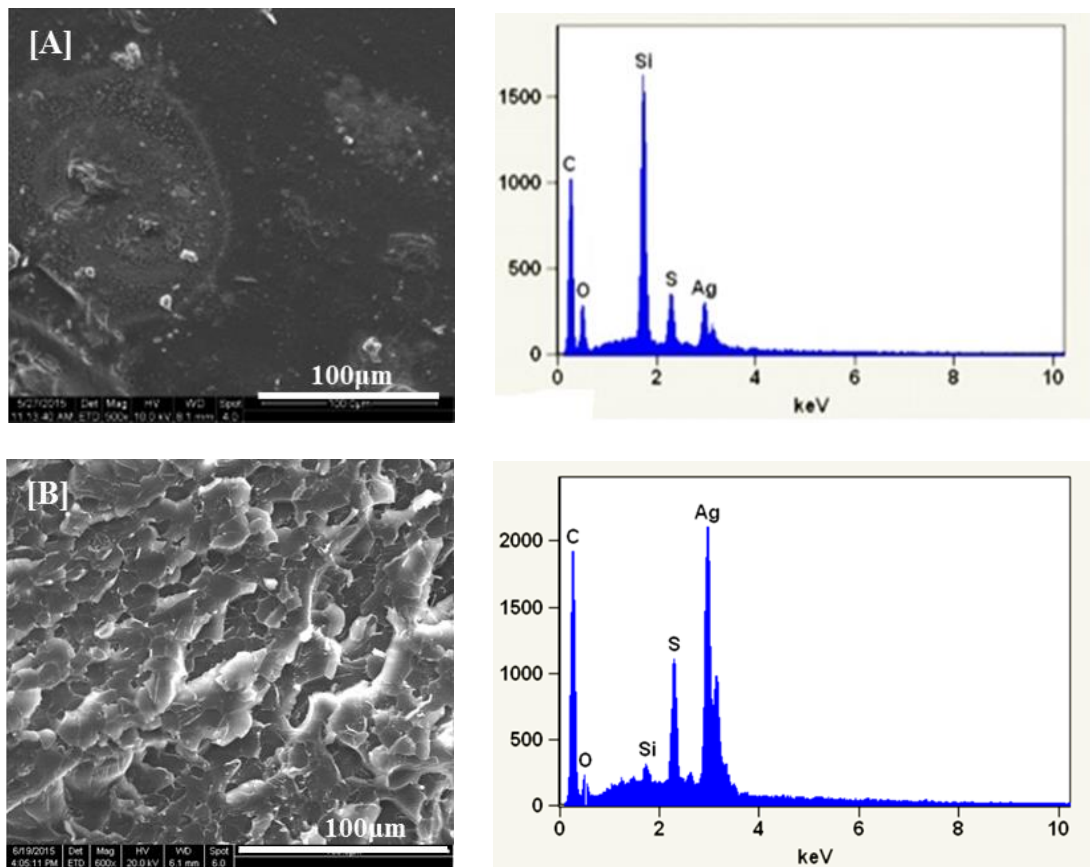
Figure 34. SEM-EDX of hybrid network with prereaction at 100°C: [A] surface, [B] bulk.

There appear to be several large agglomerations of smaller particles presumably held together by Van der Waals forces. As confirmed by EDX analysis the surface contains around 11% silicon by weight. This represents the aggregated POSS particles, which may have partly formed during the migration process, or after reaching the surface. A different image is seen in Figure 35 in which the sample, prepared at 120° C, the surface contains around 2.36 wt. % of silicon on the surface which is further reduced to 1.31 wt. % at the higher temperature of 150° C (Figure 36).
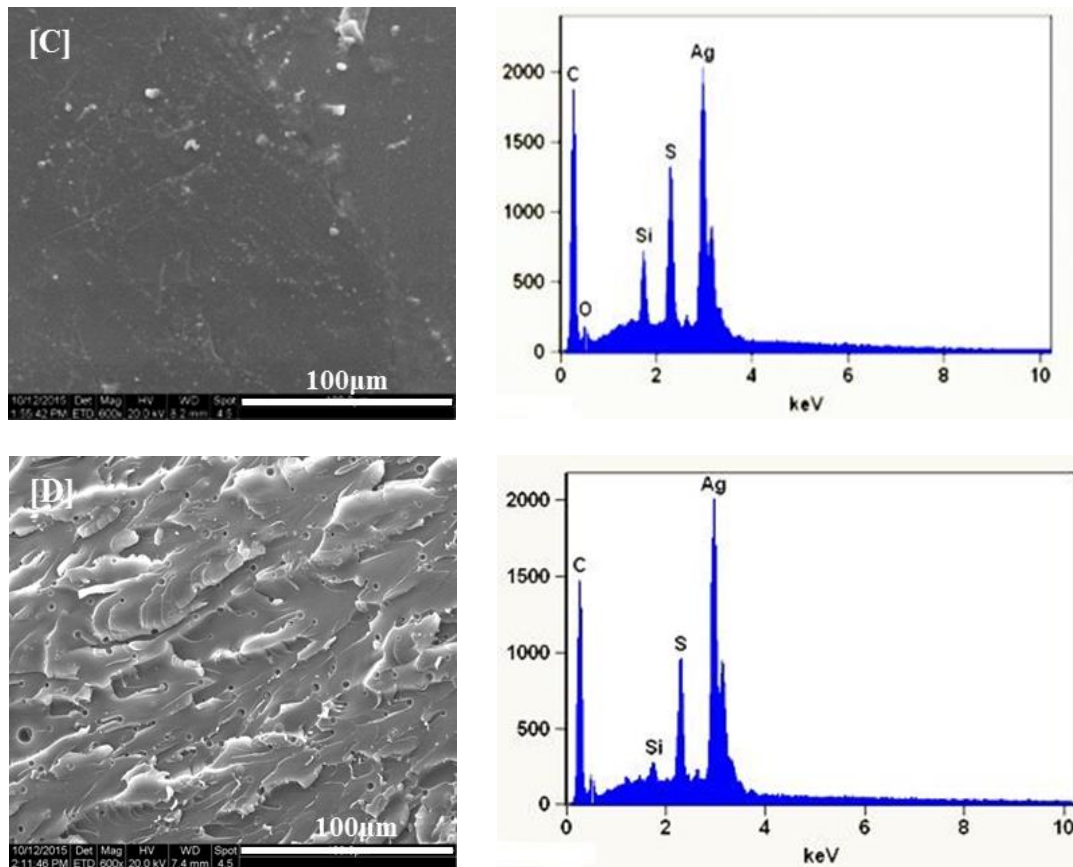
Figure 35. SEM-EDX of hybrid network with prereaction at 120°C: [C] surface, [D] bulk.
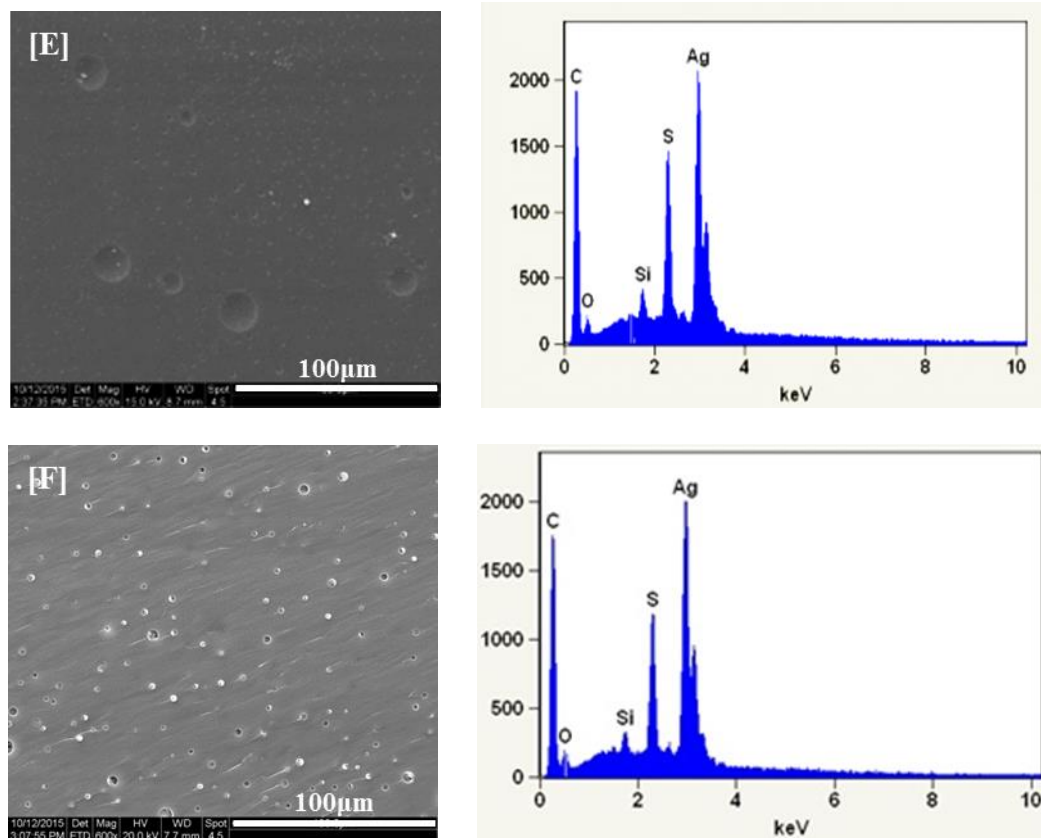
Figure 36. SEM-EDX of hybrid network with prereaction at 150°C: [E] surface, [F] bulk.

This was evidence that migration of POSS to the surface decreased sharply with increased prereaction temperature. This was likely because, at a higher temperature, the formation of extended epoxy molecules effect on POSS reactivity to form adducts. It provided additional sites for POSS to react because of hydrogen bonding between the hydroxyl group and epoxide oxygen, resulting in more POSS molecules bound as pendant into the network. The elemental analysis of the air-exposed surface and bulk for hybrid networks prepared with POSS-DGEBA precursors at varying prereaction temperature is given in Table 12. As observed, increase in prereaction temperature can stop POSS migration on the surface during curing reaction.

Table 12

SEM-EDX analysis of hybrid networks at varying prereaction temperature

Element	Amino POSS, %	100°C		120°C		150°C	
		Bulk, %	Surface, %	Bulk, %	Surface, %	Bulk, %	Surface, %
C	65.17	80.65	79.50	71.73	75.02	73.72	76.76
O	19.15	12.15	6.39	3.05	5.72	0.4	0.25
Si	12.57	0.27	10.52	0.34	2.36	0.42	1.31
S	-	1.99	0.12	3.27	2.78	3.72	3.67
Ag	3.10	4.95	3.47	21.6	14.09	21.74	18.00
Total	100	100	100		100	100	100

TEM was also utilized to image morphologies of hybrid networks with the same

loadings, prepared by POSS-DGEBA precursors at different temperatures. The images in

Figure 37 for the hybrid networks display a number of heterogeneities on the scale of

microns. Samples are not stained because good contrast arises from electron density

differences between POSS particulates and the matrix. The micron-scale dark spots could

be the oligomeric POSS-DGEBA aggregates as proposed earlier. As a consequence of

aggregation, a large fraction of POSS monomers was assumed to be trapped in domain

interiors which prevented them from being covalently tethered to the network. The

tendency of POSS to aggregate subject to steric effects would seem to be the key factor

driving phase separation. At higher prereaction temperature (Figure 37[B]) less POSS

aggregated in the bulk hybrid networks compared to networks for low prereaction

temperature (Figure 37[A]), where different sizes of aggregates and phase separation of POSS was observed. In short, there was more uniform POSS distribution with higher prereaction temperature.
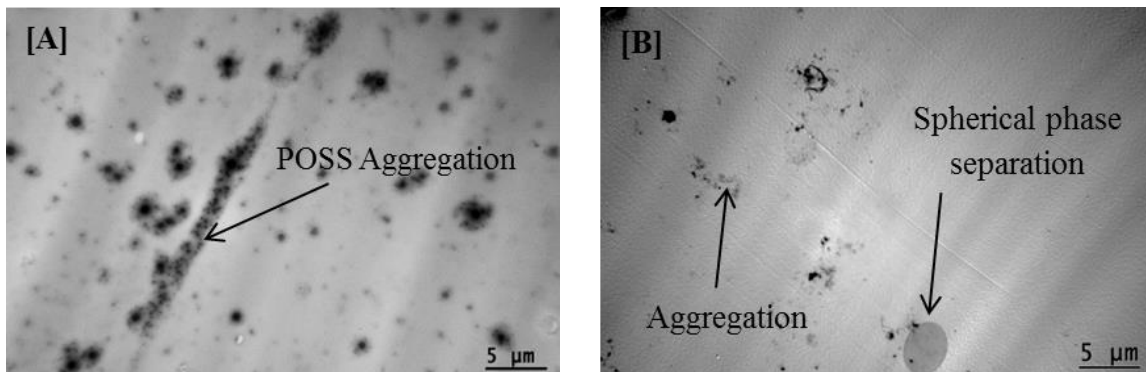
Figure 37. TEM image of hybrid networks with prereaction at [A]100°C and [B] 150°C.

Hybrid Networks with POSS-DGEBA Precursor at Varying EW DGEBA: For the same loading level, the POSS incorporation in the epoxy network was greatly improved by using a prereacted precursor with increasing DGEBA EW. As evidenced by NMR results shown in Figure 31, more POSS reacted with higher EW DGEBA monomers to form precursor. In addition, a liquid-liquid phase separation does not occur at the time of adding DDS. However, given that the phase separation is dominated by the competition between POSS-POSS interactions and cure kinetics, a secondary phase separation occurred in the epoxy-rich phase in the course of polymerization, and produce droplets of POSS domains. Figures 38-40 show droplet morphology in fractured surface of hybrid networks prepared with varying EW DGEBA monomers.
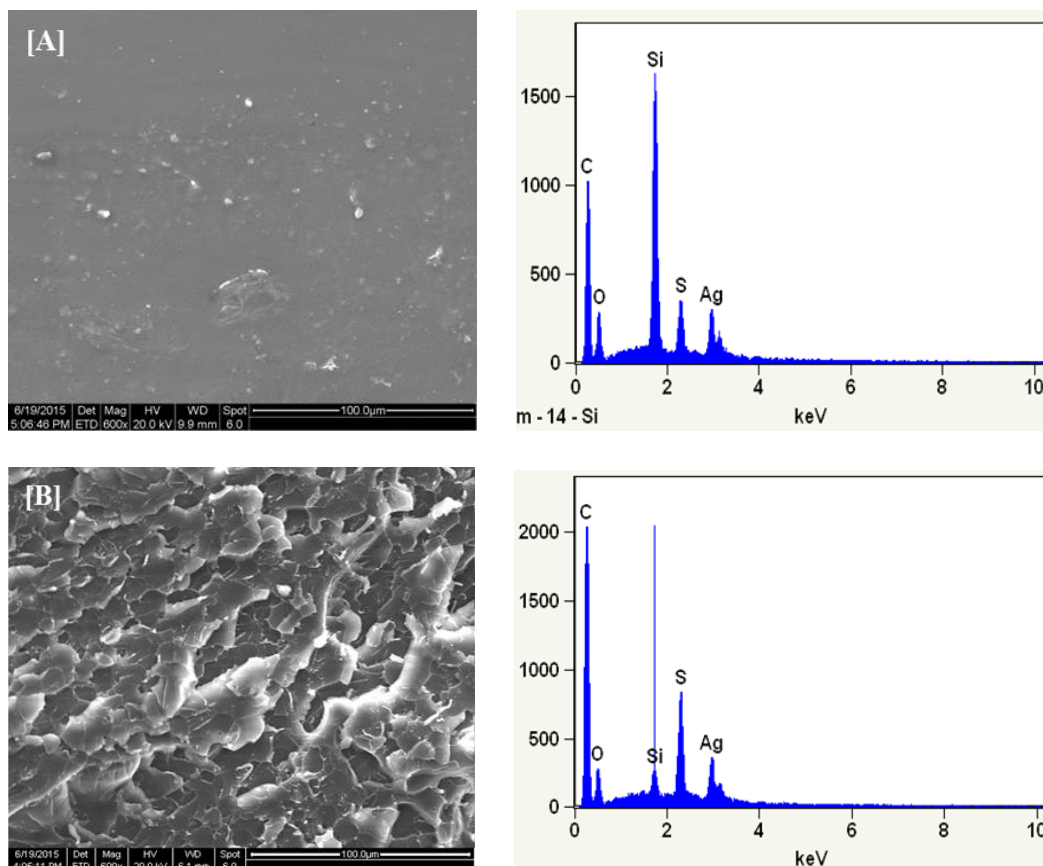
Figure 38. SEM-EDX of hybrid network with precursor at EW 177.5: [E] surface, [F] bulk.

The quantity and size of these droplets were bigger with increasing DGEBA EW; this variation can be explained by the elemental analysis of sample surface and bulk. With EW177.5, more unreacted POSS remains in the reaction mixture, this unrestricted POSS migrated to the surface due to the thermodynamic consideration as explained earlier. With increasing DGEBA EW, unreacted POSS in product mixture significantly decreased as observed by NMR. Although, a cure induced phase separation occurred but migration of bound POSS was significantly reduced. As more POSS remains in bulk, the size of droplets increased with increasing DGEBA EW.
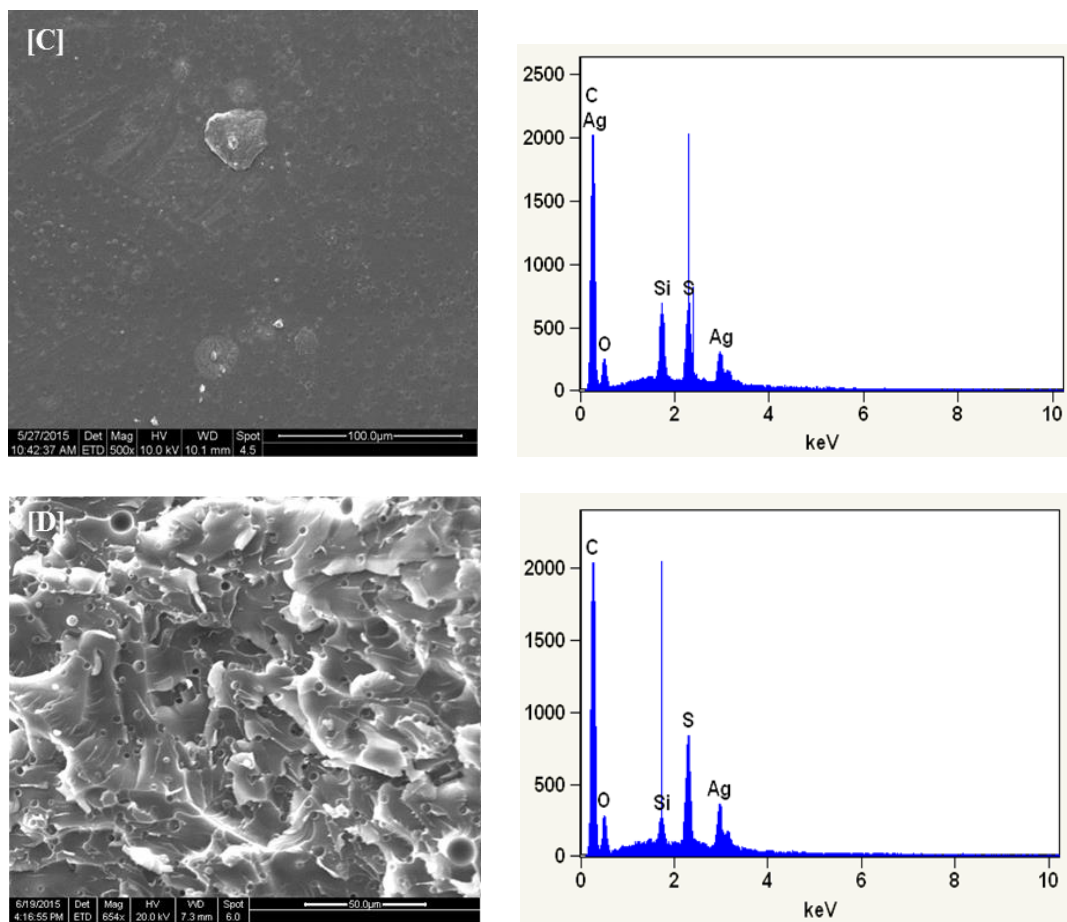
Figure 39. SEM-EDX of hybrid networks with EEW 245 precursor [E] surface, [F] bulk.

As confirmed by EDX analysis the network surface corresponding to EW177.5 contained around 7% silicon, followed by 1.51% silicon and 0.74% silicon by weight on EEW245 and EEW540 network surface respectively. In addition, the bulk samples of EEW177.5, EEW245, and EEW540 contained 0.31%, 0.44%, and 0.64 % silicon by weight, respectively
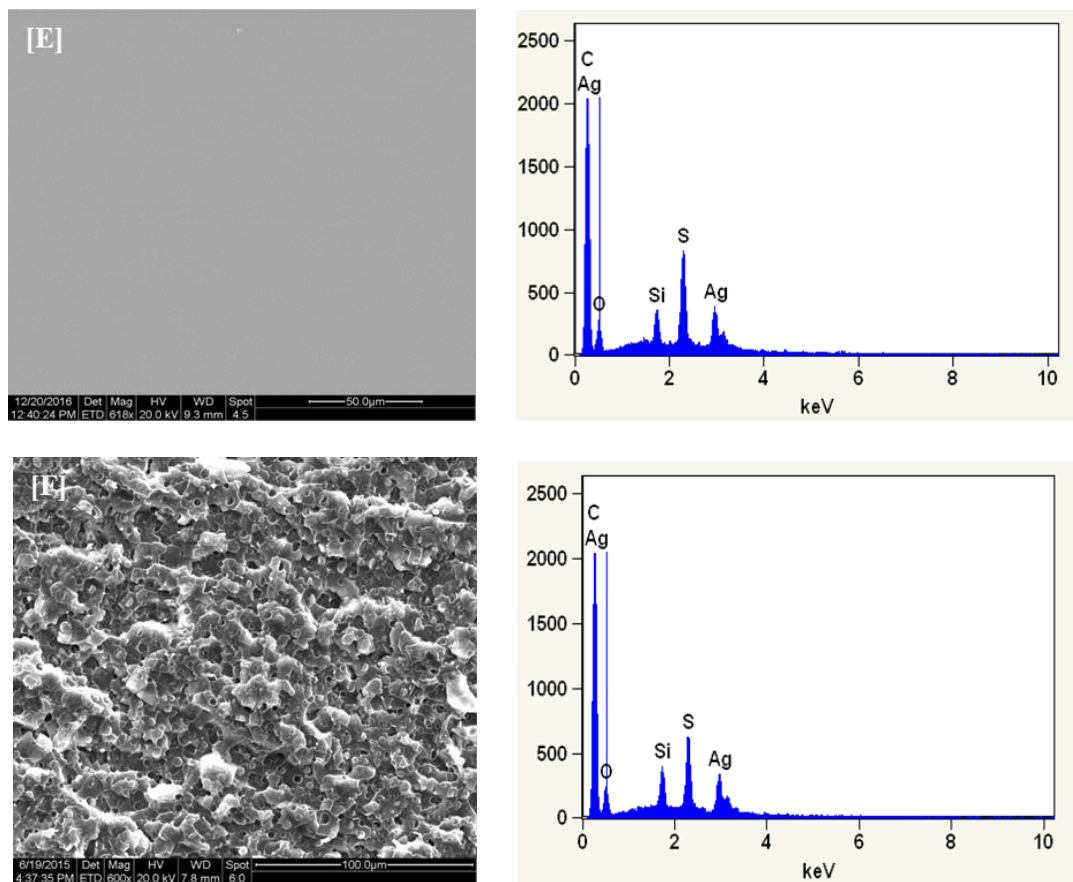
Figure 40. SEM-EDX of hybrid network with EEW 540 precursor [E] surface, [F] bulk.

Elemental analysis of air-exposed surface and bulk surface for hybrid network prepared with POSS-DGEBA precursor at varying DGEBA EW is shown in Table 13. This was evidenced that migration of POSS to the surface was sharply reduced by using precursor synthesized with higher EW DGEBA monomer. This was due to the fact that bigger epoxy molecules attached with POSS cage restricted the POSS cage mobility towards the surface, hence reduced diffusion during the reaction. However, lack of compatibility induced phase separation of POSS-rich and epoxy/amine-rich phases.

Table 13

SEM-EDX Analysis of Hybrid Networks at Varying EEW Precursors

	EEW177.5		EEW245		EEW540	
Element	Bulk, %	Surface, %	Bulk, %	Surface, %	Bulk, %	Surface, %
C	79.18	66.59	76.49	60.98	77.81	80.57
O	10.51	20.67	10.72	23.05	14.88	13.53
Si	0.31	6.69	0.44	1.51	0.64	0.74
S	2.09	1.68	2.94	6.45	1.68	1.89
Ag	7.91	4.38	9.41	8.01	5.01	3.27
Total	100	100	100	100	100	100

The TEM images of ultra-microtome and without stained treatment samples of the hybrid networks prepared with POSS-DGEBA precursor at varying EW DBEGA monomer is shown in Figure 41. On the basis of the size of dark spots consists of aggregated POSS moieties, there was a more uniform dispersion of POSS in the networks corresponding to EW540 compared to a phase separated morphology formed in the network corresponding to EW177.5 and EW245. These results also showed that it is not possible to generate a nanoscale dispersion of monofunctional POSS in a thermosetting polymer if the POSS is not functionalized with an organic group compatible with the polymer network (in our case, a possibility could be to replace the isobutyl groups by phenyl groups). The lack of compatibility induced phase separation during cure, generating different morphology in hybrid networks with varying DGEBA EW. As shown in Figure 41[A], the EW177.5 network showed bigger POSS aggregation. With

increasing EW, the samples showed droplet morphology as discussed earlier. For

EW245, the size of aggregates was small compared to EEW177.5, and the aggregates

size dramatically decreased with EEW540. As shown in Figure 41[C], a more

homogenous and continuous dispersion of POSS domains observed throughout the bulk.

POSS-rich domains are clearly isolated to each other and there was no obvious presence

of agglomeration.
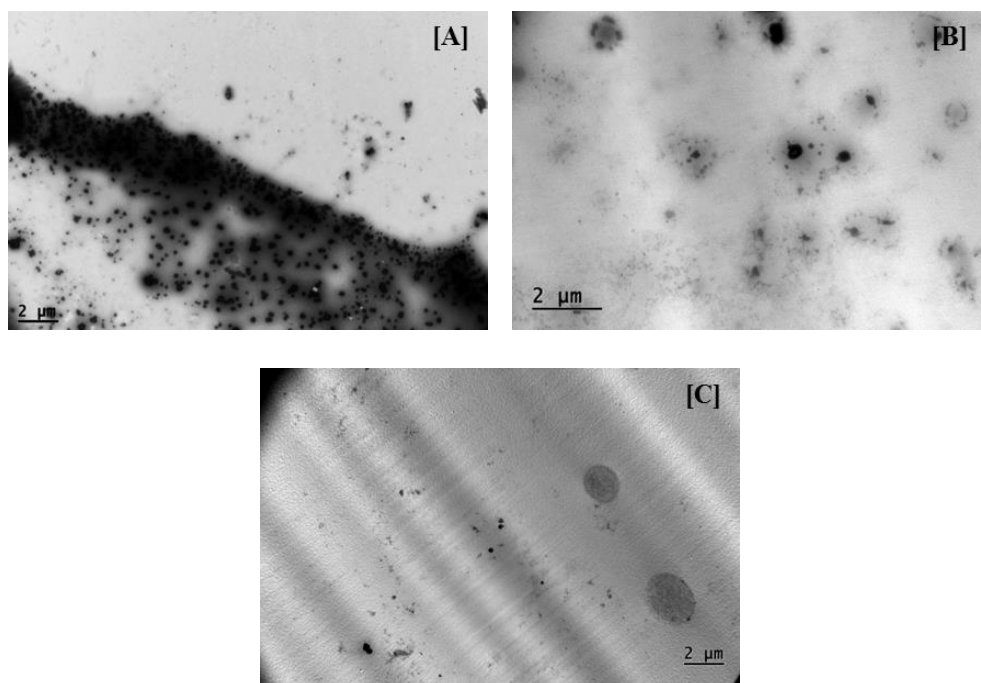
Figure 41. TEM of hybrid network corresponding to [A] EW177.5, [B] EW 245, and [C] EW 540

Thermomechanical Properties of Hybrid Networks

　　Effect of Prereaction Temperature: All of the samples tested using DMA for the

synthesized networks have 5 wt. % POSS content. The Figure 42(A) shows tan δ vs.

temperature for samples prepared by using POSS-DGEBA adducts synthesized at varying

prereaction temperatures. The α-relaxation peaks in each case are visible at high

temperature in these plots. Expanded view of the tan δ vs temperature curve at low

temperature is shown in the inset, where a β-relaxation and POSS associated relaxations at low temperature are also visible. Although, there was no significant influence on α transition caused by incorporation of POSS, however, a small shift to lower temperatures relative to the control network is observed. In addition, the α peak height increased with increasing prereaction temperature, while the peak shape remained essentially the same.

Incorporation of POSS, as adduct into epoxy, might be thought to cause a form of epoxy plasticization. More specifically, a decrease in chain packing density caused by an increase in free volume affected by the insertion of these bulky units diminished interactions between adjacent polymer chains.[116,117] However, at higher prereaction temperature, there was a more uniform dispersion of POSS in the networks compared to a phase separated morphology formed in the network prepared with low prereaction temperature. Given the strong tendency to aggregate, pendant POSS particles proceeded to form domains which are more uniformly distributed over the network. Molecular mobility is thereby restricted around POSS units resulting in a slightly higher α transition temperature as compared to that for lower prereaction temperature.

The broad β relaxation at a lower temperature is reasonably assigned to local conformational fluctuations along chain sections. The broadness of the β peak is interpreted as reflective of a broad range in microstructural heterogeneity on a local (nanoscopic) level.

In Figure 42(A), a third relaxation is visible, especially for the highest prereaction temperature, at temperatures beneath that of the β relaxation. This could possibly be the pure POSS relaxation reported by Schonhals et al.[118] According to ^{29}Si NMR results at a higher temperature, as more POSS molecules are consumed in reaction than at lower

temperature. The intensity of the pure POSS relaxation process increases with increasing

concentration of bound POSS into the network as a pendant. This is also confirmed by

SEM and TEM studies.
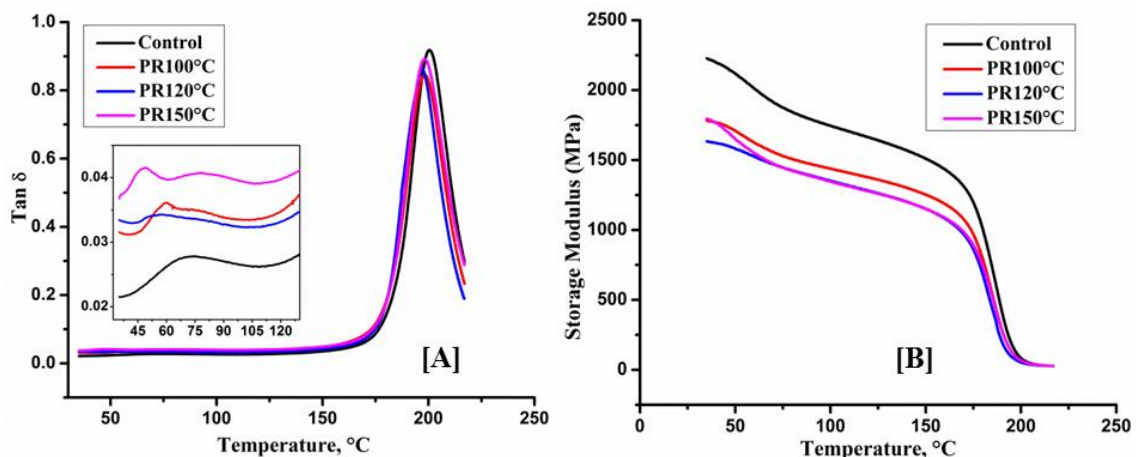
Figure 42. DMA data of hybrid networks at varying prereaction temperature:[A] Tan δ
vs. temperature (inset: expanded view of β peak over limited temperature range); [B]
dynamic storage modulus vs. temperature

The Figure 42(B) shows the corresponding storage modulus vs. temperature

curves. The curves for all three prereaction temperatures did not differ greatly and lied

beneath that of the control network. The most precipitous drop at high temperature,

somewhat over three orders of magnitude, was concurrent with the onset of α relaxation.

The inflection points correspond to the β transition.

Effect of EEW: The thermomechanical behavior of hybrid networks prepared with

varying EW DGEBA monomers is shown in Figure 43. As confirmed by SEM and TEM

studies that POSS existed in a variety of dispersion states, which gave rise to a variety of

POSS-matrix interactions with varying EW DGEBA. The glass transition temperature,

characterized by the position of the maximum of tan δ, was surprisingly not significantly

affected by the presence of POSS in the networks. However, a reduction and slightly

broadening in α relaxation peaks in hybrid networks corresponding to higher EW implied

a diminishing fraction of free epoxy network chains due to POSS-network chain

interaction. A secondary phase separation occurred in the epoxy-rich phase in the course

of polymerization and produced droplet POSS domains in the hybrid network

corresponding to higher EW, which was also observed in SEM. DMA results for EW 540

network also confirmed a phase separated morphology. Two peaks appeared at the tan δ

vs temperature curve as shown in Figure 43[A]. The one at the temperature of c.a 200°C

corresponded to the glass transition temperature of epoxy-rich phase whereas the other

one at around 80°C corresponds to the glass transition of POSS-rich phase. However, at

EEW 245, the peak was not significantly visible. The glassy storage modulus of the

hybrid networks decreased with increasing epoxy EW. These variations in storage

modulus are shown in Figure 43[B] may be attributed to the complex effects of a

decrease in crosslink density due to the presence of higher EEW epoxies in the network

and the inherent influence of POSS domains. The POSS domains contribute by a large

free volume and do not display any strong interactions with the polymer chains of the

network as having seen in SEM images.
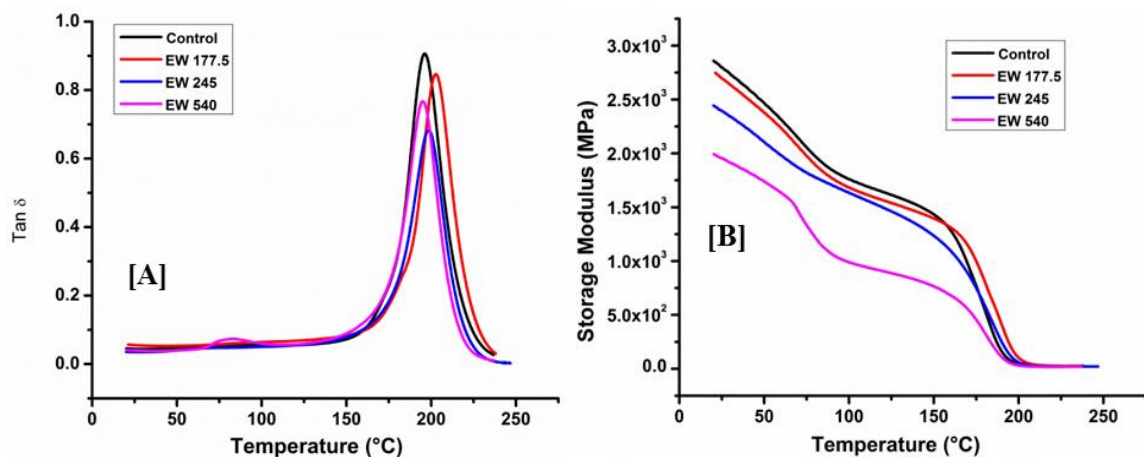
Figure 43. DMA of hybrid networks with precursors at varying EEW: [A] Tan δ vs. temperature; [B] dynamic storage modulus vs. temperature.

Conclusion

POSS- DGEBA precursors were synthesized at varying prereaction temperatures and varying DGEBA EW, to study the reaction kinetics and morphology of final networks prepared by these precursors. Dielectric and NMR studies at varying prereaction temperature confirmed that during the reaction, the mobility of bulky POSS molecules became more difficult and the reaction was controlled by diffusion such that full conversion of amino POSS not achieved. At higher prereaction temperature, more conversion of amino POSS was observed and it was concluded from SEC data that formation of extended epoxy molecules drives the reaction by reducing diffusion or by catalyzing the reaction by hydroxyl groups formed during extended epoxy molecule formation. A similar observation with increasing DGEBA EW also confirms this suggestion. Temperature dependent kinetic parameters for prereaction were determined by fitting ^{29}Si data into the Kamal & Sourour model expanded by a diffusion factor. The fitting of the kinetic model to experimental data agreed very well over the entire

83

conversion range. The behavior of prereaction between amine functionalized POSS and epoxy is the same as that for a neat epoxy-amine system.

SEM-EDX and TEM indicate that migration of POSS to the surface was reduced with increased prereaction temperature and DGEBA EW. At lower prereaction temperatures, phase separation was observed in the final network, which changed to more uniform and continuous POSS-rich phase distribution with increased prereaction temperature and DGEBA EW.DMA results showed that incorporation of POSS at 5 wt. % caused a slight reduction in glass transition temperature compared to non-POSS networks. While the tan δ peak height decreased with increased prereaction temperature, the peak shape remained essentially the same suggesting little change in the degree of microstructural heterogeneity on the scale of this relaxation. On the other hand, with increased DGEBA EW, the peak height was also reduced, however, a slight peak broadening was observed. This indicated the heterogeneity in the network structure. Storage modulus vs. temperature curves for all network studied did not differ greatly among themselves but lied beneath that of the non-pre-reacted control. More heterogeneity in crosslink density was evidenced in higher DGEBA EW.

CHAPTER IV – DEVELOPMENT OF CONTINUOUS REACTOR PROCESS FOR

POSS-DGEBA PRECURSOR SYNTHESIS: CHARACTERIZATION AND

NETWORK STRUCTURE-MORPHOLOGY

Abstract

In the previous chapter, reaction kinetics of the prereaction and effect of DGEBA EW on POSS conversion were studied in a batch process. Migration of POSS on the surface, phase morphologies, and resulting thermomechanical properties were correlated with the chemical composition. In spite of the fact that prereaction between higher EW DGEBA monomer and POSS demonstrate good conversion, DGEBA (EW177.5) monomer is a preferred choice for the synthesis of POSS-DGEBA precursors due to processing feasibility. This chapter describes a high shear continuous reactor method to synthesize POSS-DGEBA precursor with the aim of incorporating pendant POSS into epoxy networks at the molecular level and fabricate transparent nanocomposites. As evident, by using the continuous reactor, full conversion of POSS into precursor was achieved in less than a minute compared to several hours in a batch process. The structure of this precursor at the end of the reaction was determined to be close to ideal one by ^{29}Si NMR spectroscopy. The molecular weight distribution of reaction product was determined by SEC. The results confirmed that the use of high shear mixing provide excellent heat transfer, and can greatly increase the efficiency of POSS and DGEBA prereaction for the synthesis of POSS-DGEBA precursors while enhancing system entropy. Hybrid networks were prepared to contain up to 50 wt. % POSS by curing these precursors with DDS and DDM. In addition, SEM and TEM were employed to confirm the cured network morphologies for resulting networks.

Results and Discussion

Synthesis and Structure of POSS-DGEBA Precursor in Continuous Reactor

Although POSS has been reportedly reacting with DGEBA monomers in a batch process in order to synthesize POSS-DGEBA precursor, however, the batch process has been unable to achieve a full conversion of POSS into POSS-DGEBA precursor even after 18 hour reaction time at 150°C. A high shear continuous reactor method developed in this work was able to synthesize POSS-DGEBA precursor with greater efficiency. The final conversion of POSS into POSS-DGEBA precursor and molecular weight distribution of precursor formed during the reaction in the continuous reactor were studied similarly using ^{29}Si NMR and SEC, as discussed in chapter III. In order to develop a continuous reactor method for prereaction, 1:3-mol ratio of POSS: DGEBA was maintained in a high shear continuous reactor, as described in Chapter II.

Impact of Screw Speed and Reaction Temperature on Conversion: It is expected as screw speed increases the volumetric flow augments, and the residence time decrease, which should lead to a decrease in conversion; however, in this case, higher screw speed results in more conversion. This fact can be explained by the increase in effective shear energy with screw speed in the continuous reactor. The high shear continuous reactor used in this work was based on intermeshing co-rotating twin screws and was good for converting input power into hydrodynamic shear force. The reactor was efficient enough to mix immiscible phases such as DGEBA and POSS. By increasing screw speed at a fixed reaction temperature (200°C), a more hydrodynamic shear force is generated, which acts to break the POSS aggregates to a reduced size. Since there are no large aggregates and the volumes are very low in a continuous reactor, the POSS mixing with the DGEBA

is favorable. High mixing, low reactant volume and high collision frequency between reactant molecules in the continuous reactor could result in more conversion. According to the experimental results, there is a significant amount of unreacted POSS present in the reaction mixture at 100 rpm screw speed. Although the residence time is greater than one minute at this speed, there is not enough shear force to break all the POSS aggregates and drive the reaction. As screw speed increases, more conversion is achieved, which is evident that higher speed creates more shear energy to break the aggregates.

Shown in Figure 44 are the ^{29}Si peaks of the POSS-DGEBA precursors at different screw speeds. As expected, the peak corresponding to atom "1" (-67.3 ppm) shifted upfield. The appearance of two new peaks at -67.42 ppm and -67.55 ppm during the reaction are corresponding to silicon atom '1' bonded with a secondary and tertiary amine, respectively, as the bond polarity of the N-C bond is lower than that of N-H. These peak regions were integrated and the integral values were converted to moles in order to determine the concentrations of POSS molecules with primary, secondary, and tertiary amine functionalities. Based on the peak integration it is evident that nearly 20 wt.% of POSS remains unreacted in the product mixture at a screw speed of 100 rpm, whereas unreacted POSS concentration in product mixture is nearly 8 wt% at a screw speed of 200 rpm. At higher screw speeds, 300 and 400 rpm, no unreacted POSS was noticed by ^{29}Si NMR. Also, as can be seen from NMR spectra for product mixtures at different screw speeds, it is evident that formation of amine terminated POSS-DGEBA precursor is also higher at lower screw speeds. The concentration of such precursor reduces with increased screw speed, which is due to the fact that at higher screw speed volumetric flow rate also increases (residence time at 300 rpm- 50 s, and at 400 rpm- 35

s), which further reduces the reactant volume in the continuous reactor and hence further increases collision frequency between reactant molecules which could further drive the reaction.
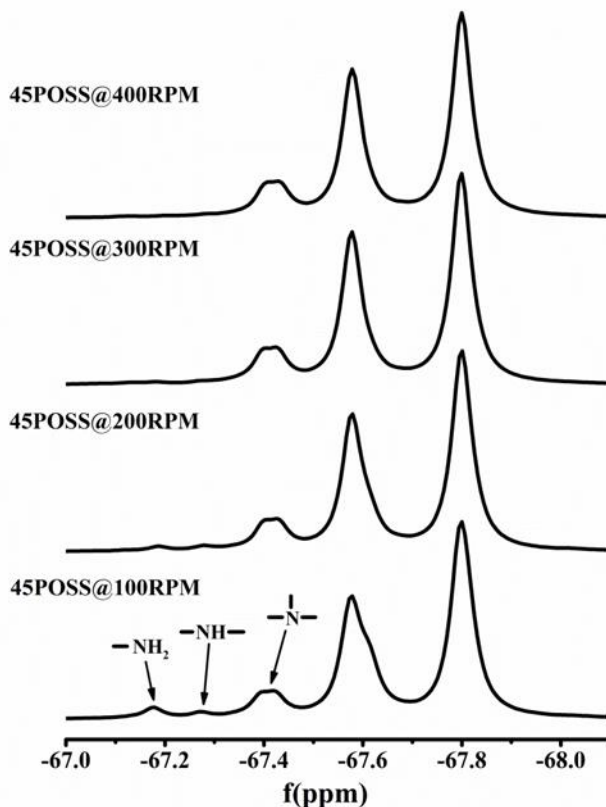
Figure 44. ^{29}Si NMR spectra of 45POSS with screw speeds (200°C)

A qualitative observation of molecular weight distribution of product mixture was shown in Figure 45, it can be seen that the DGEBA peak height at 17.35 min decreased with screw speed and at the same time height of peaks corresponding to the different molecular weight POSS-DGEBA precursors increase as we increase screw speed. Another important feature of SEC data is the peak observed at 15.85 min, this peak represents a combined peak for extended DGEBA monomer and monoamine functional POSS used in this study. As seen, a decrease in peak height at 15.85 min confirms that

unreacted POSS content in product mixture decreases with increasing screw speed, which

eventually supports the results obtained from NMR experiment. However, at a screw

speed of 400 rpm, a very short residence time lead to a slight increase in unreacted POSS

compared to 300 rpm. This concludes that for maximum conversion, an optimum screw

speed is between 300and 400 rpm.
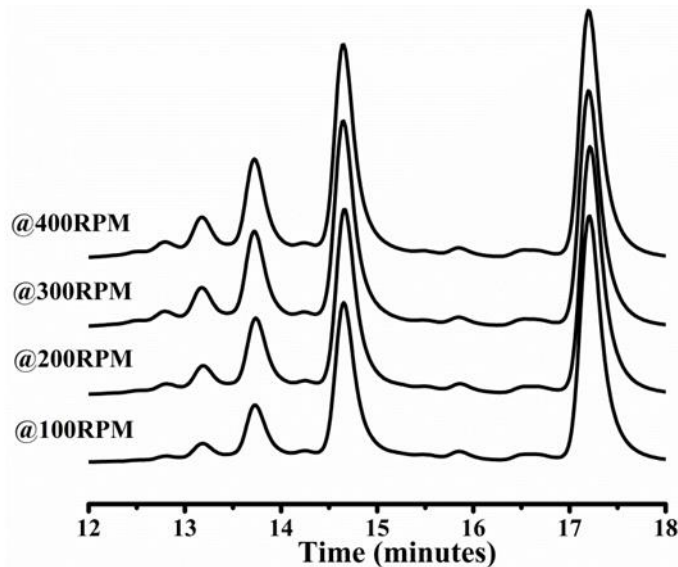
Figure 45. SEC spectra of 45POSS with screw speeds (200°C)

A similar approach was used to study the effect of reaction temperature on

conversion at a fixed 200 rpm screw speed. At a constant residence time and a constant

volumetric flow rate of the reaction mixture, the reaction conversion in the final product

was studied with respect to temperature. The reaction temperatures between 150 °C and

240 °C were studied in this study. Figure 46 shows the ^{29}Si NMR spectra of product

mixtures at various temperatures; here we see a more significant impact on conversion

with respect to reaction temperature. As observed, at 150 °C reaction temperature there

was almost 80 wt.% unreacted POSS present in product mixture, which eventually

decreased to 50 wt.% at 180 °C and 10 wt. % at 200 °C. At temperature 220 °C, there

was no unreacted POSS observed in product mixture; however, less than 10 wt % amine terminated POSS-DGEBA was observed. At temperature 240 °C, essentially complete conversion of POSS into POSS-DGEBA precursors was observed. A similar trend was observed in SEC data also in Figure 47: the peak heights corresponding to POSS-DGEBA adduct increased with greater rate till 200 °C, and thereafter it increased at a slower rate. As previously discussed, the decrease in peak intensity corresponding to unreacted POSS also confirmed the effect of reaction temperature on conversion. These results are in great agreement with the ^{29}Si NMR results to study conversion. The effect of reaction temperature on monoamine functional POSS conversion into POSS-epoxy precursor is due to the very well-known fact that epoxy-amine reactions are exothermic and the reaction proceeds faster as the temperature increase. In this case particularly when the reaction proceeds under high shear and low volumes with the assistance of greater efficacy in heat transfer provided by a continuous reactor, a more efficient reaction is evident with respect to the reaction temperature.

Since both screw speed and reaction temperature affect the conversion of this pre-reaction in a continuous reactor, an optimized screw speed and reaction temperature were used to develop a continuous reactor process for 100% conversion. Based on the observations of screw speed effects and temperature impact on conversion, a continuous high shear reactor method was developed to successfully synthesize POSS-DGEBA precursors in 30-40 s at a reaction temperature of 220 °C throughout the screws length and with a screw speed of 350 rpm.
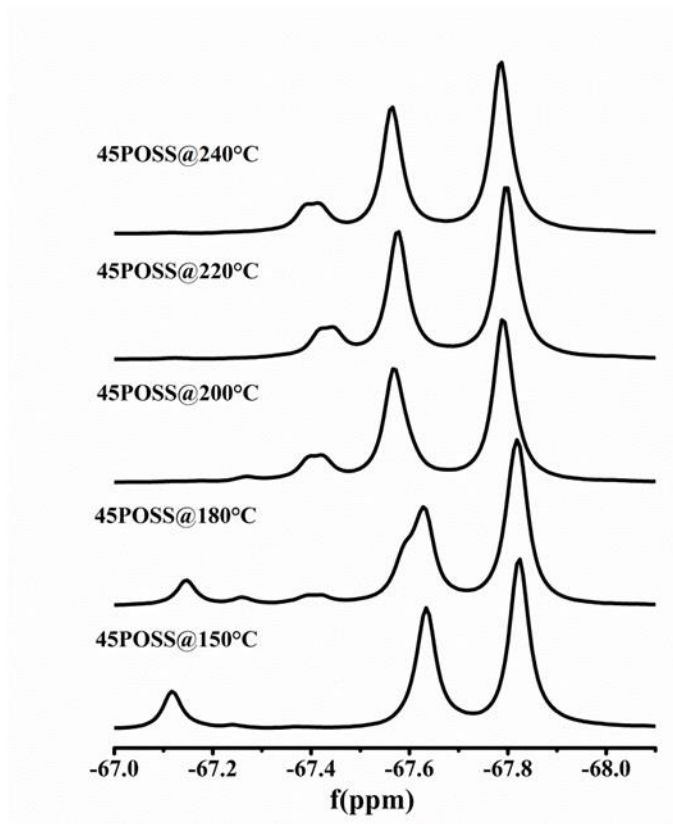
Figure 46. ^{29}Si NMR spectra of 45POSS with temperatures (200RPM)

Elimination of any post-processing method and any solvent in this method is an added advantage of using a continuous reactor process for the synthesis of POSS-DGEBA precursors. Furthermore, the final product demonstrated complete conversion of POSS into POSS-DGEBA precursor for all the molar compositions, which is as discussed, the result of excellent heat transfer efficiency and ultra-high collision frequency of reactant molecules in a high shear continuous reactor.
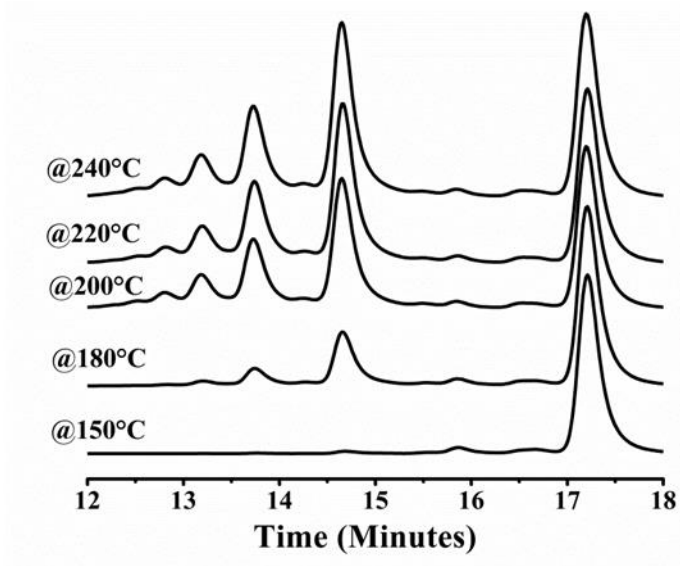
Figure 47. SEC spectra of 45POSS with temperatures (200 rpm)

Comparison between Continuous Reactor and Batch Reactor: Figure 48 shows a comparison of 29Si NMR spectra of the product mixtures in a batch reactor at 100 °C, 150 °C and in a continuous reactor. It was observed that in a batch reaction at 100 °C, there was over 40% un-reacted POSS remaining in the product mixture. At 150 °C, above 20% un-reacted, POSS remained in the product mixture. Reaction temperature higher than 150 °C in a batch reaction can lead to possible side reactions, such as homopolymerization of epoxy, etherification between neighboring epoxides and hydroxyls, cyclization and side transformation reactions. The homopolymerization and etherification are observed with an excess of epoxides, at high temperature and in presence of a base.[106] Whereas, in a continuous reactor there is no such side reaction observed at high temperature.
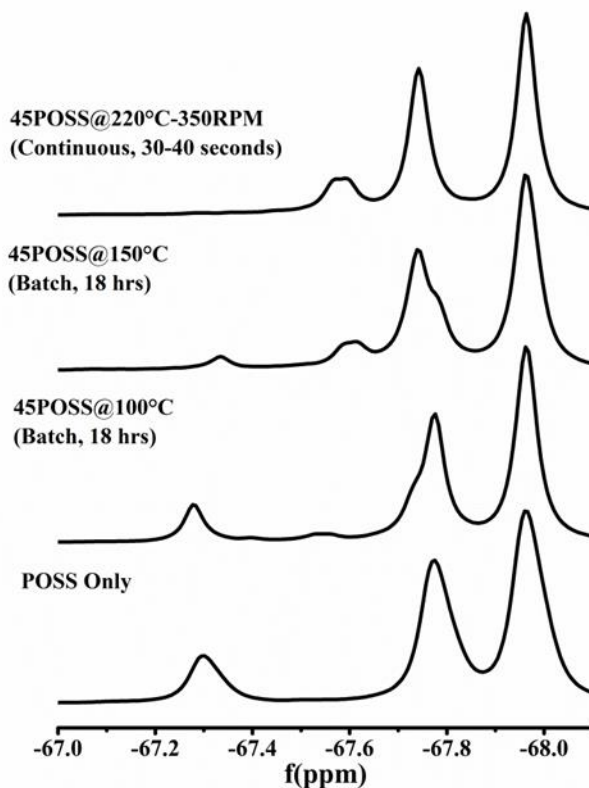
Figure 48. Comparison of ^{29}Si NMR spectra- batch vs. continuous reactor.

It is worth noting a significant advantage for the high-shear continuous reactor process over the batch process is associated with the ability to increase reaction temperature and reduce reaction time in a manner which drives the desired reaction while minimizing side reactions. In a continuous reactor, POSS completely reacted within 30-40 s as compared to 18 h to react less than 60% at 100 °C and less than 80% at 150 °C in a batch reactor. As observed, the disappearance of the peak at -67.3 ppm in product mixture confirms a complete conversion in a continuous reactor process to synthesize POSS-DGEBA precursor.

This was followed by SEC to determine the evolution of precursor molar mass distribution. The SEC chromatogram in Figure 49 demonstrates a comparison between

POSS-DGEBA precursor molar mass distributions in a batch and a continuous reactor.
As seen, peaks representing the formation of POSS-DGEBA trimer, pentamer, and so on,
are much more defined in continuous reactor compared to a batch reactor.
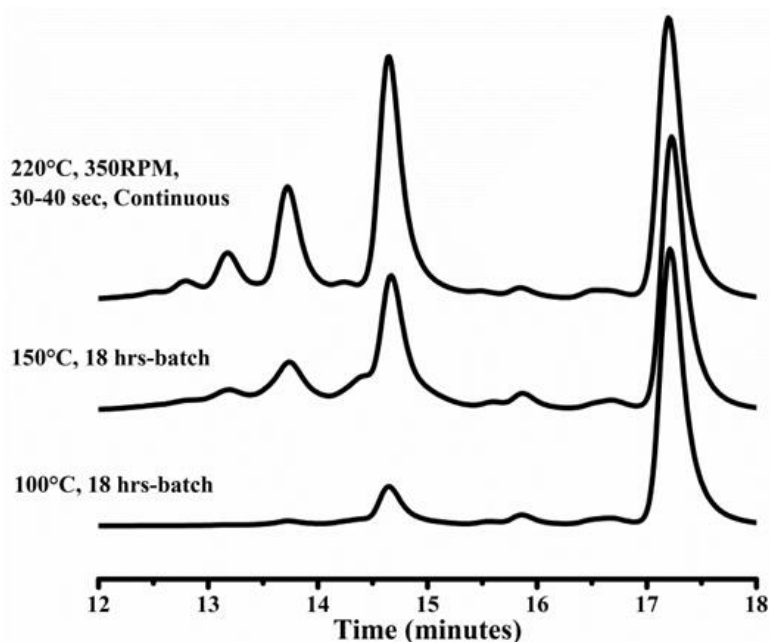
Figure 49. Comparison of SEC record- batch vs. continuous reactor.

It was also observed that in a batch reactor at 150 °C, the fraction of higher
molecular weight precursors was higher, but the peaks were not clearly defined. This
could be because of the formation of extended epoxy molecules through
homopolymerization during the reaction at a higher temperature. More defined formation
of trimer was observed at a low reaction temperature (100 °C) in batch; however, the
peak intensity of unreacted DGEBA is much higher compared to another process which
suggested more unreacted POSS in product mixture, this was also confirmed by [29]Si
NMR experiment.

Formation of POSS-DGEBA Precursors with Varying Composition: POSS was
reacted with DGEBA in a high shear continuous reactor at varying weight percentages

94

from 1.75 to 70 wt. % (or 1:140 to 1:1.05-mol ratio). The product of the reaction was characterized via SEC and ^{29}Si NMR for molar mass distribution and POSS conversion during the reaction as describe previously. The reactant feed rates for the synthesis of POSS-DGEBA precursor in a continuous reactor were discussed in chapter II (Table 3).

SEC results shown in Figure 50 confirm that the primary product of the reaction was a 'DGEBA-POSS-DGEBA' trimer molecule until 45 wt. % (1:3-mol ratio of POSS: DGEBA) of POSS in the reaction mixture. As POSS content increased, the concentration of trimer molecule in the product mixture decreased while the concentration of higher molecular weight adduct increased. At 54 wt. % and 70 wt. % (1:2, and 1:1.05-mol ratio), the majority of the product were higher molecular weight precursors. Interestingly, the work reported by Matejka et al. also confirmed that 1:3-mol ratio was an optimum composition of POSS: DGEBA for in the synthesis of sufficient content of POSS precursor in a batch process.[77]
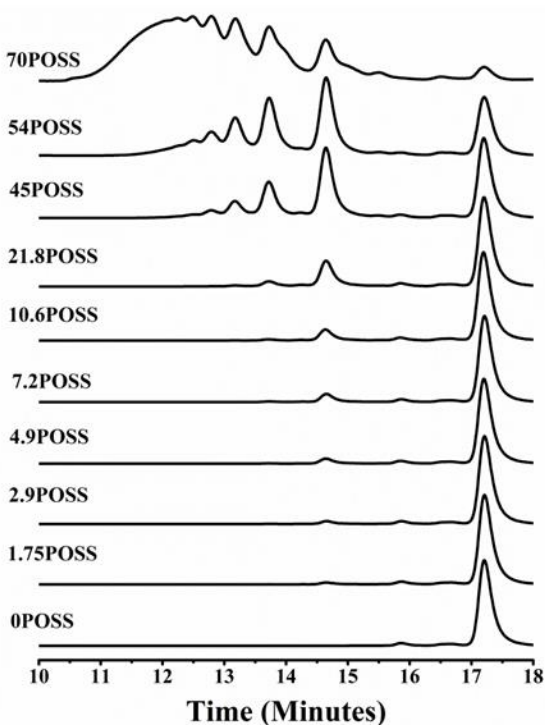
Figure 50. SEC record of POSS-DGEBA precursor prepared in a continuous reactor

The final conversion of POSS into precursor with varying POSS content in a

continuous reactor was determined by ^{29}Si NMR spectra, as described previously. It was

observed in Figure 51 that the peak at -67.3 ppm completely disappeared after reaction in

a continuous reactor. Also, other than the 70 wt. % (or 1:1.05-mol ratio) case there was

no amine terminated POSS-DGEBA precursor observed in ^{29}Si NMR spectra for all

compositions of POSS. At 70 wt. %, only 8% amine terminated POSS-DGEBA precursor

was present in the product mixture, which is due to the stoichiometric balance of epoxide

and active hydrogen at 70 wt. % POSS loading. For all other POSS contents, where

epoxy was in excess, the only peak observed after reaction in a continuous reactor was

silicon atom peak attached with a tertiary amine, which confirmed complete conversion

of POSS. At very low POSS content, the peaks were not clearly visible because of the

low concentration effect.

96
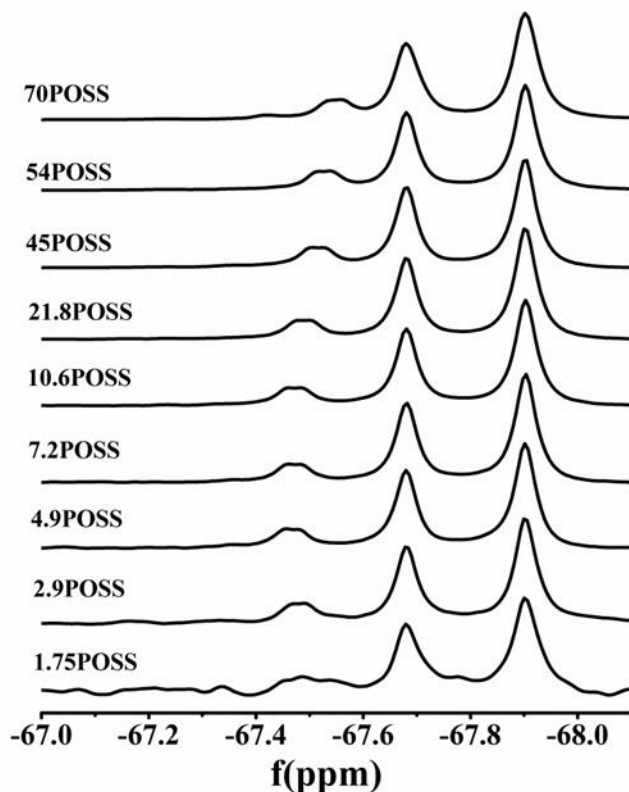
Figure 51. ^{29}Si NMR data of POSS-DGEBA precursors prepared in a continuous reactor

The physical state of the POSS-DGEBA precursors synthesized in a continuous reactor with varying POSS contents varies from liquid to solid at ambient conditions. DSC was used to determine the effect of POSS addition on the melting and crystallization behavior of these precursors. Shown in Figure 52, at low POSS contents (less than 5 wt. %) the crystalline and melting behavior of precursor follows DGEBA monomer, indicating the addition of low POSS content did not affect the crystalline structure of the POSS-DGEBA precursor. For higher POSS contents, the crystalline content increased, suggesting that the POSS molecules possibly acted as nucleating agents. An increase in the melting temperature of POSS-DGEBA precursor confirmed the presence of the POSS crystalline domains in POSS-DGEBA precursor. As observed in Figure 52(a), a small melting shoulder appears at ca. 65 °C for adduct with POSS contents of 7.2 - 10.6 wt. %.

97

Melting temperature further increased with POSS content as sharp melting peaks are observed at 75 °C, 88 °C, 97 °C, and 125 °C for precursors with 21.8, 45, 54, and 70 wt. % POSS contents, respectively.
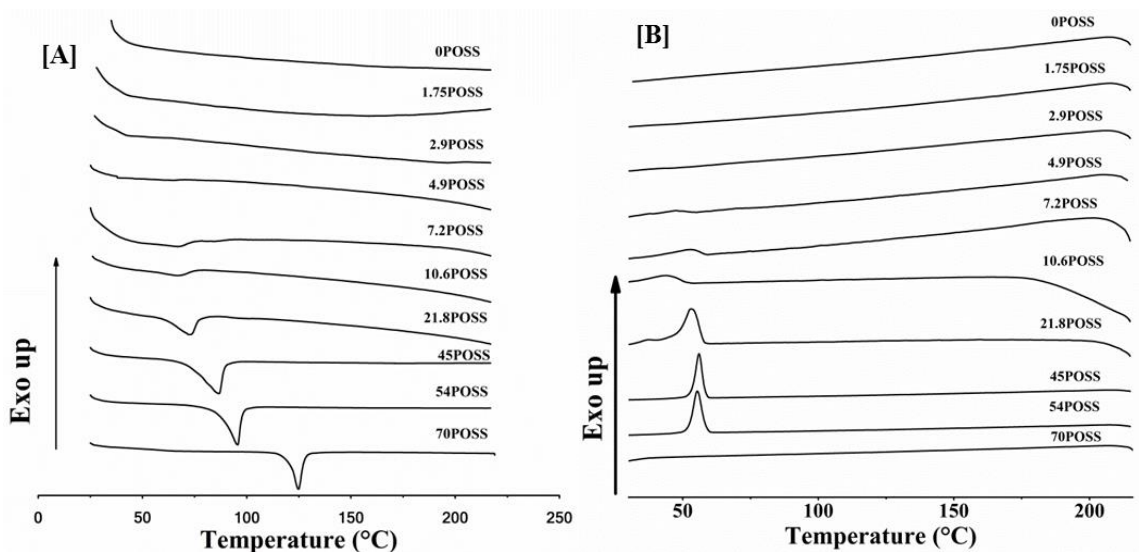
Figure 52. [A] Melting and [B] Crystallization temperature of POSS-DGEBA precursors

Morphology of POSS-containing Hybrid Composites Cured by Aromatic Amine

Curatives

The miscibility of POSS in the epoxy monomer is the biggest challenge in order to prepare the POSS-based hybrid composites. Continuous reactor method greatly improved the miscibility of POSS cage as pendant unit into the epoxy monomer. The miscibility of amine curative in POSS-DGEBA precursor is also important in order to prepare epoxy hybrid network. It was observed that mixtures of POSS-DGEBA precursor with DDS or DDM were a transparent solution, which suggested that the DDS or DDM are miscible in synthesized POSS-DGEBA precursor. The transparent mixtures were cured under the conditions described in chapter II. The composition of the epoxy hybrid

network formulated by using POSS-DGEBA precursor and aromatic curing agent were described in experimental section (Table 8 & 9).

DGEBA-POSS-DDS Networks: Fractured surfaces of DGEBA-POSS-DDS networks were observed by SEM, as shown in Figure 53. In all images presented here, droplet morphology was observed. Spherical globules corresponding to POSS-rich domain were dispersed uniformly in bulk networks as observed in SEM micrographs. The size of these globules increased with increasing POSS content into the hybrid network, it varied from a few microns to around 20 microns with increasing POSS contents up to 10.6POSS-DDS hybrid networks. Further increase in POSS content was unable to form an integrated network. A layered phase separation was observed in hybrid networks corresponding to 21.8POSS-DDS, 45POSS-DDS, and 54POSS-DDS.
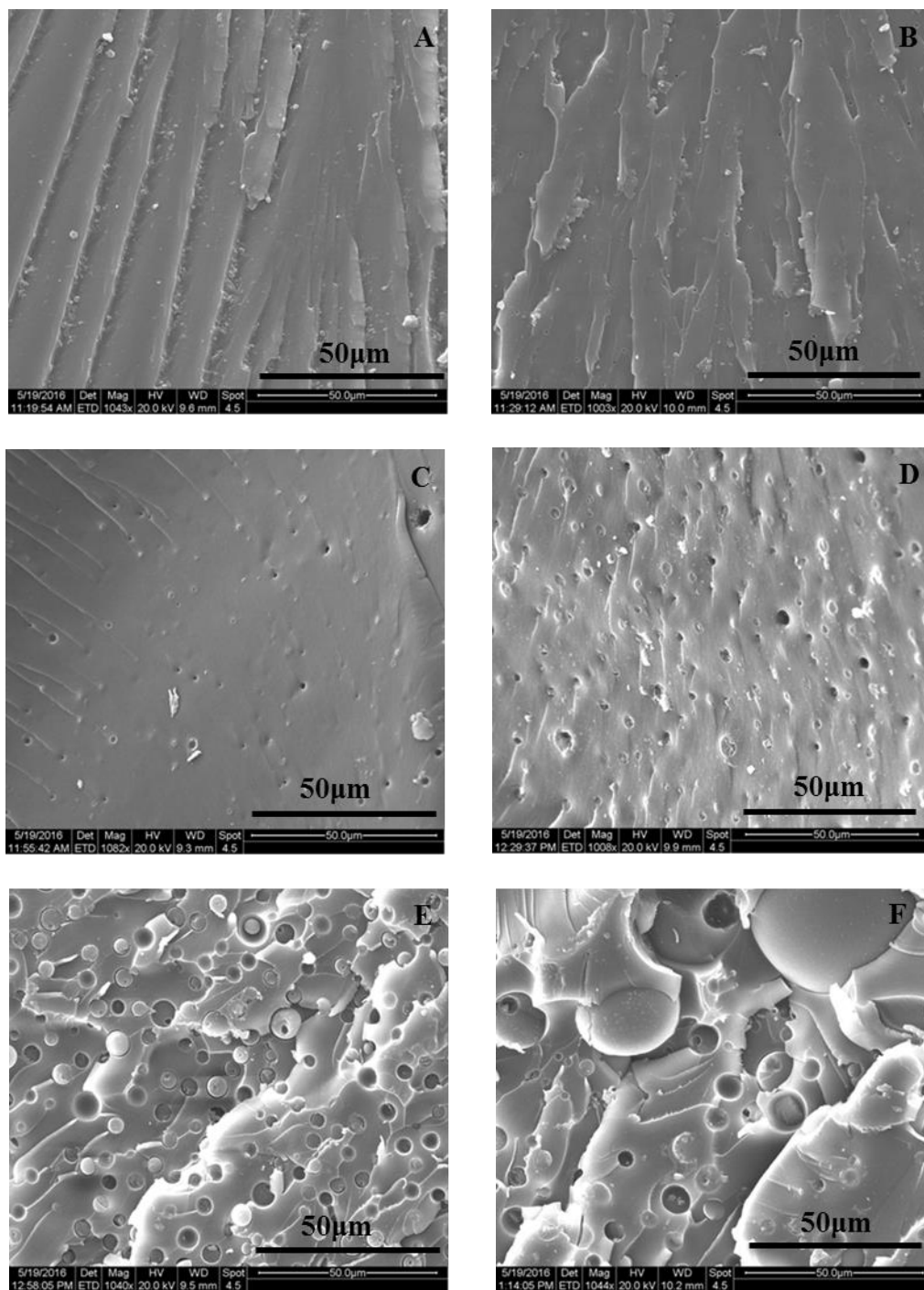
Figure 53. SEM images of hybrid networks corresponding to [A] 0, [B] 1.75, [C] 2.9, [D] 4.9, [E] 7.2, and [F] 10.6POSS-DDS

Variation in droplet size and formation of layered phase separated morphology

resulted from the polymerization induced phase separation as also observed previously

with DDS curative. Interestingly, these phase-separated domains or layered phase had a very weak interphase, which was attributed to poor compatibility between isobutyl groups and the DGEBA-DDS polymer matrix.

The morphology of hybrid networks cured by DDS curative was also seen in TEM images. As observed in Figure 54, the size of POSS domains in 10.6POSS-DDS network were around 10 microns compared to 1-5 microns for 4.9POSS-DDS. However, in comparison to POSS-DGEBA-DDS network containing 5wt. % POSS prepared by prereacted precursor in a batch reaction (discussed in the previous chapter), more POSS was incorporated into the network. This could be due to the fact that there is no unreacted POSS into the system compared to a batch process where unreacted POSS was evident after prereaction.
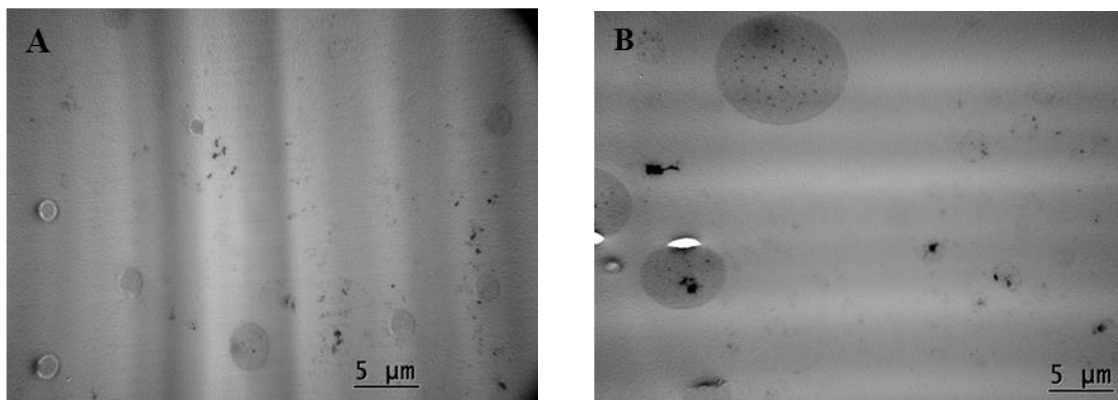
Figure 54. TEM micrographs for epoxy-POSS-DDS networks containing [A] 4.9POSS-DDS and [B] 10.6POSS-DDS

Epoxy-POSS-DDM Networks: DGEBA-POSS-DDM networks show good miscibility. Unlike DDS systems, DDM based network does not show secondary phase separation. It was observed that all the hybrids containing POSS at various concentration (0–50 wt. %) are transparent (Figure 55), which indicated molecular level dispersion or homogeneously dispersed POSS domains having domain size less than the average

wavelength of the visible light in the epoxy matrix. The micro-features of the fractured

surface of hybrid networks containing POSS were investigated by SEM. Shown in Figure

56 are the SEM micrographs of the fracture surfaces of the control epoxy, and epoxy

hybrid networks corresponding to 7.2POSS, 21.8POSS, and 54POSS. As observed, the

POSS-containing hybrid networks exhibited similar homogeneous morphology as the

control epoxy network with no POSS, and no distinguishable POSS aggregates were

visible in SEM micrographs of hybrid networks over the total range of POSS

concentrations.
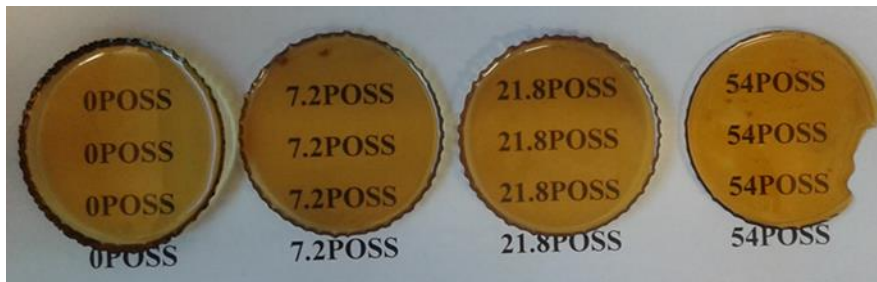
Figure 55. Hybrid network corresponding to 0POSS, 7.2POSS, 21.8POSS, and 54POSS, illustrating optically transparent hybrid networks.
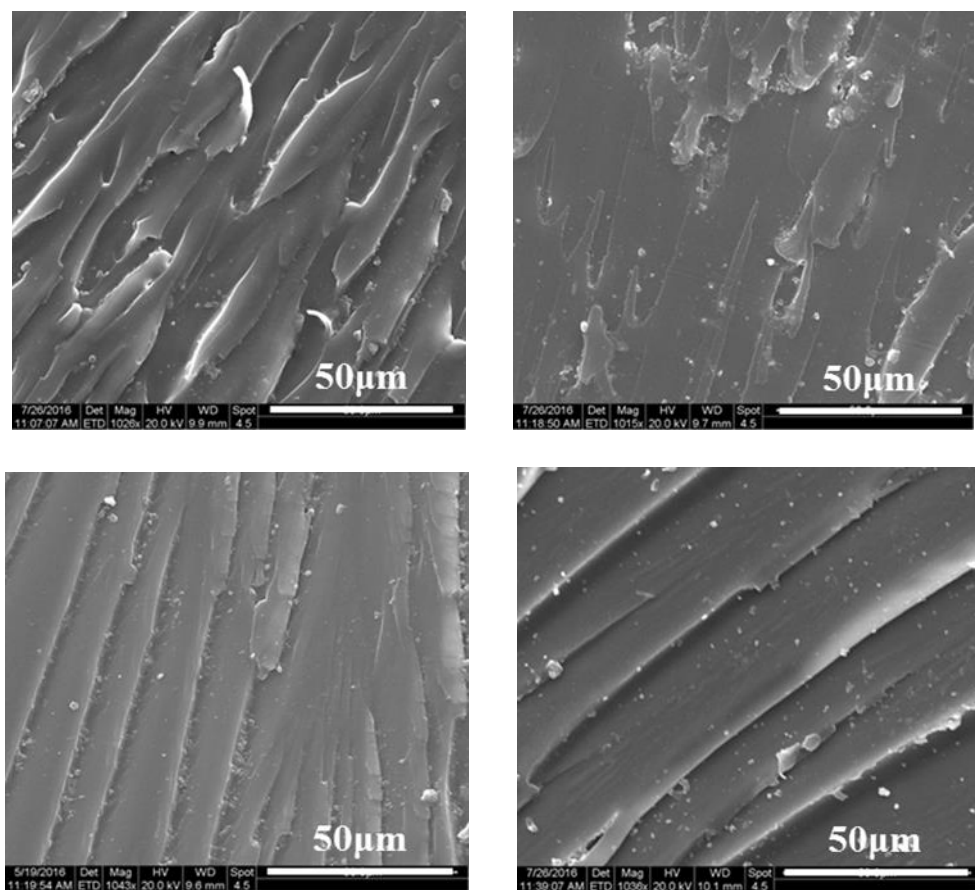
Figure 56. SEM micrographs of hybrid networks: [A] 0POSS; [B] 7.2POSS; [C] 21.8POSS; [D] 54POSS

The morphology of the epoxy hybrid networks containing POSS was further investigated by transmission electron microscopy (TEM) in order to better understand the nanoscale dispersion of pendant POSS. Figure 57 shows the TEM micrographs of hybrid epoxies corresponding to 21.8POSS and 54POSS contents. The TEM images of the POSS-containing epoxy networks showed indistinguishable morphologies of epoxy hybrid networks and no phase separation was detected within experiment resolution. The lack of aggregates in these systems suggested a high level of pendant POSS dispersion within networks was achieved by continuous reactor method.

This could be explained by thermodynamic considerations. The miscibility of POSS-DGEBA precursor and DDM was mainly because of larger entropy contribution which was the result of low molecular weight components mixture. Also, the high compatibility between POSS cage and DDM was ascribed to similar polarity between isobutyl groups on the POSS cage and methane group of the DDM molecules. Generally, with the curing reaction proceeding, the systems go through structural changes, like an increase in molecular weight by chain extension and an increase in system viscosity. The increased molecular weight and viscosity eventually led to decreased system entropy. This resulted in a decreased in entropy contribution to miscibility.[119] However, in this case, hydrophobic isobutyl side groups on POSS cage and methane group of the DDM interact with each other, which can cause the entropy to increase (ΔS is positive). According to the relation,

$$\Delta G = \Delta H - T\Delta S \qquad \text{(Eq 9)}$$

ΔG is negative for favorable mixing. As temperature increases, the strength of hydrophobic interactions increases as ΔG become more negative. Hence, utilization of fully reacted POSS in a continuous reactor with DDM resulted in the formation of a molecular level dispersion of POSS in epoxy-POSS nanocomposites.
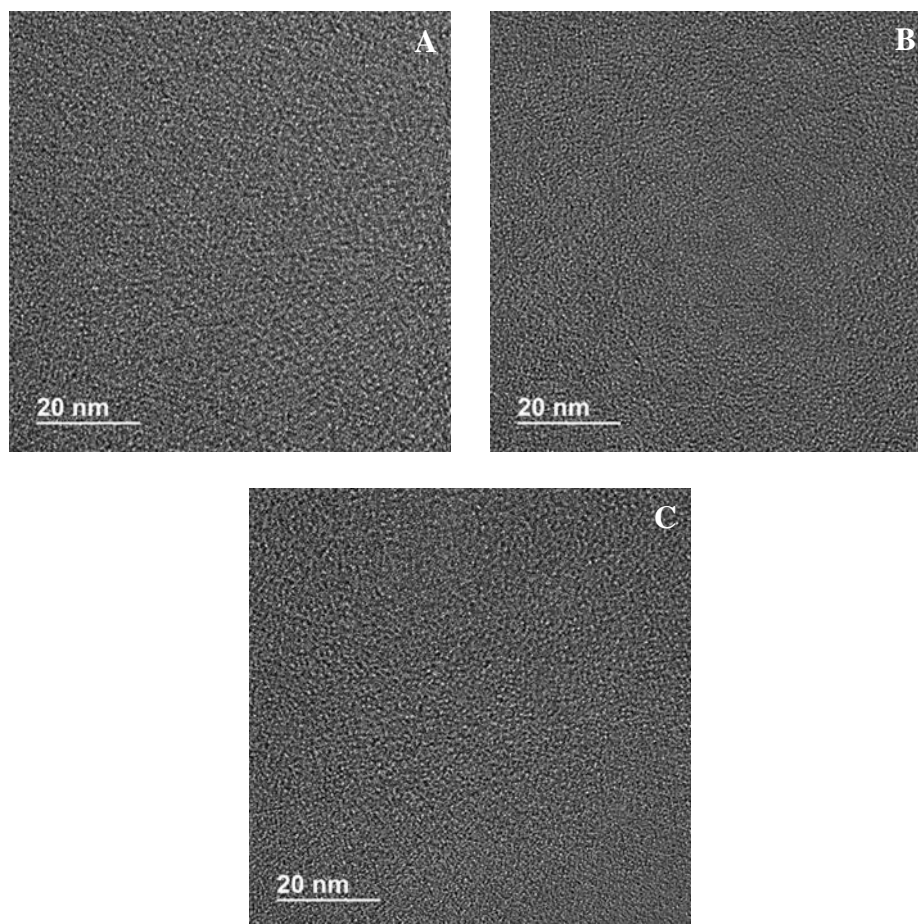
Figure 57. TEM of hybrid networks: [A] 0POSS; [B] 21.8POSS, [C] 54POSS

A TEM-EDX analysis of samples corresponding to 0POSS and 54POSS is given

in Figure 58. As observed, significant presences of silicon element in the epoxy hybrid

network corresponding to 54POSS clearly indicate a molecular level dispersion. Since no

aggregates were observed at a scale of 20 nm in the epoxy hybrid network corresponding

to 54POSS (shown in Figure 58), It is plausible to claim that a molecular level

incorporation of pendant POSS into epoxy networks has been achieved by using

continuous reactor method.
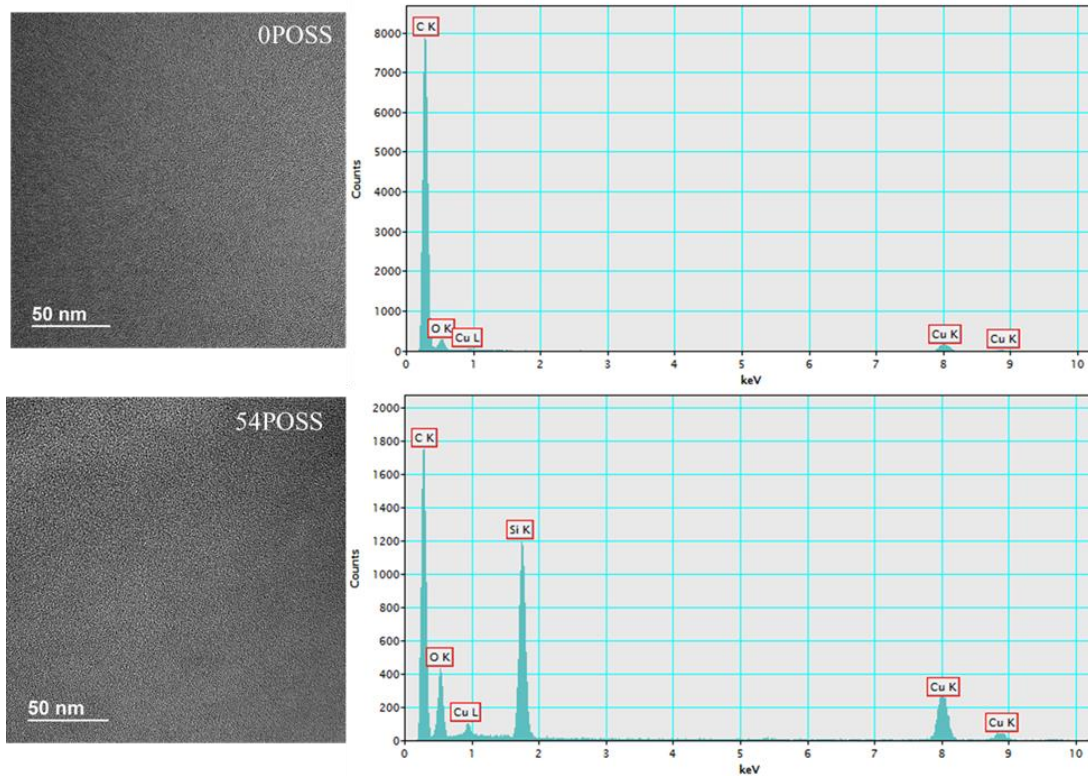
Figure 58. TEM-EDX analysis for hybrid network corresponding to 0POSS (Up) and 54POSS (Below)

Conclusion

Incorporation of monofunctional POSS into epoxy networks as a pendant unit at a molecular level is the main objective of this work. Following a two-step synthesis proposed by Liu et al,[74] a continuous reactor method was developed to synthesize POSS-DGEBA precursors. In contrast to a batch process, a full conversion of monoamine functional POSS into POSS-DGEBA precursor with more defined molecular weight distribution has been achieved using this continuous reactor method. The reaction time has been reduced significantly by using a continuous reactor. Compared to 18 hours in the batch process, full conversion was achieved in 40 seconds using a continuous reactor. The epoxy hybrid networks were prepared by curing POSS-DGEBA precursor with

aromatic amine curatives, DDS or DDM. The resulting networks have POSS covalently

bound as pendant unit. For these networks, we have followed network structure formation

with respect to POSS loadings. The epoxy hybrids cured by DDS showed droplet

morphology, suggesting a secondary phase separation process during cure. On the other

hand, the epoxy hybrid cured by DDM show a featureless morphology at multi-scale

from visual observations, SEM, and TEM experiments for all POSS concentrations,

suggesting a molecular level dispersion of pendant POSS in epoxy hybrid networks.

CHAPTER V –HYBRID NETWORKS BASED ON HIGH MASS FRACTION OF PENDANT POSS: STRUCTURE-MORPHOLOGY AND PROPERTIES

Abstract

The molecular level incorporation of monofunctional POSS into epoxy networks up to 50 wt. % loading has been achieved using high shear continuous reactor technology. However, the ability to tailor performance properties depends on the network architecture and its effects on the physical properties of the nanocomposite. This chapter evaluates the performance of POSS-based epoxy hybrid networks focusing on viscoelastic, mechanical (compression) and thermal analyses. Special attention is given to the correlation of molecular packing and free volume of hybrid networks with POSS concentration since it directly influences the viscoelastic and mechanical behavior of hybrid networks. Another important correlation defined is the dependency of Si-O-Si cage incorporation at the molecular level on flammability, which most likely favors the formation of a moderate amount of char residue during combustion. This study gives new insights into the effects of structural changes in POSS-containing thermosets on their performance properties.

Results and Discussion

Hybrid networks containing up to 50 wt. % pendant POSS dispersed at molecular level were prepared by polymerizing POSS-DGEBA precursors with DDM. A direct comparison of structure-property relationships of these networks is presented in this chapter. In order to establish structure-property relationships, the variations in free volume, crosslinking density, and chain packing in the network with respect to pendant POSS incorporation has been correlated with networks performance properties.

Glass Transition Behavior of Hybrid Networks with POSS Loading

Measurement of T_g provides a direct insight into the mobility of polymer chains. Incorporation of POSS in a polymer can result in an increase, decrease, or unchanged glass-rubber transition (T_g).[55,120] Generally, the hybrid network's behavior is determined by two competing effects: the restriction of chain mobility due to presence of a robust POSS cage, which results in an increase in Tg and a local chain reinforcement; or an increase in free volume due to voluminous POSS molecule which leads to acceleration of chain dynamics and diminishing of T_g as well as modulus. POSS thus acts either as nanofiller or as a plasticizer.[55]

DSC measurements were performed for the hybrid networks containing pendant POSS; for the purpose of this study, T_g was taken as the midpoint in the specific heat transition. DSC curves of hybrids networks are presented in Figure 59. For all POSS-containing hybrid networks, DSC thermograms displayed single glass transition temperatures (T_g's) within the experimental temperature range (25–300°C) indicating POSS is completely miscible in the epoxy system.[83] When compared to the T_g value of 175.1 °C for the neat DDM-DGEBA polymer, the hybrid network T_g was reduced with increased loading of POSS.
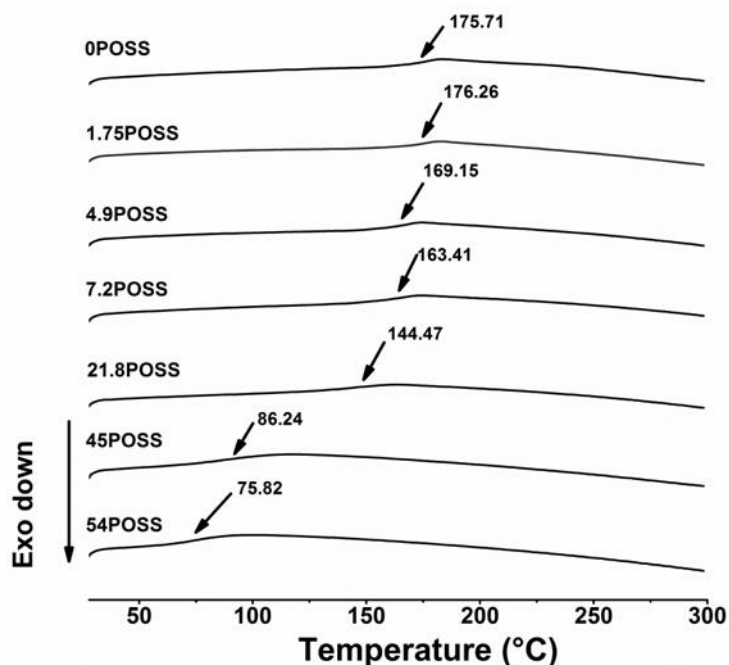
Figure 59. DSC curves of the epoxy hybrid containing pendant POSS

Incomplete curing of epoxy resin upon incorporation of the POSS is a possible explanation of the depression in the glass transition temperature.[121] In order to examine possible unreacted epoxides, infrared spectra of neat epoxy, and hybrid networks corresponding of 0POSS, 1.75POSS, 4.9POSS, 7.2POSS, 21.8POSS, 45POSS, and 54POSS were determined by FTIR in the near IR range. As mentioned, FTIR results are qualitative as the samples are of different thicknesses, but the presence of epoxide groups in neat DGEBA and cured samples were visible as shown in Figure 60. The absorption peak at 4530 cm^{-1} is characteristic of epoxide as the combination band of the second overtone of the epoxy ring stretching with the fundamental C-H stretching is centered at 4530 cm^{-1} in near IR region for DGEBA.[122] As evident from FTIR spectra, the curing reaction of the neat DGEBA-DDM network was essentially complete as verified by the disappearance of the epoxide peak. The similar spectra were observed for the hybrid

110

networks containing POSS; the epoxide peak completely disappeared in all the networks

containing POSS. This confirmed that complete curing in hybrid networks containing

POSS was achieved. Based on FTIR results, it was concluded that neat DGEBA-DDM

and hybrid networks were completely cured and the depression in T_g was not the result of

uncured networks.
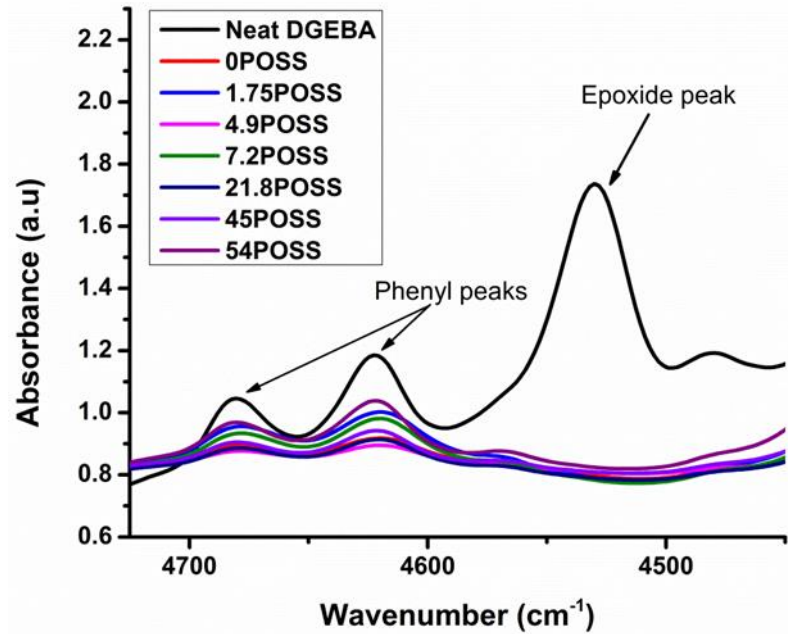
Figure 60. Near-IR curves of the epoxy hybrid containing pendant POSS

The decrease in T_g could be the result of an increase in free volume in hybrid

networks containing pendant POSS. This suggestion is in agreement with the free volume

hole size $\langle V_h \rangle$ values measured by PALS, as described in chapter II. In PALS, the time

between emission of positrons from a radioactive source and detection of gamma rays

due to the annihilation of positron through interaction with electrons corresponds to the

lifetime of the positron. Based on the lifetime of these interactions, the $\langle V_h \rangle$ can be

calculated using various models.[123] The $\langle V_h \rangle$ for epoxy network corresponding to 0POSS

and hybrid network containing pendant POSS is shown in Figure 61. The $\langle V_h \rangle$ value for

hybrid networks corresponding to 7.2POSS, 21.8POSS, and 54POSS was increased by 18 %, 60 %, and 135 % relative to the 0POSS network. The increased free volume is reminiscent of the crosslinking density of these networks since the decrease in crosslinking can give rise to free volume as reported by Dlubek et al.[124]
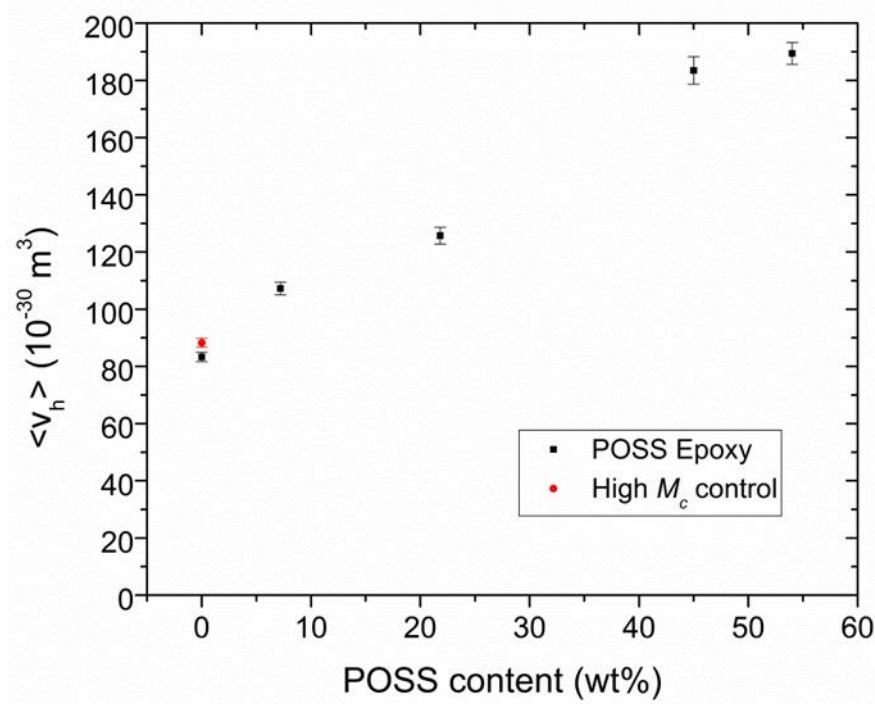
Figure 61. PALS data of the epoxy hybrid containing pendant POSS

The number of crosslinks per unit volume, *Nc,* was calculated using the equation below based on network density and curative weight fraction:

$$N_C = \frac{\rho\, w_{cu}}{M_{cu}} A_v \qquad \text{(Eq 10)}$$

where, ρ is the density, measured based on Archimedes principle as described in the experimental section, A_v is the Avogadro's number, w_{cu} is weight fraction of curative (DDM), and M_{cu} is the molecular weight of curative. In addition to that, a control precursor, 0POSS-PA, shown in Figure 62 was prepared to quantify the effect of pendant

112

POSS cage on network free volume. Two moles of DGEBA were reacted with one mole

of 1-propylamine (PA) at 60°C under reflux for 1 hour to prepare 0POSS-PA precursor.

In order to prepare an epoxy network to exhibit the same crosslinking density

corresponding to 54POSS, but without a cage, 25.04 grams of 0POSS-PA precursor were

mixed with 3.22 grams of DDM. The control network corresponding to 0POSS-PA also

showed complete conversion in an FTIR experiment as described previously. The $<V_h>$

value for the control network is measured as 88 $\mathring{A}^3$ through PALS experiment. Different

levels of molecular packing and free volume were expected despite having the same

crosslinking density, considering the absence of bulky inorganic Si-O-Si cage in the

control network corresponding to 0POSS-PA.
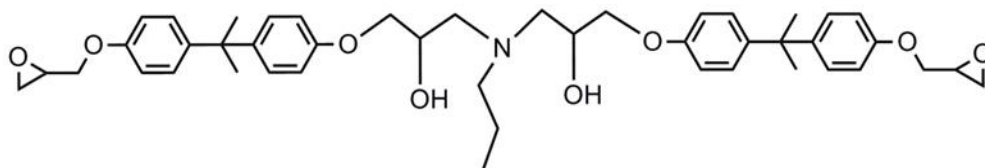
Figure 62. Structure of DGEBA precursor without inorganic Si-O-Si cage (0POSS-PA)

Figure 63 shows the variation in T_g between neat epoxy network, hybrid network

corresponding to 54POSS, and control network corresponding to 0POSS-PA.

Additionally, Table 14 shows the density values and number of crosslinks per unit

volume in the network with respect to POSS loading. As anticipated, the number of

crosslinks per unit volume in networks decreased with POSS loading. The results

indicated that 0POSS-PA network displayed a higher T_g value compared to 54POSS

network, however, 0POSS-PA network had a lower T_g value compared to the 0POSS

network. Interestingly, the free volume hole size of 0POSS-PA shown in Figure 61 was

close to the 0POSS network. This suggested that the depression in T_g could be the result

113

of decreased crosslinking density but the crosslinking density has minimal impact on free volume. It is reasonable to assume that increased free volume was mainly attributed to the pendant POSS cages.
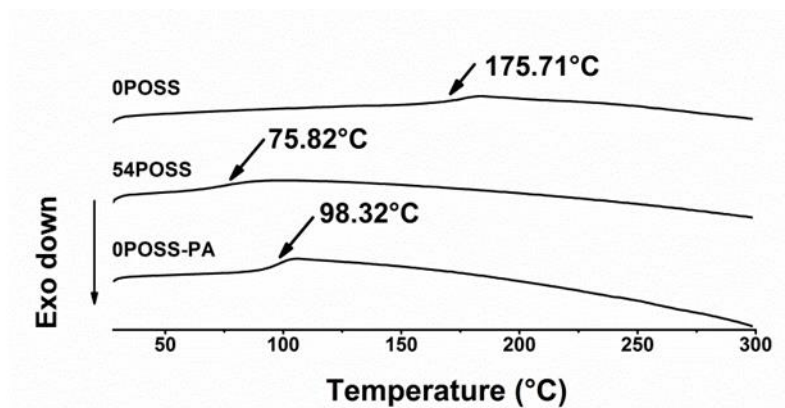
Figure 63. DSC curves of hybrid networks corresponding 0POSS, 54POSS, and 0POSS-PA

From Figure 63, higher T_g value for 0POSS-PA network than 54POSS network indicated that bulky substitution on epoxy chains disrupted the ordered structure of the hybrid network containing pendant POSS. As shown in Table 14, density and number of crosslinks per unit volume for 0POSS-PA network were much higher than the 54POSS network. This suggested that the presence of pendant POSS cages affected chain packing in the network. In literature, several researchers reported phase separation, or formation of POSS-rich domains, caused by the poor compatibility between POSS and isobutyl side groups in epoxy-amine networks as discussed in chapter I. In this case, pendant POSS was dispersed at a molecular level and only interacted with other POSS molecule on nearby chains. However, the known incompatibility between pendant POSS isobutyl groups and the epoxy-amine network influenced chain packing within networks containing pendant POSS. A proposed illustration of network structure may be found in Figure 64.

114

Table 14

Density and Number of Crosslinks per unit Volume for Hybrid Networks

Network ID	POSS wt. %	DDM wt. fraction	Density, ρ (g/cm^3)	No. of crosslinks per unit volume, *Nc*
0POSS	0	0.218	1.18	7.82 x 10^{20}
1.75POSS	1.58	0.212	1.169	7.55 x 10^{20}
4.9POSS	3.94	0.206	1.161	7.28 x 10^{20}
7.2POSS	5.89	0.2	1.159	7.05 x 10^{20}
21.8POSS	18.26	0.162	1.154	5.70 x 10^{20}
45POSS	40.8	0.093	1.104	3.13 x 10^{20}
54POSS	50.37	0.064	1.096	2.13 x 10^{20}
0POSS-PA	0	0.114	1.162	4.03 x 10^{20}
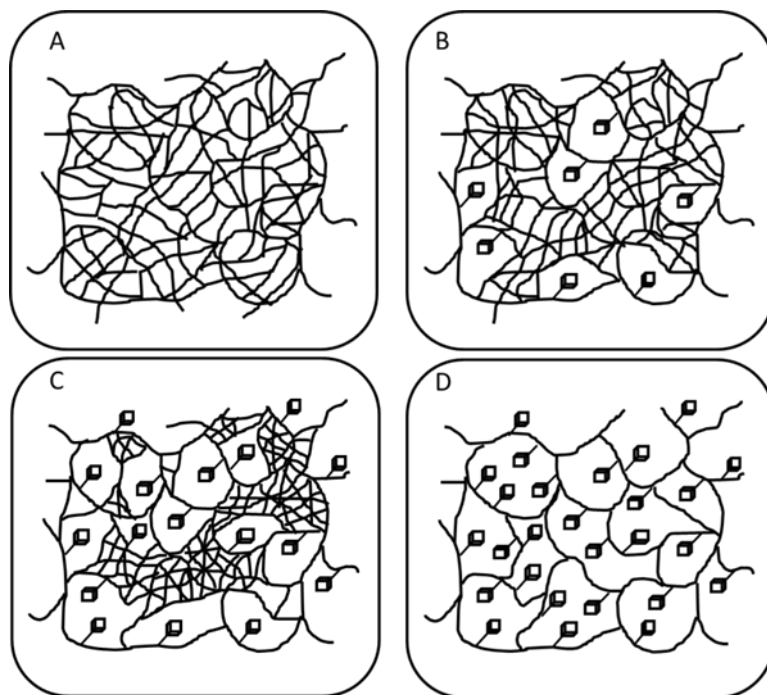
Figure 64. Illustration of network structure depicting POSS dispersion, chains packing and free volume; A- 0POSS, B- 7.2POSS, C- 21.8POSS, and D- 54POSS

It is reasonable to suggest for hybrid networks containing molecularly dispersed pendant POSS the glass transition temperatures can be determined by free volume and crosslink density. Obviously, a decrease in crosslinking density of the network will decrease glass transition temperature. Also, the inclusion of the bulky POSS cage could result in a decreased T_g due to an increase in free volume and disruption of the ordered structure of the system. Therefore, the behavior of glass transition temperature of the hybrids containing POSS is the cumulative effect of these two factors.

Thermomechanical Properties with POSS Loadings

Thermomechanical properties of the hybrid networks containing POSS were determined by DMA. Storage modulus with respect to the temperature of 0POSS-PA and hybrid networks corresponding to 0POSS, 1.75POSS, 4.9POSS, 7.2POSS, 21.8POSS, 45POSS, and 54POSS are given in Figure 65. The trend shown in Figure 65 and their

dependence on POSS incorporation in epoxy networks indicated a few important observations. First, the glassy state storage modulus of all pendant POSS-containing hybrid networks was lower than that of the network corresponding to 0POSS and decreased with increasing concentrations of pendant POSS. Another important observation in Figure 65 was the dependence of rubbery storage modulus on POSS incorporation (inset). Table 15 shows glassy storage modulus and rubbery storage modulus with POSS concentration. The decreased moduli values could be attributed to decreased number of crosslinks per unit volume in hybrid networks with the incorporation of pendant POSS. It is apparent that the POSS concentration and the number of crosslinks per unit volume are strongly related, as the N_c value of hybrid networks further decreased with increasing pendant POSS concentration. Another important factor to be considered is the chain packing in the network, which is evident from the storage modulus value of 0POSS-PA network in the glassy state (-50°C) compared to 54POSS network that more free volume caused by incorporation of pendant POSS decreases the network's resistance to deform. As these are glassy state relaxations, they must involve motions of short macromolecular fragments within small free volumes.[125]

Storage moduli decreased with increased temperatures and finally drop off at glass transition temperature to an equilibrium state as shown in Figure 65. Interestingly, the decreased moduli in transition regions were steeper in networks corresponding to 0POSS, 1.75POSS, 4.9POSS, and 0POSS-PA. The slope of the decrease in storage moduli in transition regions was gradually reduced with POSS loading. This is explained by the presence of inhomogeneous crosslink densities in the network structure, as

proposed in Figure 64B & C, where the number of crosslinks per unit volume (N_c) is varied because of incompatibility between the POSS cage isobutyl groups and epoxy-amine system. However, for the 54POSS network, a slightly steeper decrease than that of other POSS loadings (45POSS, 21.8POSS, and 7.2POSS) suggest a more homogeneous network structure and crosslink density as shown in Figure 64D. It is also noted the rubbery state storage modulus for the POSS-containing epoxy hybrids was lower than that of the network corresponding to 0POSS (shown in inset). This discrepancy can be interpreted as decreased crosslink density for the epoxy hybrid systems and an absence of any nano-reinforcement caused by nanosized aggregates. Incorporation of pendant POSS lowers crosslink density and storage modulus in the rubbery state.
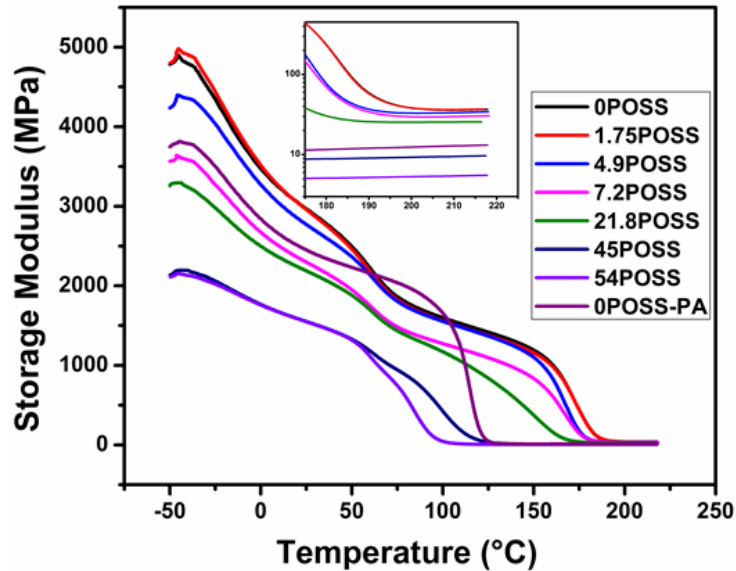
Figure 65. DMA storage modulus for epoxy hybrid networks containing pendant POSS

Table 15

DMA Data for Storage Modulus and Glass Transition Temperature

Network ID	DMA T_g (°C)	E'@ -50°C (MPa)	E'@ 25°C (MPa)	E''@ 220 (MPa)
0POSS	184.65	4784	2965	36.76
1.75POSS	184.57	4800	2958	37.01
4.9POSS	178.01	4235	2770	34.22
7.2POSS	178.03	3565	2298	30.58
21.8POSS	166.94	3257	2189	25.62
45POSS	121.75	2139	1551	9.69
54POSS	100.82	2110	1548	5.53
0POSS-PA	124.51	3746	2453	13.19

The tan δ curves with respect to the temperature shown in Figure 66 depict a clear dependency of the α-relaxation with POSS concentrations. The α-relaxation peak of the network corresponding to 0POSS with respect to temperature at 1 Hz frequency is 184.22 °C. For epoxy hybrid networks corresponding to 1.75POSS, 4.9POSS, 7.2POSS, 21.8POSS, 45POSS, and 54POSS, a transitions are 181.57 °C, 176.84 °C, 175.72 °C, 162.9 °C, 117.87 °C, and 97.48 °C, respectively.
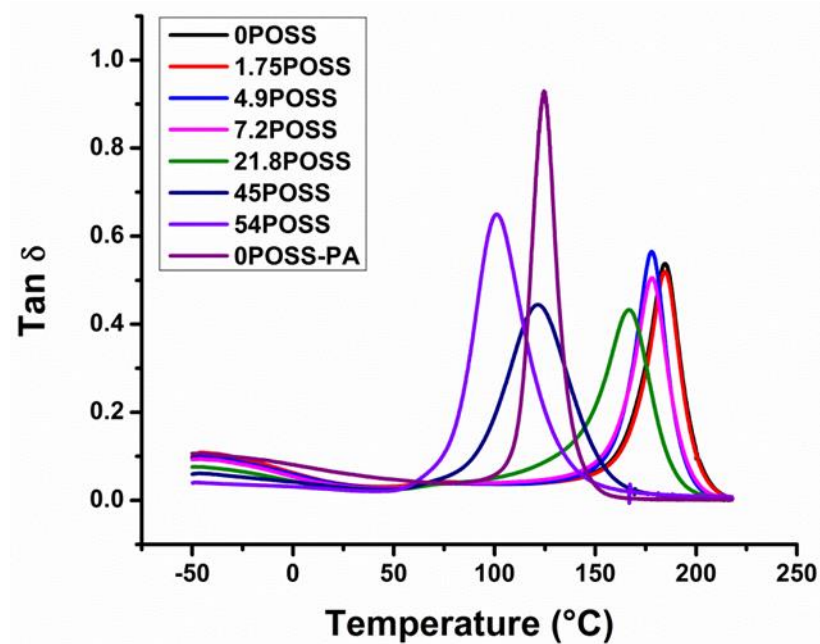
Figure 66. DMA tan δ for epoxy hybrid containing pendant POSS

Reduction of peak height and peak broadening occurred with increased POSS

concentration in epoxy hybrid networks associated with the distinct regions of varying

crosslinking density. The 0POSS network displayed a slight secondary transition at ca. 75

°C, which was assigned to local fluctuations within the networks. For epoxy hybrids

containing pendant POSS, as seen in Figure 67, the secondary relaxation peak shifted to

lower temperatures upon increased POSS loadings suggesting POSS increases free

volume in the networks. This increased free volume facilitates the motion of these local

fluctuations, and these results are in good agreement with lower glass transition
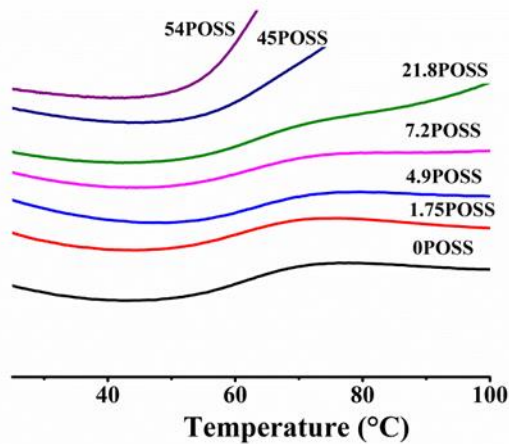
temperatures.

Figure 67. Tan δ vs temperature – β transitions of hybrid networks containing pendant POSS

Mechanical Properties with POSS Loadings

The mechanical properties of the hybrid networks containing pendant POSS were measured using a Wyoming Test Fixtures compression apparatus with an MTS 810 universal test machine. Quality dispersion of POSS cages is critical for the improvement of mechanical properties of POSS-containing networks. As seen in literature, pendant POSS cages can give reinforcement depending on their state of dispersion in pendant POSS-containing polymeric systems.[77,81] This was believed to be caused by the tendency for pendant POSS units to aggregate through interaction forming strong physical crosslinks which play a dominant role in the reinforcement of polymers.[120,125] As discussed earlier, incorporation of pendant POSS cage through chemically reacting monoamine functional POSS into the epoxy network at molecular level decreased the number of crosslinks per unit volume and creates distinct regions with different crosslinking density within the network structure. The yield stress of the networks decreased with increasing POSS concentrations as shown in Figure 68 (stress vs strain

121

curves). There is a well-established relationship between yielding behavior and the T_g of

epoxy networks,[126] and incorporation of POSS at molecular level decreased T_g. A

generalized model for the yield behavior of epoxy networks developed by Lesser et al.

suggests that yielding in epoxy resins is governed by intermolecular forces between

network chains.[126] Furthermore, it was suggested that at lower crosslinking densities the

only effect on yield stress was a change in T_g. In this sense, the T_g and the yield stress of

the epoxy networks are intimately related. Therefore, it should be expected that

incorporation of POSS would decrease the yield stress of the network, which was

supported by the observation of the mechanical behavior in hybrid networks (Figure 68).
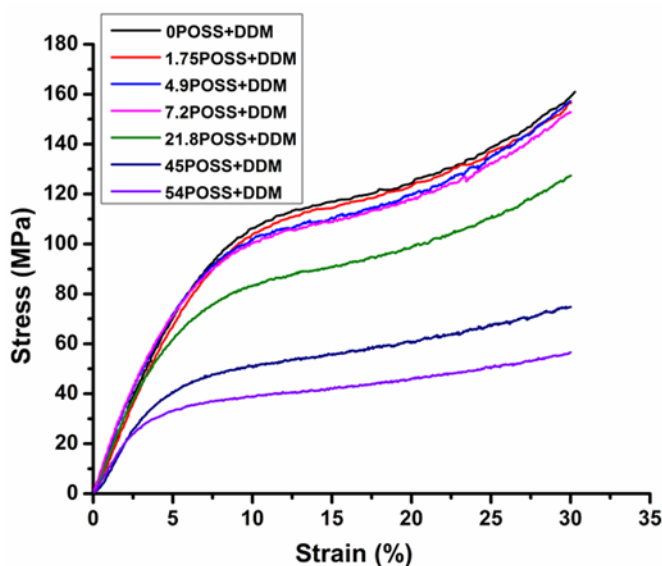
Figure 68. Stress-strain data in compression mode for epoxy hybrid networks containing pendant POSS

Thermal Stability with POSS Loadings

Thermal stability of hybrid networks containing POSS was evaluated by TGA.

Curves shown in Figure 69 are the studied networks recorded in a nitrogen atmosphere at

10°C/min. For the pure POSS, the initial decomposition temperature was defined as 5%

mass loss and was found to be 220 °C where a sharp degradation occurred above 220 °C. The degradation process of isobutyl POSS is a volatilization phenomenon influenced by the substitution size; small molecule substituted POSS was recognized to undergo almost complete sublimation.[127,128] For 0POSS, the initial decomposition occurred at 363 °C, which was much higher than that of the pure POSS. The initial decomposition temperature for POSS-containing hybrids decreased from 363 °C to 359 °C, 347 °C, and 350 °C for hybrid networks corresponding to 7.2POSS, 21.8POSS, and 54POSS as expected based on initial decomposition temperature of pure POSS and structural variation introduced by the incorporation of POSS. Another important feature observed from the TGA data is the char yield at 595 °C, which increased from 16 wt. % for 0POSS to 19, 18, and 26 wt. % with hybrid network corresponding to 7.2POSS, 21.8 POSS, and 54 POSS respectively. Based on TGA decomposition temperatures and char yields, it was clear that the thermal stability of hybrid networks was enhanced with increasing POSS content in hybrid networks. According to the trend shown in TGA data, it is plausible that presence of POSS in hybrid networks does not significantly change the degradation mechanism of these networks. This was likely due to POSS cages covalently attached to the epoxy chains as pendant units which are molecularly dispersed in hybrid networks as discussed earlier. The mass loss from segmental decomposition via gaseous fragments could be suppressed by well miscible POSS cages in hybrid networks.[129]
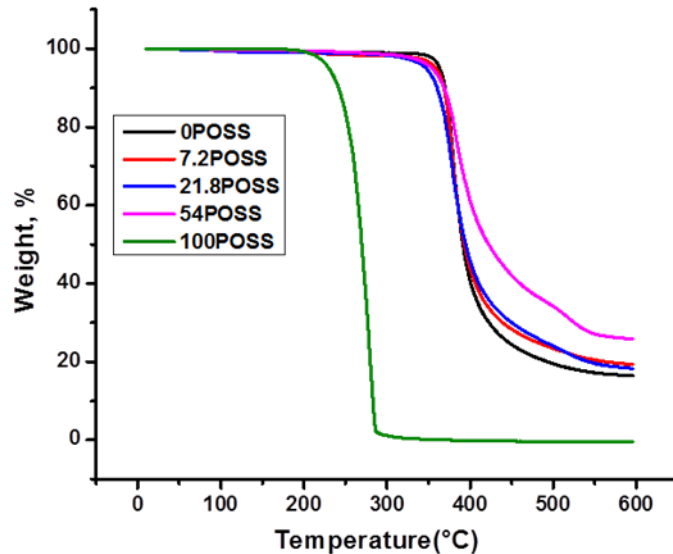
Figure 69. TGA data of epoxy hybrid networks containing pendant POSS

Similar results were found with cone calorimetry evaluations for the flammability of hybrid networks containing pendant POSS. Cone calorimetry provides robust and repeatable data for both 'time of ignition' and 'rate of surface flame spread'. The hybrid networks containing POSS with their weights are given in Table 16. All samples studied were exposed to a heat flux of 50 kW/m^2 (594 °C) during cone calorimetry experiment. The test was stopped when the flame extinguished. As observed, 0POSS, followed solid phase combustion with non-continuous char after complete combustion. The hybrid networks showed solid phase combustion initially, but gradually a boiling liquid was observed during the combustion process, which indicated liquid phase combustion. The char volume increases with the POSS concentration in the hybrid network. Also, heavy smoke release was observed during combustion process for hybrid networks containing POSS which increased with higher loadings of POSS.

Four parameters were derived from the cone calorimetry measurement to characterize the ignition and flammability behaviors of epoxy hybrid networks. Time of

124

ignition (T_{ig}) is defined as the time to achieve a sustained fire, peak heat release rate (PHRR) is characterized by the highest heat rate occurred during combustion process, time for peak heat release rate (tPHRR) is defined as the time at which highest heat release occurred, and total heat release (THR) is defined as the total heat release during the combustion process. Table 16 shows the variation in typical combustion parameters in cone calorimetry experiments.

Table 16

Cone calorimetry parameters to characterized ignitability and flammability

Network ID	Sample wt. (g)	T_{ig} (sec)	PHRR (kW/m^2)	tPHRR (sec)	THR (MJ/m^2)
0POSS	35.52	47.656	1307.5	105.5	86.8
7.2POSS	34.65	44.326	880	136	83.6
21.8POSS	44.62	36.312	584.8	100	97.7
54POSS	28.94	32.167	615.5	89.5	65.3

Figure 70 shows the rate of heat release of the hybrid network containing POSS with respect to time. As evident in heat release curves, the heat release rate during combustion process decreased with increasing POSS content in the hybrid networks. The peak heat release rate (PHRR) dropped linearly along with tPHRR with the concentration of POSS content. PHRR also decreased with increased loading of POSS by 32.7%, 55%, and 53% for epoxy hybrid networks corresponding to 7.2POSS, 21.8POSS and 54POSS compared to the control epoxy network.
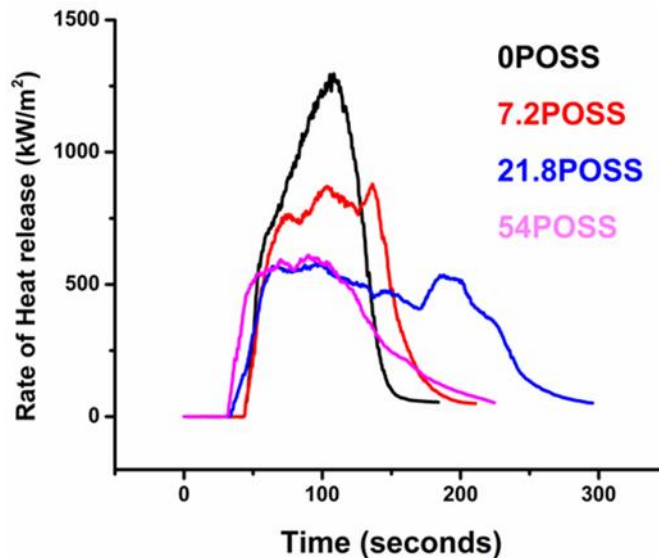
Figure 70. The Cone calorimetry data of epoxy hybrid networks containing pendant POSS

As hybrid networks containing POSS cages are exposed to severe environments such as high temperatures, only Si-O bonds survive while weaker bonds degrade and form volatile organic compounds. The Si-O bonds are significantly stronger than other bonds in the system like C-H, C-C, and even C-Si. More importantly, the surviving Si-O bonds can form a SiO_2-like surface layer on the POSS material to prevent further etching and consumption.[125,130,131] This surface layer lowers the time for ignition of these networks compared to the 0POSS network and decreases with POSS concentration. This was attributed to the readily oxidized isobutyl side groups on the POSS cage during combustion and was accompanied by the release of the generated volatiles such as carbon dioxide and vapor. There are two stages of combustion for POSS-containing networks: the long chain combustion and the small molecule combustion stages.[132] With greater POSS loading in the network, more isobutyl groups were available which led to more rapid combustion. Early ignition time and heavy smoke generation with POSS loading

126

were due to the presence of isobutyl groups. As mentioned, POSS cages were terminated by isobutyl groups at seven corners of the Si-O bonded cage. The dissociation energy of Si-C is lowest of all the bonds in the system, and upon high-temperature exposure, the Si-C bond broke first resulting formation of small volatile molecules which burned more rapidly than the crosslinked network. Complete combustion of these small molecules in the early stage of burning led to faster ignition time and heavy smoke generation. The liquid phase combustion and char expansion during the burning process with POSS-containing samples were due to the formation of a SiO_2-like surface layer on the POSS materials, preventing the escape of more volatiles produced during the combustion process. This trapped volatiles resulted in bubbling and increased char volume after the burning process.

Water Uptake Properties

Water uptake in hybrid networks was largely governed by the network architecture. Previous studies showed that in monofunctional POSS-based systems, POSS was present in the network either as a microscale crystalline phase or as dispersed pendant unit. Pendant POSS was expected to increase free volume hole size (V_h) in the material which should increase the water absorption as suggested by Jackson et al.[133] The phase separated crystalline POSS domains were primarily formed by inorganic Si-O-Si skeleton present in the POSS molecules and the material containing these crystalline phases expected to be impervious to water absorption.[134] It was expected that water absorption would be reduced as the POSS crystalline domains increased in the network.

It is widely accepted that water absorption in epoxy networks follow Fickain diffusion, where epoxy networks show an almost linear relationship between the moisture

127

uptake and the square root of time at the beginning of the absorption process. The diffusion coefficient can be estimated as follows.

$$\frac{M_t}{M_{inf}} = \frac{4}{L} \left(\frac{Dt}{\pi}\right)^{1/2} \qquad \text{(Eq 11)}$$

where M_t is the water absorption at time t, M_{inf} is the equilibrium water absorption, L is the half the sample thickness, and D is the diffusion coefficient. Water uptake results of epoxy hybrid networks containing pendant POSS incorporated at molecular level showed large variation with POSS content. The samples were submerged in water and the weight gain was measured over a fixed period of time, Figure 71 presents the plots of water absorption curves for POSS-containing hybrid networks with respect to time. The shapes of the curves suggest networks containing low POSS fractions absorbed water more quickly initially, but the rate of uptake decreased until equilibrium was reached. This water concentration gradient was the driving force that led to water absorption in the networks.[135] In addition, Figure 71(B) plots M_t/M_{inf} as a function of square root of time, where the slope is proportional to the diffusivity of water through the individual network. A Fickian behavior was observed since all samples show almost linear water absorption initially with the square root of time except the very high loading (54POSS). As discussed for increased pendant POSS content in the network, free volume hole size significantly increased which should result in increasing water uptake as suggested by Jackson et al.[133] However, water uptake behavior of the hybrid networks studied present a competing effect dominated by the free volume and the network hydrophobicity. With increasing pendant POSS content the chemical composition and polarities of the network also change and the resulting networks were more hydrophobic due to the presence of

128

hydrophobic Si-O-Si inorganic cage into the epoxy network at the molecular level. As the loading level of pendant POSS increased the networks clearly showed a restriction blocking behavior for water molecules into the network due to the presence of more numbers of Si-O-Si skeletons.
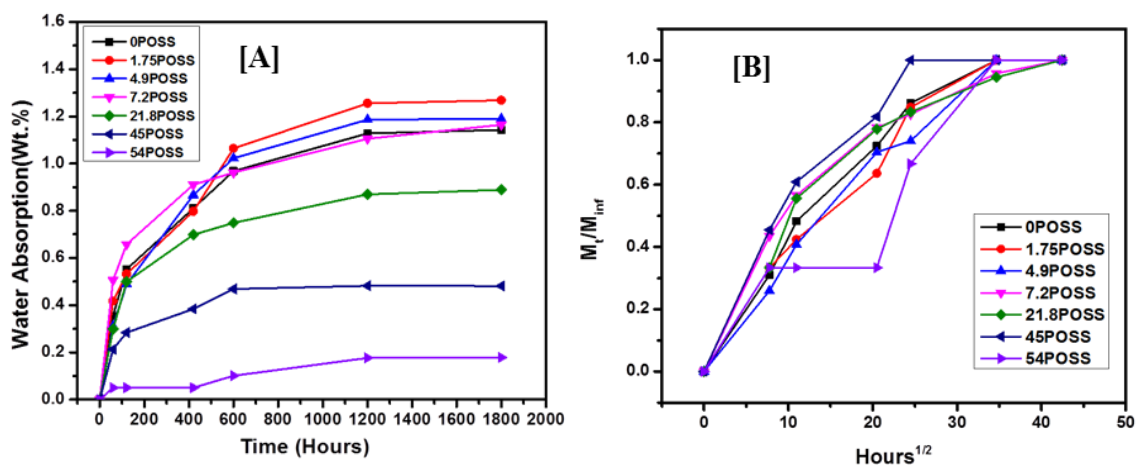
Figure 71. [A] Water uptake vs. time, [B] M_t/M_{inf} vs. square root of time

Incorporation of pendant POSS at molecular level resulted in increased in free volume hole size, but simultaneously the network polarity restricted the water molecules ability to transport through the network. This characteristic of pendant POSS-containing networks can have a promising use in selective fluid transport application. However, a detailed analysis of these networks for selective fluid transport application is required to understand their true potential.

Conclusion

The DDM cured hybrid networks were prepared using POSS-DGEBA precursors with POSS covalently bound as pendant unit. For these hybrid networks, we have:

a) observed network structure formation with respect to POSS loadings

b) explained the effect of concentration of pendant POSS dispersed at the molecular level on glass transition temperature

c) studied the effect of concentration of pendant POSS dispersed at the molecular level on thermal properties of hybrid networks containing POSS

Glass transition temperature of the epoxy hybrid networks revealed a complex relationship with respect to the incorporation of pendant POSS dispersed at a molecular level. Factors which affect the glass transition temperature are the large free volume associated with voluminous pendant POSS cage and a decrease in crosslinking density by incorporating POSS as pendant cage. A control precursor without a POSS cage but with a similar network structure was prepared to study the effect of the POSS cage on free volume. It was determined the free volume is associated with POSS cage, of which the presence of voluminous POSS cage disrupts chain packing in the networks and is mainly responsible for depression in T_g in crosslinked networks. It was also observed that even at very high loading (>50 wt. %) of POSS content, epoxy hybrid networks do not show a reinforcing effect and the physical interactions between POSS-POSS cages are absent. A decrease in storage modulus was observed for epoxy hybrid networks at temperatures above the glass transition temperature.

The effect of POSS concentration on network thermal behavior was evaluated. The effects of inorganic Si-O-Si cage thermal stability and the organic substituent on the POSS cage were taken into account to elucidate the effect of pendant POSS concentration on thermal properties. We have proven that formation of the hybrid network with the molecular level incorporation of pendant POSS resulted in increased char yield of epoxy hybrid network despite the fact that initial decomposition temperature decreased with

130

POSS concentration. The thermal stability of epoxy hybrid network containing POSS was enhanced with increased POSS loading. However, the presence of small organic substituents on the POSS cage affected the combustion process of these networks adversely in terms of increased smoke generation and reduced time for ignition. In absence of POSS-POSS interactions, the mechanical behavior of epoxy hybrid networks was clearly dominated by the decrease in crosslink density by incorporation of POSS as a pendant cage. At high loading levels, hybrid networks showed significant flexibility compared to no POSS network and hybrid networks containing low POSS loading levels.

CHAPTER VI – EPOXY NETWORKS CONTAINING POSS AND SILICA NANOPARTICLES: NANOSTRUCTURED MORPHOLOGY AND PROPERTIES

Abstract

Hybrid networks containing pendant POSS and silica nanoparticles (SNP) were prepared to exploit POSS-POSS and POSS-SNP interactions and control the network nanostructure. These interactions mandate ultimate morphologies and the mechanical properties of the hybrid networks. The POSS-POSS and POSS-SNP interactions were studied through controlled experiments to observe influence for generating nanostructured morphologies in epoxy networks cured by DDS or DDM. Our approach combined the successful strategies for incorporating pendant POSS at the molecular level with a dispersion of silica nanoparticles to form novel nanostructured morphologies. Hybrid networks were characterized via SEM, and TEM, to study nanostructure evolutions during cure and the mechanical properties were investigated in compression mode to determine bulk modulus and strain at the yield of these hybrid networks. Favorable interactions between pendant POSS cage and non-functional SNP surface were correlated to the load bearing properties of hybrid networks. Additionally, thermomechanical properties of cured hybrid networks containing pendant POSS and SNP have been determined and correlated with corresponding nanostructured morphologies.

Results and Discussion

Physical properties of polymer nanocomposites are strongly influenced by the dispersion level of inorganic nanoparticles. However, uniform dispersion of inorganic nanoparticles is somewhat difficult due to their high surface area and large surface

132

energies. Kinetically driven dispersion of multi-walled carbon nanotubes in epoxy matrices by high shear mixing in a continuous reactor has been systematically studied by Cheng[136] and Greenhoe.[137] This research demonstrated that reducing process temperature and increasing shear provided a better dispersion state in epoxy prepolymers. However, maintaining a homogeneous dispersion during cure was determined to be a critical factor as lower viscosity which occurs during cure lead to secondary agglomeration. In order to maintain inorganic nanoparticles dispersion state in cured composites, Cheng and Greenhoe used matrix viscosity to prevent secondary agglomeration during cure.[136,137] In our previous work, we prepared epoxy resins modified with pendant POSS and demonstrated a full conversion of POSS into POSS-DGEBA precursors. The work herein aims to introduce SNP and monoamine POSS concurrently into the epoxy system in order to maintain the silica nanoparticle dispersion by utilizing surface interaction between pendant POSS and silica nanoparticles. Two different nanostructured morphologies formed in the hybrid network will be discussed in this chapter to study the influence of these interactions on nanostructured morphology, mechanical, and thermomechanical properties.

Microscale Interactions between SNP and POSS

Nanostructured Morphology. POSS-DGEBA (EEW 540) precursor was prepared in a batch process as described in chapter II & III. SNP was dispersed in a mixture of POSS-DGEBA (EW540) precursor, DGEBA, and DDS. The epoxy and amine stoichiometry were adjusted to maintain 5 wt. % of POSS and 0.5, 1.0, 1.5, 2.0, 3.0, 5.0 wt. % SNP in final network compositions to study nanostructured morphology, and network physical properties. SEM micrographs of fractured surfaces are shown in Figure

133

72. In all SEM micrographs, dispersed droplet morphologies were observed. As discussed previously, the spherical droplets are POSS-rich domains dispersed in a continuous epoxy matrix and their sizes are uniform throughout the samples studied in this section. With SNP loadings, the fractured surface morphology presented isolated SNP aggregates and the size of these aggregates increased with SNP loadings. Aggregates of less than 2 microns can be observed in the network containing 0.5 wt. % of SNP. The size of these aggregates increased to around 5 microns for 1 wt. % SNP loading. With further increased loading, larger aggregates (>10 microns) of SNP were observed; however, migration of SNP to the surface of POSS domains were also observed. The migration of SNP on the surface of POSS domains confirmed the presence of interactions between POSS and SNP.
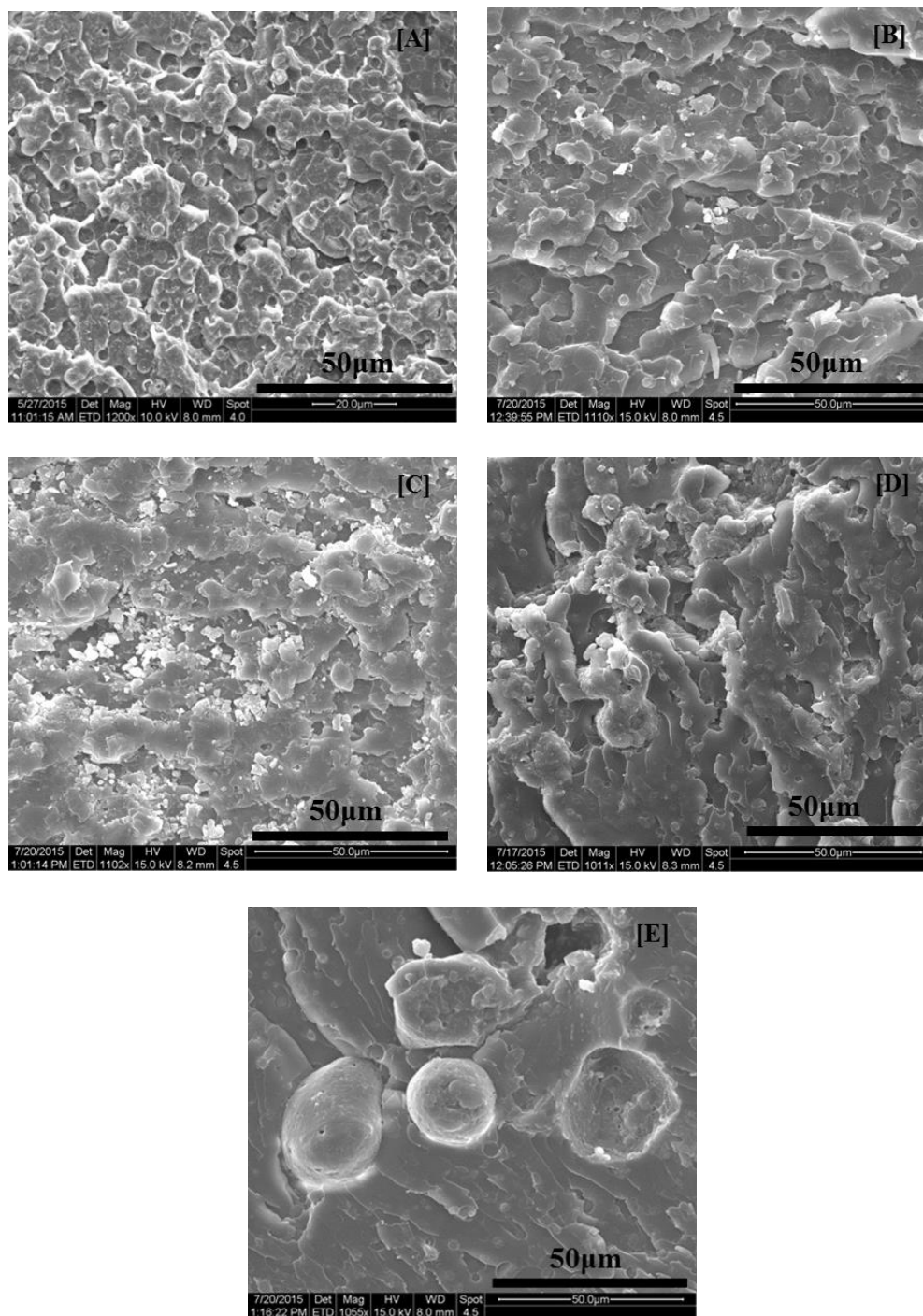
Figure 72. SEM micrographs for hybrid networks containing 5wt.% POSS and [A] 0, [B] 1, [C] 2, [D] 3, and [E] 5 % SNP loadings by weight.

The interactions between POSS and SNP led nanoparticles to assemble on the spherical POSS domain surface and form a layer. As the SNP content and size of the SNP

layer around the POSS domains increased, a growth of isolated aggregates resulted as shown at higher magnification SEM micrographs (Figure 73). Therefore by observing the morphology of hybrid networks containing POSS and SNP, it is postulated that POSS and SNP interaction directed the formation of nanostructured morphology.
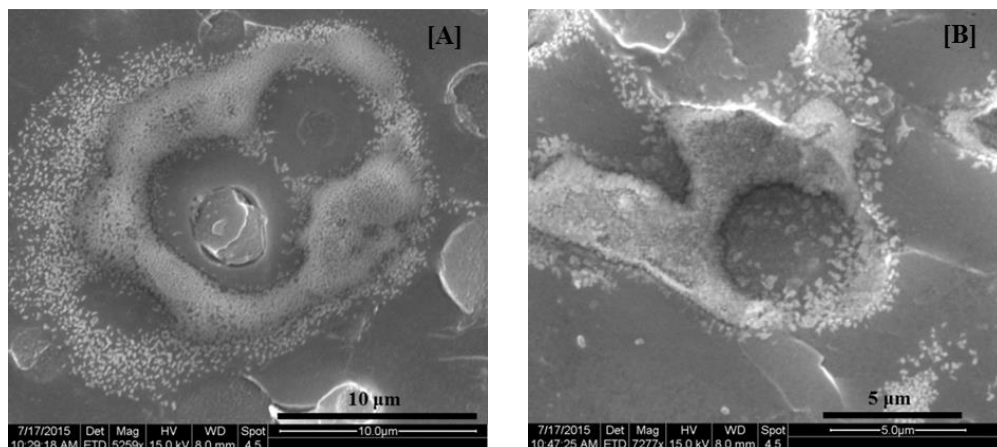
Figure 73. SEM for 5wt.% POSS and 5 wt.% SNP.at [A] 5259 x- magnification, and [B] 7277 x- magnification

Bulk morphology was observed using TEM. The micrographs shown in Figure 74 depict the dispersion of isolated spherical droplet corresponding to POSS-rich domains in the epoxy network and the bright objects correspond to SNP aggregates. The TEM analyses provide clear evidence of favorable interactions between POSS and SNP.
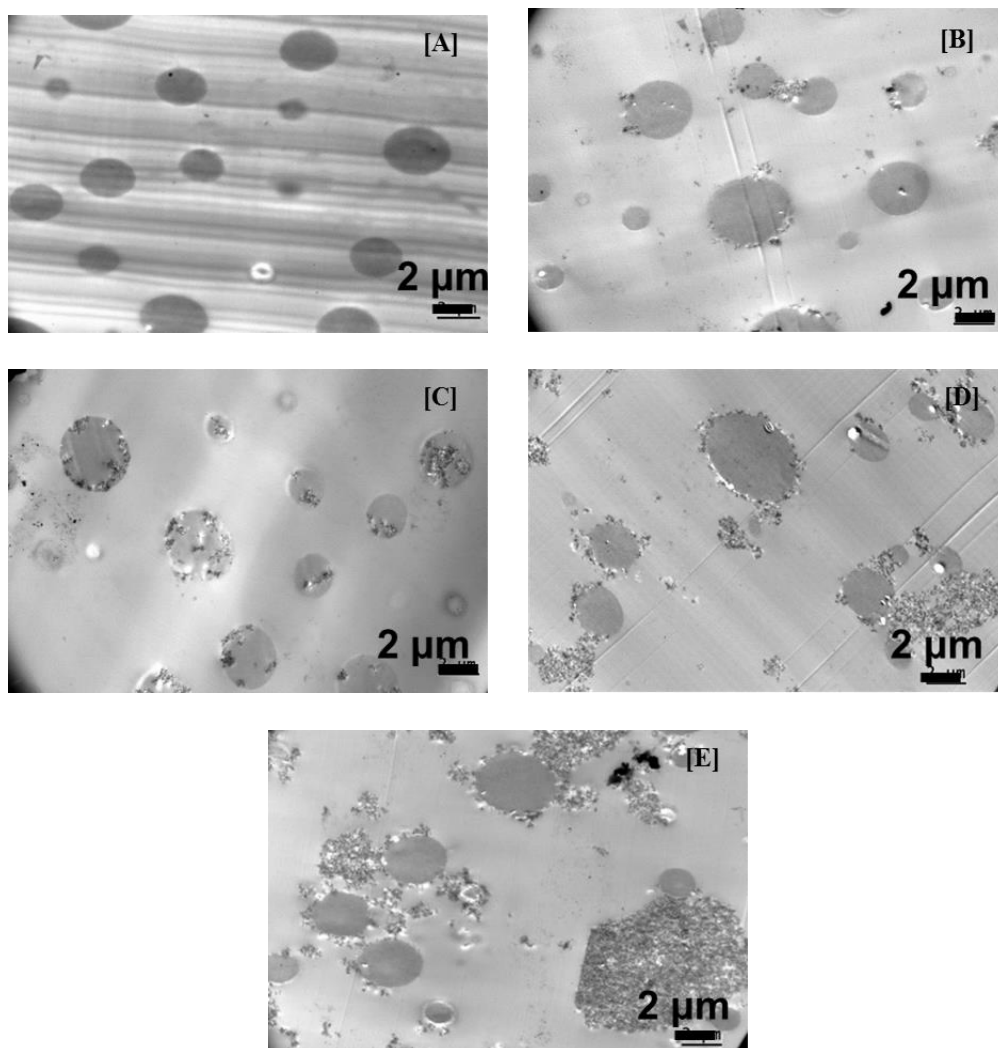
Figure 74. TEM of hybrid networks 5wt.% POSS and [A] 0, [B] 1, [C] 2, [D] 3, and [E] 5.% SNP loadings by weight

As observed for 0.5 wt. % SNP loading, SNP assembled on the POSS domain surface and almost no isolated SNP aggregates were observed in the network. As SNP loading increased to 1.0 wt. %, many fine isolated SNP aggregates were observed along with SNP migration on the surface of POSS domains. Further increase in SNP loading levels led to increased SNP aggregates and more migration of SNP to the surface of POSS domains. This was due to differences in surface energies between POSS, SNP and

137

epoxy chains. A Smaller difference between POSS and SNP surface energies led to favorable enthalpic interactions.

Formation of large SNP aggregates interacting with POSS domains was further verified through TEM analyses. Figure 74[E] corresponds to 5.0wt. % SNP loading into the network and depicts formation of a continuous layer on the POSS domain. Despite the hybrid structure, POSS molecules are structurally similar to SNP and appear to have favorable interactions. However, in this case, POSS molecules are covalently attached to the epoxy network chains and therefore POSS facilitate nanoparticle dispersion in the networks through these interactions. Surface interactions between unmodified SNP and POSS domains can be understood by similar thermodynamics considerations for POSS-POSS interactions as reported by Morgan at el.[138] A large difference in the surface energies of the polymer and the unmodified SNP led to the higher thermodynamic driving force of the nanoparticles to aggregates. On the other hand, a small difference in the surface energies of POSS and SNP led to favorable enthalpic interactions, as previously described. The homogenous dispersion of SNP in the hybrid network depends on these favorable interactions, but the size scale of these interactions must be considered and play a major role in the properties of hybrid networks.

Thermomechanical Properties: All samples tested were prepared by using POSS-DGEBA (EW540) precursor, and have 5 wt. % POSS in final network composition. Additionally, variable amounts of SNP, 0.5, 10, 1.5, 2.0, 3.0, 5.0 wt. %, based on final network composition, were added to the network. The variation in dynamic storage modulus vs. temperature is shown in Figure 75[A]. With increased temperature, storage moduli decreased for all samples. This behavior is attributed to increased molecular

138

mobility of the polymer chains.[139] At a higher temperature in the rubbery region, hybrid

networks containing POSS and SNP displayed higher storage modulus compared to

hybrid networks containing only POSS. The values of storage moduli in the rubbery

regions increased with increasing in SNP loading, was due to increased network rigidity

with the reinforcing effect provided by the inorganic nanoparticles.[140]
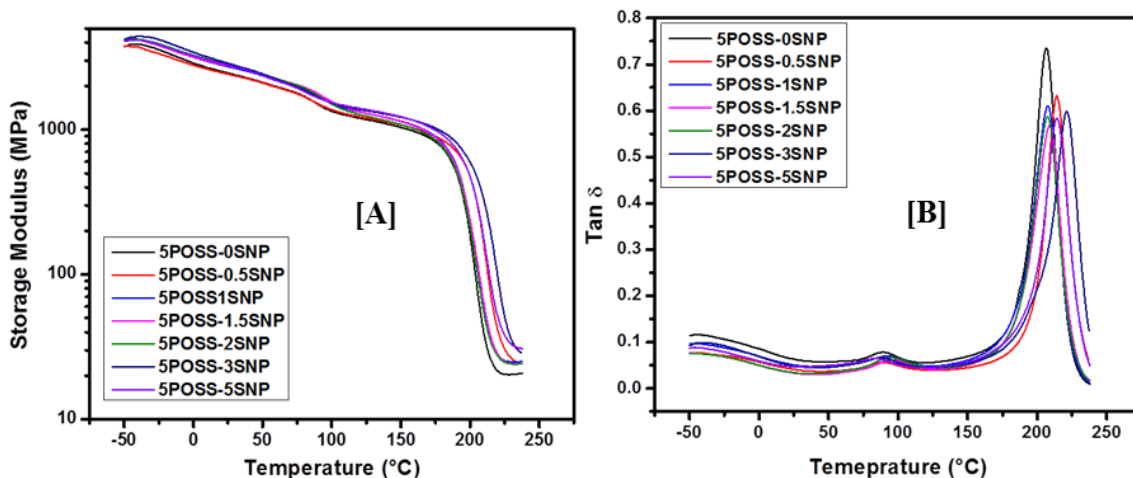
Figure 75. DMA data of hybrid networks containing 5wt.% POSS and 0 -5.0 wt.% SNP
[A] Storage modulus vs. temperature, and [B] Tan δ vs. temperature

At low temperature and in the glassy region, the storage moduli increased with

SNP loading related to the good SNP /matrix interaction and facilitated by pendant POSS

and the high rigidity of inorganic nanoparticles.[139,141] In other words, the small difference

in storage moduli of SNP filled hybrid networks clearly show a reinforcing effect. Figure

75[B] shows the tan δ vs. temperature curves with increasing SNP concentration in

hybrid networks. The α relation peak corresponding to T_g is visible in all curves at high

temperature. Adding 0-10 wt.% of SNP in epoxy networks generally resulted in a

reduction in T_g due to the free volume associated with SNP.(4) However, we observed a

slight increase in T_g with SNP loading associated with the additional surface interactions

between POSS and SNP as observed in the microstructure of these networks. Increased SNP loading did not affect the T_g of hybrid networks significantly. T_g discounted the restrained polymer chains and increased free volume caused by isolated SNP aggregates. The height of tan δ peak was indicative of hybrid network properties. The tan δ of hybrid networks shifted toward the lower values with increased SNP loadings suggesting favorable interactions between SNP and matrix were facilitated by pendant POSS. In general, lower α transition peaks indicated a good interaction between matrix and nanoparticles.[142] Reduced sub-T_g motions (side group motions, crankshaft, or localized motions) were observed in hybrid networks containing SNP, as peak height corresponding to β transition at c.a 75°C and γ transition at c.a. -50°C were reduced with increased SNP loadings. This indicated that in a vitrified state, fewer chains contributed to cooperative motions because of SNP –matrix interactions, facilitated by pendant POSS, which resulted in less damping.[140,143,144]

Mechanical Properties: Further insights into network structure-properties were gained by investigating the mechanical properties of these networks. The mechanical properties of hybrid networks containing POSS and SNP were measured in compression mode. Figure 76 show the stress vs. strain curves of hybrid networks. A clear trend is observed in the stress-strain behavior of hybrid networks with respect to SNP loadings. The bulk modulus was found to increase with the SNP contents. The increased bulk modulus and yield stress were afforded by the stiffness of inorganic nanoparticles. Table 17 shows the mechanical properties in compression mode with respect to SNP loading of hybrid networks.
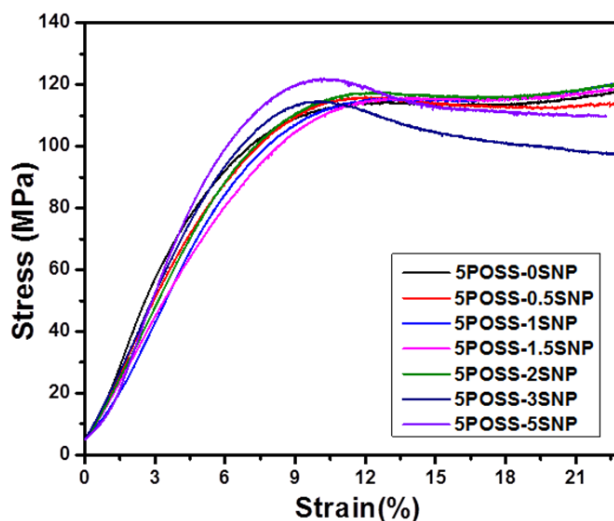
Figure 76. Stress-strain curves of hybrid networks containing 5wt.% POSS and 0 -5.0 wt. % SNP

In the post yield region, stress-strain curves showed increased strain softening with higher SNP loadings in hybrid networks. Strain softening is indicative of the network's ability to dissipate applied stress.[145] Addition of higher SNP content in the hybrid network imparted less resistance to the stress induced flow resulting in decreased strain at yield. This was attributed to a reduction in intermolecular interactions between network chains due to larger and isolated SNP aggregates. Subsequently, lower stress was required to flow in the post yield region once flow begin at the yield point. At low SNP loadings, improved interfacial interaction between SNP and POSS provided greater resistance to flow under applied stress and increased yield strain was observed.

Table 17

Compressive Properties of Hybrid Networks Containing 5 wt.% POSS and Varying SNP

Network ID	Modulus, MPa (Std. Deviation)	Yield Stress, MPa (Std. Deviation)	Yield Strain, % (Std. Deviation)
5POSS-0SNP	1281.75 (22.1)	110.2 (4.83)	12.57 (1)
5POSS-0.5SNP	1301.8 (74.8)	113.11 (3.87)	13.29 (0.29)
5POSS-1SNP	1338.12 (65.4)	114.11 (1.67)	13.14 (0.62)
5POSS-1.5 SNP	1430.09 (55.1)	115.12 (2.61)	12.98 (0.2)
5POSS-2SNP	1566.63 (54.8)	117.49 (1.14)	12.38 (0.5)
5POSS-3SNP	1674.07 (55.5)	117.94 (2.41)	11.04 (0.92)
5POSS-5SNP	1729.6 (45.3)	121.94 (1)	10.1 (0.88)

Nanoscale Interactions between SNP and POSS

  Nanostructured Morphology. Incorporation of pendant POSS at the molecular level in epoxy networks has been discussed, as well as the unique continuous reactor technology which led to the incorporation of high mass fraction pendant POSS. A kinetically favored pre-reaction, along with the simultaneous dispersion of SNP by high shear mixing in a continuous reactor, provided an opportunity to further study nanoscale interactions between POSS-SNP on nanostructure morphology and network properties. At first, various loadings of SNP were dispersed in POSS modified epoxy precursors simultaneously in a continuous reactor. These precursors/dispersions were cured using DDM in order to prepare hybrid networks. The compositions of hybrid networks are given in Table 10 of chapter II. The fractured surface morphologies of hybrid networks

corresponding to 0POSS-4SNP, 10POSS-4SNP, 20POSS-4SNP, and 40POSS-4SNP

were observed by SEM to study the dispersion dynamics of SNP with respect to POSS

loading. Figure 77 shows the SEM micrographs of the fracture surfaces for these

networks.

Figure 77. SEM of 4 wt. % SNP in hybrid network corresponding [A] 0 POSS, [B]
10POSS, [C] 20POSS, and [D] 40POSS

Interestingly, the micrographs reveal that SNP dispersion improved as POSS

content increased. SNP dispersed hybrid networks without POSS show formation of large

aggregates of SNP up to 10 microns in size. It was observed that the size of these

aggregates was significantly reduced with increased POSS loading in the hybrid

networks. At 40wt % POSS a significant reduction in the size of aggregates was

observed in the hybrid network. As discussed, the POSS molecules chosen for this

research have favorable surface interactions with SNP. The molecular level incorporation

of POSS into network chains was achieved through covalent bonding and favorable

surface interaction with SNP and was helpful in controlling the SNP dispersion in hybrid

networks. The favorable surface interactions between SNP and POSS decrease the inter-

particle forces and stabilize dispersion during cure. The effect of POSS loading on SNP

dispersion in hybrid networks was further confirmed by TEM. As seen in Figure 78, the
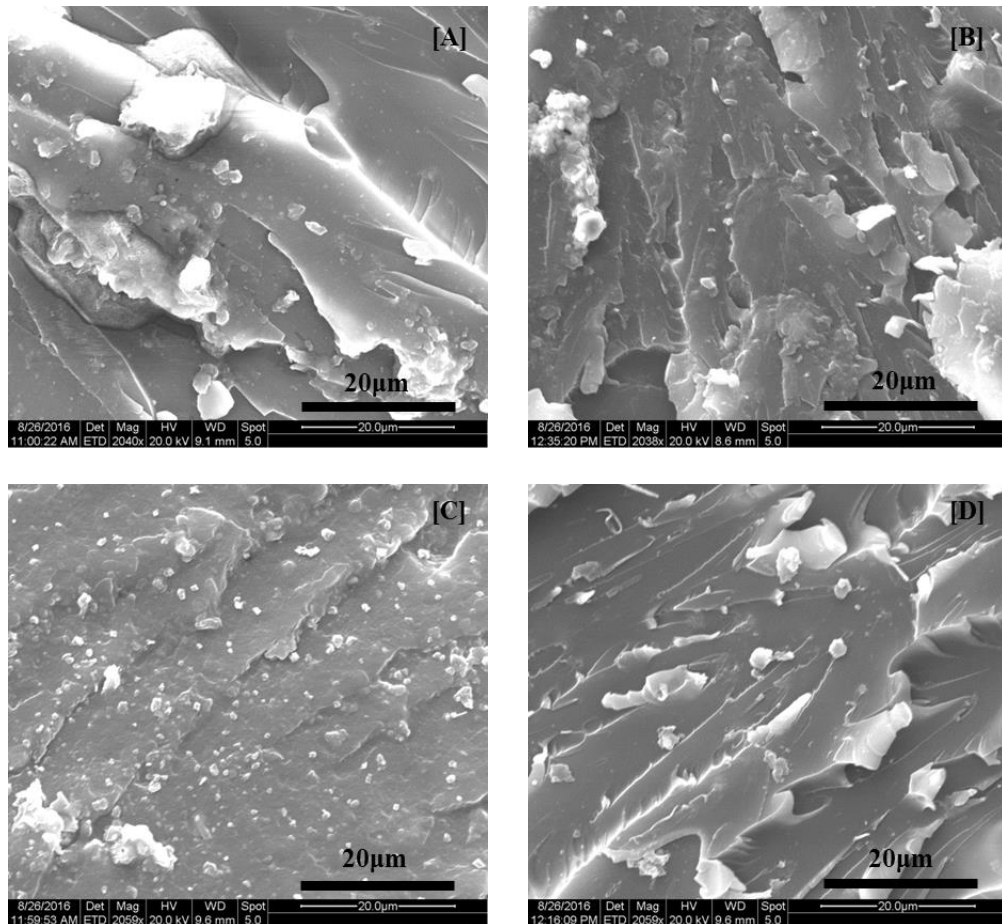
sizes of SNP aggregates were significantly reduced with increased POSS loading.
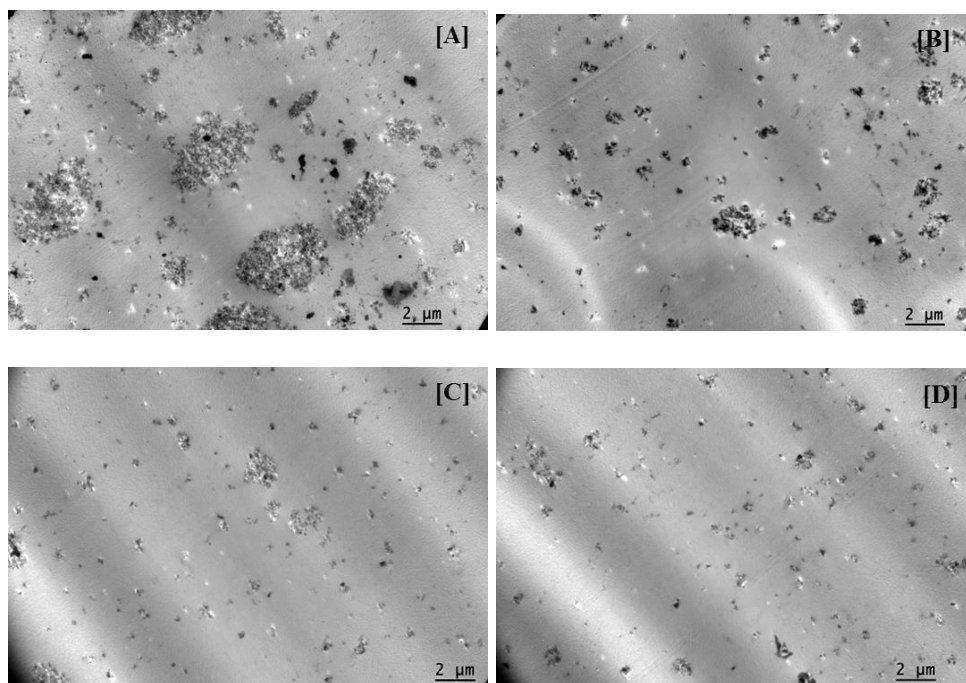
Figure 78. TEM of 4 wt. % SNP in hybrid network corresponding [A] 0POSS, [B] 10POSS, [C] 20POSS, and [D] 40POSS

This was attributed to a very interesting thermodynamic process. According to

Gibbs free energy equation,

$$\Delta G = \Delta H - T\Delta S$$

144

For favorable mixing, the enthalpy term should be minimized and the entropy term should be maximized. However in the present systems solubility of the unmodified SNP in epoxy is very poor and the enthalpic interactions are significantly higher than entropic interactions. These favorable enthalpic interactions led to nanoparticle aggregations. Nonetheless, pendant POSS moieties reacted into network chains provide additional enthalpic interactions between POSS and SNP since they are structurally similar. With increased number of molecularly dispersed POSS moieties in the network, enthalpic interactions between POSS and SNP increased. This increased number of POSS moieties on the surface of SNP resulted in decreased interparticle forces between SNP, which resulted in maximizing the entropy term in the Gibbs free energy equation. Hence, increased POSS moieties in the system led to better SNP dispersion in cured networks.

Thermomechanical Properties: A series of hybrid networks containing POSS and SNP were prepared to study the effect of nanostructured morphology on thermomechanical properties. Three SNP concentrations (0 wt.%, 4 wt. %, and 12 wt.%) were dispersed in POSS-containing hybrid networks corresponding to 0POSS, 10POSS, 20POSS, and 40POSS as described in chapter II (Table 10). Dynamic mechanical analysis (DMA) was performed on these networks and elucidated the variation in dynamic storage modulus and α relaxation peak indicated network structure and SNP-matrix interactions with respect to POSS loading. Variations in storage modulus with temperature are shown in Figure 79. The value of the storage modulus decreased with temperature for all networks due to the molecular mobility of network chains at higher temperatures.[139]

As reported in chapter V, storage moduli value of hybrid networks decreased with increased POSS loading. Conversely, storage modulus values increased with increased SNP content. In the glassy state, higher storage moduli values with SNP loadings were observed in hybrid networks containing both POSS and SNP. For example, addition of 12 wt. % of SNP into hybrid networks corresponding to 10P-0SNP, 20P-0SNP, and 40P-0SNP resulted in increased storage modulus values by 161, 220, and 791 MPa, respectively. Whereas a, 12 wt. % addition of SNP into 0POSS-0SNP network resulted in decreased storage modulus value by 165 MPa. This was associated with strong SNP-matrix interphase, due to favorable interactions between pendant POSS moieties and SNP. Another important observation was the noticeable increase in storage modulus value in the rubbery region with increased SNP loadings. This observation is attributed to a reinforcing effect provided by nanoparticles which increased rigidity in the hybrid networks. At high POSS and high SNP loadings, a prominent decrease in storage modulus around the glass transition temperature was observed. This was due to the entrapment of POSS-DGEBA precursors into SNP aggregates at very high loading levels leading to a reduction in the crosslink density and a sharp decrease in storage modulus values around glass transition temperature.
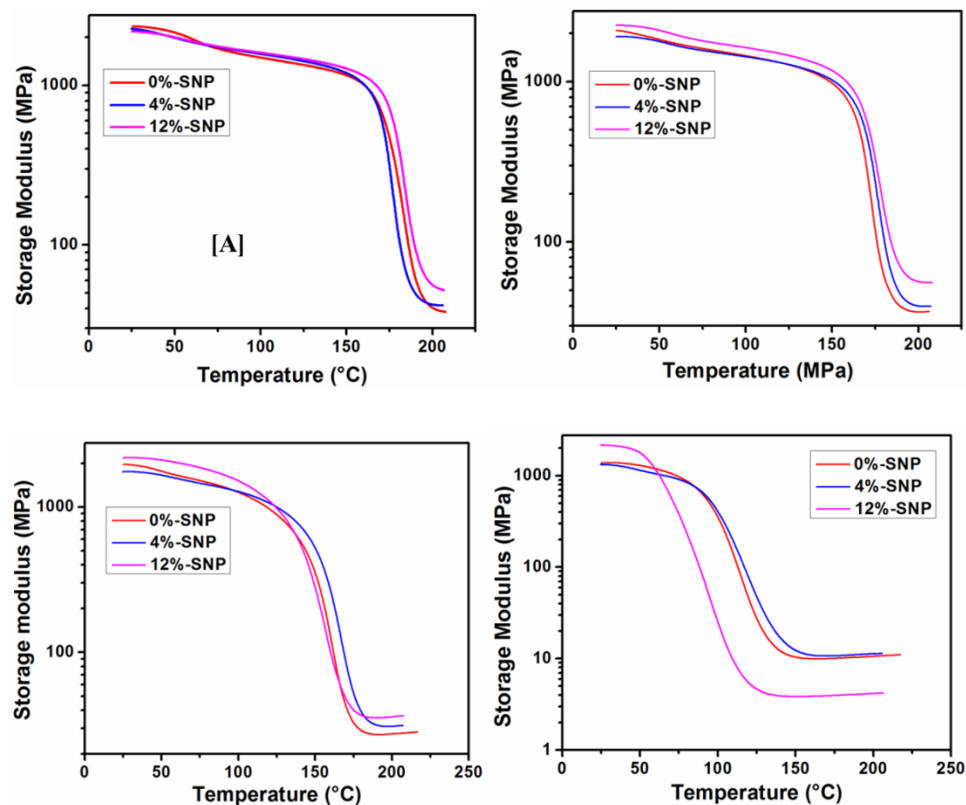
Figure 79. Storage modulus vs. temperature networks containing 0, 4, and 12 wt. % SNP, and [A] 0POSS, [B] 10POSS, [C] 20POSS, [D] 40POSS

It is also important to note that in the glassy state storage moduli were influenced by the inter-molecular interactions between chains and their ability to pack in the network.[143] In all networks studied, the glassy state storage modulus was slightly higher with the respective POSS-containing network which proves favorable interactions between SNP and pendant POSS moieties.
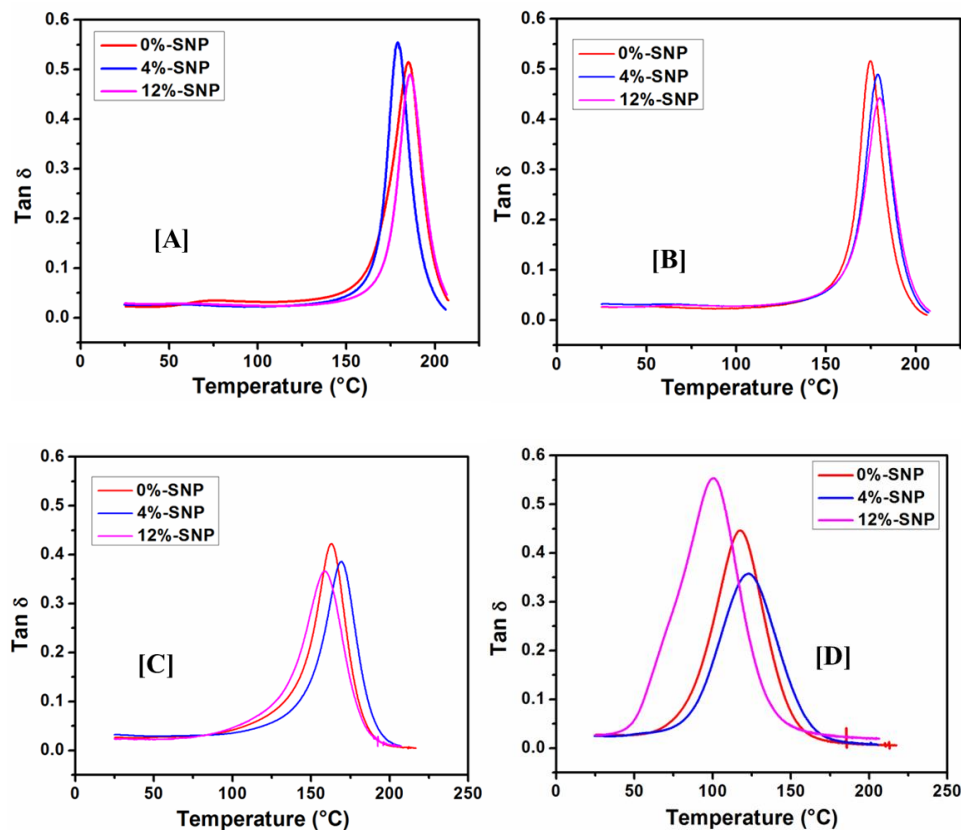
Figure 80. Tan δ vs. temperature for hybrid networks containing 0, 4, and 12 wt. % SNP, and [A] 0POSS, [B] 10POSS, [C] 20POSS, [D] 40POSS

All networks studied display a single α relaxation peak corresponding to the T_g of hybrid networks. Figure 80 shows tan δ vs. temperature curves. All samples showed a maximum value of tan δ in α relaxation region indicating cooperative motions of chains between crosslinks.[141] The α relaxation peaks shifted to lower temperatures with increasing POSS loadings, as discussed earlier in chapter IV. However, with the incorporation of SNP into POSS-containing networks, the α-relaxation peak height and position shifted suggesting a strong dependence on the interaction between SNP and matrix. The peak height and position of α-relaxation are important for describing structure-property relationships of hybrid networks. In general, peak heights in the glass transition regions are reduced if the nanoparticle-matrix interaction is favorable since

148

nanoparticles and matrix restrict polymer chains mobility and permit less energy dissipation through the interface.[142] Hybrid networks containing 10 wt. % POSS demonstrated favorable interactions between SNP and the matrix with SNP loading, whereas hybrid networks containing higher POSS loading (20 and 40 wt. %) displayed favorable interactions with low SNP loading (4 wt. %) but a poor interface with high SNP loading (12 wt. %). This was attributed to the formation of SNP aggregates which entrapped POSS-DGEBA precursors within these aggregates resulting in low crosslinking and poor interface. This behavior was enhanced with increased POSS loadings, as more POSS was entrapped into SNP aggregates more network heterogeneity was observed. This behavior is evident in Figures 79[C] & [D] where reduced reinforcement effect in the rubbery region was observed with increased POSS loading with 12 wt. % of SNP in a hybrid network.

Mechanical Properties: Mechanical properties of the hybrid networks were studied to provide more insight into the effects of nanostructured morphology on the compressive stress-stain response of hybrid networks. Stress-stain curves for all DDM cured hybrid networks containing POSS and SNP studied in this chapter are presented in Figure 81. Generally, it was observed that a good dispersion of SNP in epoxy networks enhanced the tensile stress-strain behavior [146] However, the stress-strain behavior strongly depends on the dispersion state and the nanoparticle-matrix interactions. According to the stress-strain curves, 0POSS-4SNP (or 0P-4S) showed slightly higher compressive modulus and lower yielding than 0POSS-0SNP. The increased modulus is likely due to greater stiffness of SNP,[147] and lower yield indicated the existence of plastic behaviors due to poor interactions between the nanoparticles and epoxy matrix.[148] On the

other hand, the stress-strain curve corresponding to 0P-12S showed reduced compressive modulus and high yield compared to 0POSS-0SNP. This observation was due to a lower crosslink density caused by increased incorporation of nanoparticles. However, the large area under the stress-strain curve for the 0POSS-12SNP hybrid network indicated increased fracture toughness compared to the 0POSS-0SNP hybrid network. Higher content of SNP into neat matrix also caused more interactions between nanoparticles and the neat matrix, which results in increased yield behavior and toughness.
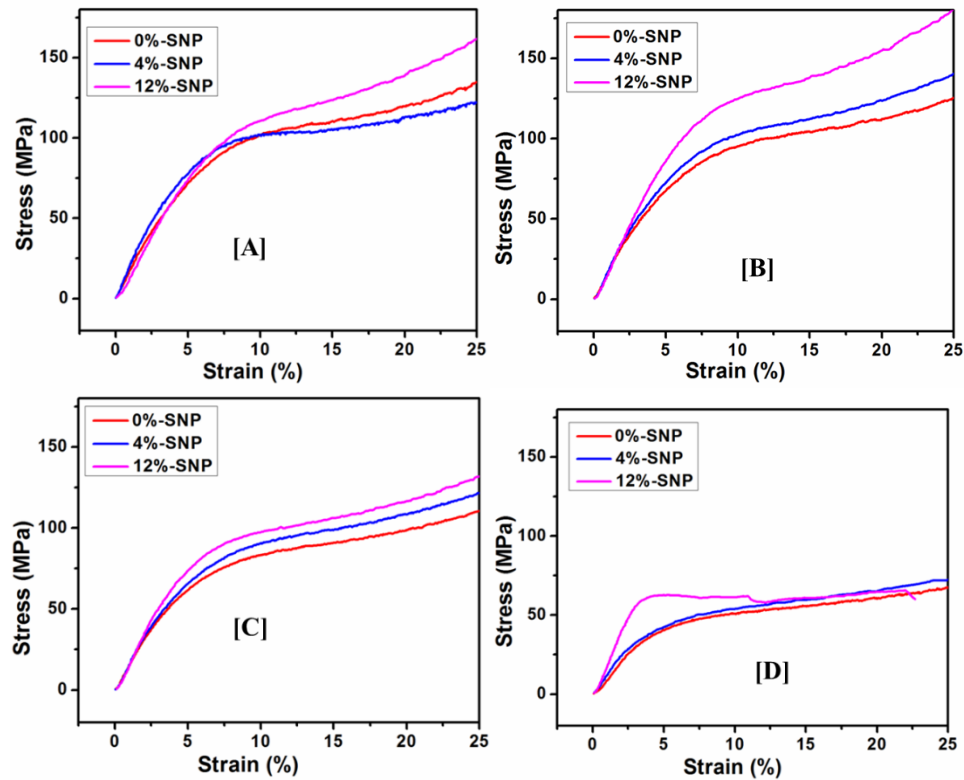
Figure 81. Stress-strain curves for hybrid networks containing 0, 4, and 12 wt. % SNP, and [A] 0POSS, [B] 10POSS, [C] 20POSS, [D] 40POSS

For POSS and SNP filled epoxy networks, interactions between pendant POSS moieties and SNP play an important role in the determination of the compressive properties. For 10 wt. % POSS networks, compressive modulus and the area under the

150

curves increased with SNP loading. This indicated favorable interactions between SNP and pendant POSS moieties that introduced an additional mechanism of energy dissipation in compression. With increased compressive load and network deformation, the strong interactions between SNP and pendant POSS resist deformation by transferring the load to the SNP leading to a reduction in network deformation. Additionally, this observation suggests that POSS-SNP interactions were favorable for transfer of applied stress efficiently to high stiffness SNP. Thus, hybrid networks containing SNP and POSS with good interparticle interactions afforded higher compressive modulus and strength. Hybrid networks with higher POSS concentrations (20 wt. % and 40wt, %) exhibited a similar behavior with increased SNP concentrations, although a plastic behavior was observed in the post yield region. As discussed, increased SNP concentrations in hybrid networks decrease crosslinking in the polymer matrix. It appears this led to decreased network yield under compressive load. Furthermore, at higher SNP concentrations a reduction in the stress-strain curve area indicated a reduction in the network's fracture resistance strength. As a result, SNP aggregation in the hybrid networks at higher SNP concentrations acted as stress concentrators and led to a fracture under applied stress. These observations confirmed that compressive properties of hybrid networks strongly depend on SNP and pendant POSS interactions. However, interparticle interactions depend on SNP and POSS ratios in hybrid networks. It appears that the optimum SNP and POSS weight ratio to maximize interactions should be close to 1, supported by the observation that hybrid network containing 10 wt. % POSS and 12 wt. % SNP displayed maximum strength with improved compressive modulus.

Conclusion

A series of hybrid networks were prepared on pendant POSS and SNP. SEM and TEM micrographs depicted the formation of nanostructured morphology in a hybrid network containing pendant POSS and SNP indicating enthalpic interactions between POSS moieties and SNP surfaces. In hybrid networks where POSS domains dispersed at a micro scale, a self-assembly behavior was revealed with increasing SNP loading. POSS domains provide a favorable surface for SNP to migrate into the network during polymerization. SNP aggregates increased in size as the SNP loading increased. Moreover, in hybrid networks where POSS was dispersed at a molecular level, a reduction in SNP aggregates size was revealed with POSS loading indicating an enthalpic driven interaction exists between pendant POSS moieties and SNP surfaces. The thermomechanical properties of the hybrid networks were evaluated via DMA and hybrid networks containing POSS demonstrated a higher storage modulus with increasing SNP loading due to the reinforcing effect provided by SNP. Hybrid networks with 10 wt. % of POSS showed the good interaction between SNP and the matrix due to favorable surface interactions between pendant POSS moieties and SNP. However, hybrid networks with higher POSS content exhibited poor interactions between SNP and matrix with high SNP loading. This could be due to the formation of SNP aggregates and a reduction in the crosslink density at higher SNP loading.

Hybrid networks containing POSS afforded lower stiffness and strength compared to neat epoxy networks. With increasing SNP loading, however, the stress-strain response of hybrid networks containing POSS improved (based on the initial slope of the curve and larger area under the curve). The stress-strain curves also show that the addition of

high SNP content in hybrid networks containing a large mass fraction POSS providing plasticity in the network. This could be due to large aggregates at high SNP loading and reduced the crosslink density. By means of adding SNP continuously, compressive properties improved corresponding to pendant POSS content then decreased ultimately, so there is an optimum ratio of POSS and SNP to achieve the best performance in a hybrid network containing pendant POSS: SNP which we conclude is around 1:1 weight ratio.

REFERENCES

(1)   Lebaron, P. C.; Wang, Z.; Pinnavaia, T. J. *Appl. Clay Sci.* **1999**, *15* (1–2), 11–29.

(2)   Oliver, C.; Pharr, M. *Journal of Materials Research*. 1992, pp 1564–1583.

(3)   Vaia, R. A.; Price, G.; Ruth, P. N.; Nguyen, H. T.; Lichtenhan, J. *Appl. Clay Sci.* **1999**, *15* (1–2), 67–92.

(4)   Yano, K.; Usuki, A.; Okada, A. *J Polym Sci A Polym Chem* **1997**, *35*, 2289–2294.

(5)   Mei-Hui Tsai; Wha-Tzong Whang. *Polymer (Guildf).* **2001**, *42* (9), 4197–4207.

(6)   Sanchez, C.; Soler-Illia, G. J. D. A. A.; Ribot, F.; Lalot, T.; Mayer, C. R.; Cabuil, V. *Chem. Mater.* **2001**, *13* (10), 3061–3083.

(7)   Pyun, J.; Matyjaszewski, K. *Synthesis (Stuttg).* **2001**, 3436–3448.

(8)   Scott, B. J.; Wirnsberger, G.; Stucky, G. D. *Chem. Mater.* **2001**, *13* (10), 3140–3150.

(9)   Gomez-Romero, P. *Adv. Mater.* **2001**, *13* (3), 163–174.

(10)   Yao, X. F.; Zhou, D.; Yeh, H. Y. **2008**, *12*, 223–230.

(11)   Kim, B. C.; Park, S. W.; Lee, D. G. *Compos. Struct.* **2008**, *86* (1–3), 69–77.

(12)   Gojny, F. H.; Wichmann, M. H. G.; Köpke, U.; Fiedler, B.; Schulte, K. *Compos. Sci. Technol.* **2004**, *64*, 2363–2371.

(13)   Mathews, M. J.; Swanson, S. R. *Compos. Sci. Technol.* **2007**, *67* (7–8), 1489–1498.

(14)   Hajji, P.; David, L.; Gerard, J. F.; Pascault, J. P.; Vigier, G. *J. Polym. Sci. Part B Polym. Phys.* **1999**, *37* (22), 3172–3187.

(15)   Ou, Y. C.; Yu, Z. Z.; Vidal, A.; Donnet, J. B. *J. Appl. Polym. Sci.* **1996**, *59* (8), 1321–1328.

(16) Rong, M. Z.; Zhang, M. Q.; Pan, S. L.; Lehmann, B.; Friedrich, K. *Polym. Int.* **2004**, *53* (2), 176–183.

(17) P.M, A. *Nanocomposite Science and Technology*; P.M, A., L.S, S., P.V., B., Eds.; Wiley-VCH, 2003.

(18) Ash, B. J.; Stone, J.; Rogers, D. F.; Schadler, L. S.; Siegel, R. W.; Benicewicz, B. C.; Apple, T. *MRS Proc.* **2000**, *661*.

(19) Hergeth, W. D.; Steinau, U. J.; Bittrich, H. J.; Simon, G.; Schmutzler, K. *Polymer (Guildf).* **1989**, *30* (2), 254–258.

(20) Hergeth, W. D.; Starre, P.; Schmutzler, K.; Wartewig, S. *Polymer (Guildf).* **1988**, *29* (7), 1323–1328.

(21) Bourgeat-Lami, E.; Ph.Espiard; Guyot, A. *Polymer (Guildf).* **1995**, *36* (23), 4385–4389.

(22) Kango, S.; Kalia, S.; Celli, A.; Njuguna, J.; Habibi, Y.; Kumar, R. *Prog. Polym. Sci.* **2013**, *38* (8), 1232–1261.

(23) Zhang, Z.; Zhang, P.; Wang, Y.; Zhang, W. *Polym. Chem.* **2016**, 3950–3976.

(24) Tang, E.; Cheng, G.; Ma, X.; Pang, X.; Zhao, Q. *Appl. Surf. Sci.* **2006**, *252* (14), 5227–5232.

(25) Franczyk, A.; He, H.; Burdynska, J.; Hui, C. M.; Matyjaszewski, K.; Marciniec, B. *ACS Macro Lett.* **2014**, *3* (8), 799–802.

(26) Raus, V.; Čadová, E.; Starovoytova, L.; Janata, M. *Macromolecules* **2014**, *47* (21), 7311–7320.

(27) Zhang, W.; Müller, A. H. E. *Macromolecules* **2010**, *43* (7), 3148–3152.

(28) Zhang, W.; Hong, L.; McGowan, P. C. *Macromol. Chem. Phys.* **2014**, n/a-n/a.

(29) Zhang, W.; Yuan, J.; Weiss, S.; Ye, X.; Li, C.; Axel, H. E. M. **2011**, 6891–6898.

(30) Pyun, J.; Matyjaszewski, K. *Macromolecules* **2000**, *33*, 217–220.

(31) Tan, B. H.; Hussain, H.; He, C. B. *Macromolecules* **2011**, *44* (3), 622–631.

(32) Kim, S. K.; Kim, D. G.; Lee, A.; Sohn, H. S.; Wie, J. J.; Nguyen, N. A.; MacKay, M. E.; Lee, J. C. *Macromolecules* **2012**, *45* (23), 9347–9356.

(33) Zheng, Y.; Wang, L.; Yu, R.; Zheng, S. *Macromol. Chem. Phys.* **2012**, *213* (4), 458–469.

(34) Costa, R. O. R.; Vasconcelos, W. L.; Tamaki, R.; Laine, R. M. *Macromolecules* **2001**, *34* (16), 5398–5407.

(35) Kim, D.-G.; Kang, H.; Han, S.; Lee, J.-C. *J. Mater. Chem* **2012**, *22* (17), 8654–8661.

(36) Yang, Y. Y.; Wang, X.; Hu, Y.; Hu, H.; Wu, D. C.; Xu, F. J. *ACS Appl. Mater. Interfaces* **2014**, *6* (2), 1044–1052.

(37) Carraro, M.; Gross, S. *Materials (Basel).* **2014**, *7* (5), 3956–3989.

(38) Schubert, U. *Macromol. Symp.* **2008**, *267* (1), 1–8.

(39) Schubert, U. *Chem. Mater.* **2001**, *13* (10), 3487–3494.

(40) Judeinstein, P. *J. Sol-Gel Sci. Technol.* **1994**, *2* (1), 147–151.

(41) Judeinstein, P. *Chem. Mater.* **1992**, *4*, 4–7.

(42) Kickelbick, G.; Schubert, U. *Eur. J. Inorg. Chem.* **1998**, No. 2, 159–161.

(43) Kickelbick, G.; Wiede, P.; Schubert, U. *Inorganica Chim. Acta* **1999**, *284* (1), 1–7.

(44) Schubert, U.; Arpac, J. E.; Glaubitt, W.; Helmerich, A.; Chaulb, C. *Chem. Mater.* **1992**, *4* (13), 291–295.

(45) Kickelbick, G. *Concepts for the incorporation of inorganic building blocks into*

organic polymers on a nanoscale; 2003; Vol. 28.

(46)   Pomogailo, A. D. *Nanostructured Mater.* **1999**, *12* (1), 291–294.

(47)   Zhang, W.; Müller, A. H. E. *Prog. Polym. Sci.* **2013**, *38* (8), 1121–1162.

(48)   Scott, D. W. *J. Am. Chem. Soc.* **1946**, *68* (3), 356–358.

(49)   Baney, R. H.; Itoh, M.; Sakakibara, A.; Suzuki, T. *Chem. Rev.* **1995**, *95* (5), 1409–
         1430.

(50)   Li, G.; Charles, U. P. *Macromol. Contain. Met. Met. Elem. Gr. IVA Polym.* **2005**, *4*
         (3), 79–131.

(51)   Zhou, H.; Ye, Q.; Xu, J. *Mater. Chem. Front.* **2016**, No. 2.

(52)   www.hybridplastics.com.

(53)   Haddad, T. S.; Lee, A.; Phillips, S. *Polym. Prepr.* **2001**, *42*, 88–89.

(54)   Matejka, L.; Strachota, A.; Plestil, J.; Whelan, P.; Steinhart, M.; Slouf, M.
         Macromolecules **2004**, *37* (25), 9449–9456.

(55)   Wu, J.; Mather, P. T. *Polym. Rev.* **2009**, *49* (1), 25–63.

(56)   Kawakami; Kakihana, Y. and; Miyazato, Y. and; Tateyama, A. and; Seiji; Hoque,
         A.; Asadul, M. *Silicon Polymers*; 2011.

(57)   Barry, A. J.; Daudt, W. H.; Domicone, J. J.; Gilkey, J. W. *J. Am. Chem. Soc.* **1955**,
         77 (16), 4248–4252.

(58)   Ayandele, E.; Sarkar, B.; Alexandridis, P. *Nanomaterials* **2012**, *2* (4), 445–475.

(59)   Rahman, I. A.; Padavettan, V. *J. Nanomater.* **2012**, *2012*.

(60)   Werne, T. Von; Patten, T. E. *J. Am. Chem. Soc.* **1999**, *121* (32), 7409–7410.

(61)   Ladmiral, V.; Mantovani, G.; Clarkson, G. J.; Cauet, S.; Irwin, J. L.; Haddleton, D.
         M. *J. Am. Chem. Soc.* **2006**, *128* (14), 4823–4830.

(62)   Hadjichristidis, N.; Iatrou, H.; Pispas, S.; Pitsikalis, M. *J. Polym. Sci. Part A Polym. Chem.* **2000**, *38* (18), 3211–3234.

(63)   Fournier, D.; Hoogenboom, R.; Schubert, U. S. *Chem. Soc. Rev.* **2007**, *36* (8), 1369–1380.

(64)   Moad, G.; Rizzardo, E.; Thang, S. H. *Aust. J. Chem.* **2005**, *58* (6), 379–410.

(65)   Kuo, S. W.; Chang, F. C. *Prog. Polym. Sci.* **2011**, *36* (12), 1649–1696.

(66)   Choi, J.; Yee, A. F.; Laine, R. M. *Macromolecules* **2003**, *36* (15), 5666–5682.

(67)   Kim, G. M.; Qin, H.; Fang, X.; Sun, F. C.; Mather, P. T. *J. Polym. Sci. Part B Polym. Phys.* **2003**, *41* (24), 3299–3313.

(68)   Lee, L.-H.; Chen, W.-C. *Polymer (Guildf).* **2005**, *46* (7), 2163–2174.

(69)   Herman Teo, J. K.; Teo, K. C.; Pan, B.; Xiao, Y.; Lu, X. *Polymer (Guildf).* **2007**, *48* (19), 5671–5680.

(70)   Yang, C. C.; Chang, F. C.; Wang, Y. Z.; Chan, C. M.; Lin, C. L.; Chen, W. Y. *J. Polym. Res.* **2007**, *14* (6), 431–439.

(71)   Ni, Y.; Zheng, S.; Nie, K. *Polymer (Guildf).* **2004**, *45* (16), 5557–5568.

(72)   Choi, J.; Harcup, J.; Yee, A. F.; Zhu, Q.; Laine, R. M. *J. Am. Chem. Soc.* **2001**, *123* (46), 11420–11430.

(73)   Choi, J.; Kim, S. G.; Laine, R. M. *Macromolecules* **2004**, *37* (15), 99–109.

(74)   Liu, Y. L.; Chang, G. P. *J. Polym. Sci. Part A Polym. Chem.* **2006**, *44* (6), 1869–1876.

(75)   Lee, a; Lichtenhan, J. *Macromolecules* **1998**, *31* (15), 4970–4974.

(76)   Abad, M. J.; Barral, L.; Fasce, D. P.; Williams, R. J. J. *Macromolecules* **2003**, *36* (9), 3128–3135.

(77)   Matějka, L.; Murias, P.; Pleštil, J. *Eur. Polym. J.* **2012**, *48* (2), 260–274.

(78)   Vazquez, A.; Matejka, L.; Spacek, P.; Dusek, K. *J. Polym. Sci. Part A Polym. Chem.* **1990**, *28* (9), 2305–2319.

(79)   Xu, Y.; Ma, Y.; Deng, Y.; Yang, C.; Chen, J.; Dai, L. *Mater. Chem. Phys.* **2011**, *125* (1–2), 174–183.

(80)   Chiu, Y.-C.; Riang, L.; Chou, I.-C.; Ma, C.-C. M.; Chinag, C.-L.; Yang, C.-C. *J. Polym. Sci. Part B Polym. Phys.* **2010**, *48*, 643–652.

(81)   Frank, K. L.; Exley, S. E.; Thornell, T. L.; Morgan, S. E.; Wiggins, J. S. *Polymer (Guildf).* **2012**, *53* (21), 4643–4651.

(82)   Ni, Y.; Zheng, S. *Macromolecules* **2007**, *40* (19), 7009–7018.

(83)   Zeng, K.; Zheng, S. *J. Phys. Chem. B* **2007**, *111* (50), 13919–13928.

(84)   Jiao, J.; Wang, L.; Lv, P.; Cui, Y.; Miao, J. *Mater. Lett.* **2014**, *129*, 16–19.

(85)   Zhao, F.; Huang, Y. *Mater. Lett.* **2010**, *64* (24), 2742–2744.

(86)   Finnigan, B.; Martin, D.; Halley, P.; Truss, R.; Campbell, K. *Polymer (Guildf).* **2004**, *45* (7), 2249–2260.

(87)   Cai, C.; Shi, Q.; Li, L.; Zhu, L.; Yin, J. *Radiat. Phys. Chem.* **2008**, *77* (3), 370–372.

(88)   Shokoohi, S.; Arefazar, A.; Naderi, G. *Mater. Des.* **2011**, *32* (3), 1697–1703.

(89)   M., X. *Reactive Extrusion: priciples and practices. Hanser Publisers: Munich*; 1992.

(90)   B., B. S.; C.M, O. *Encyclopedia of polymer science and engineering, wiley: New York*; 1988.

(91)   Rauwendaal, C. J. *Polym. Eng. Sci.* **1981**, *21* (16), 1098–1100.

(92)   Rauwendaal, C. *Polymer extrusion 5E*; Hanser Publishers, Munich, 1998.

(93)   C.Martin. *Melt extrusion Materials, Technology and Drug Product Design*; Langley, N., Repka, M. A., Eds.; Springer New York, 2013.

(94)   *Thermo fisher scientific*.

(95)   Cheng, X.; Wiggins, J. S. *Polym. Int.* **2014**, *63* (10), 1777–1784.

(96)   Zhou, Z.; Cui, L.; Zhang, Y.; Zhang, Y.; Yin, N. *Eur. Polym. J.* **2008**, *44* (10), 3057–3066.

(97)   Kumar, S.; Butola, B. S.; Joshi, M. *Fibers Polym.* **2013**, *14* (3), 428–435.

(98)   Heinz, S.; Wiggins, J. In *42nd International SAMPE Technical Conference, Salt Lake City, UT, Oct. 11-14,*; 2010.

(99)   NETZSCH Instruments, Inc.

(100)   Olson, B. G.; Lin, J.; Nazarenko, S.; Jamieson, A. M. *Macromolecules* **2003**, *36* (20), 7618–7623.

(101)   Kirkegaard, K. *Comput. Phys. Commun.* **1981**, *23* (3), 307–335.

(102)   Eldrup, M.; Lightbody, D.; Sherwood, J. N. *Chem. Phys.* **1981**, *63* (1–2), 51–58.

(103)   Morgan, A. B. *Fire and Polymers VI: New Advances in Flame Retardant Chemistry and Science*; Wilkie, C. A., Morgan, A. B., Nelson, G. L., Eds.; OUP USA, 2013.

(104)   Frank, K.; Childers, C.; Dutta, D.; Gidley, D.; Jackson, M.; Ward, S.; Maskell, R.; Wiggins, J. *Polym. (United Kingdom)* **2013**, *54* (1), 403–410.

(105)   Hakmé, C.; Stevenson, I.; Maazouz, A.; Cassagnau, P.; Boiteux, G.; Seytre, G. *J. Non. Cryst. Solids* **2007**, *353* (47–51), 4362–4365.

(106)   Innocenzi, P.; Kidchob, T.; Yoko, T. *J. Sol-Gel Sci. Technol.* **2005**, *35* (3), 225–

235.

(107) Sourour, S.; Kamal, M. R. *Thermochim. Acta* **1976**, *14* (1–2), 41–59.

(108) Fournier, J.; Williams, G.; Duch, C.; Aldridge, G. A.; Fournier, J.; Williams, G.; Duch, C.; Aldridge, G. A. *Macromolecules* **1996**, *29* (22), 7097–7107.

(109) Harsch, M.; Karger-Kocsis, J.; Holst, M. *Eur. Polym. J.* **2007**, *43* (4), 1168–1178.

(110) Perrin, F. X.; Nguyen, T. M. H.; Vernet, J. L. *Eur. Polym. J.* **2007**, *43* (12), 5107–5120.

(111) Rabearison, N.; Jochum, C.; Grandidier, J. C. *J. Mater. Sci.* **2011**, *46* (3), 787–796.

(112) López, J.; López-Bueno, I.; Nogueira, P.; Ramírez, C.; Abad, M. .; Barral, L.; Cano, J. *Polymer (Guildf).* **2001**, *42* (4), 1669–1677.

(113) Francis, B.; Rao, V. L.; Vanden Poel, G.; Posada, F.; Groeninckx, G.; Ramaswamy, R.; Thomas, S. *Polymer (Guildf).* **2006**, *47* (15), 5411–5419.

(114) Tang, Y.; Lewin, M. *Polym. Adv. Technol.* **2009**, *20* (1), 1–15.

(115) R, D. *Surface Tension and Absortion*; R, D., I, P., A, B., Eds.; Wiley-Interscience: New York, 1951.

(116) Boček, J.; Matějka, L.; Mentlík, V.; Trnka, P.; Šlouf, M. *Eur. Polym. J.* **2011**, *47* (5), 861–872.

(117) Iyer, S.; Schiraldi, D. A. *Macromolecules* **2007**, *40* (14), 4942–4952.

(118) Hao, N.; Böhning, M.; Goering, H.; Schönhals, A. *Macromolecules* **2007**, *40* (8), 2955–2964.

(119) Matějka, L.; Amici Kroutilová, I.; Lichtenhan, J. D.; Haddad, T. S. *Eur. Polym. J.* **2014**, *52* (1), 117–126.

(120) Pellice, S. A.; Fasce, D. P.; Williams, R. J. J. *J. Polym. Sci. Part B Polym. Phys.*

2003, *41* (13), 1451–1461.

(121)   Li, G. Z.; Wang, L.; Toghiani, H.; Daulton, T. L.; Koyama, K.; Pittman, C. U. *Macromolecules* **2001**, *34* (25), 8686–8693.

(122)   González, M. G.; Cabanelas, J. C.; Baselga, J. *Infrared Spectroscopy - Materials Science, Engineering and Technology*; Intech, 2012.

(123)   Lesser, A. J.; Kody, R. S. *J. Polym. Sci. Part B Polym. Phys.* **1997**, *35*, 1611–1619.

(124)   Dlubek, G.; Stejny, J.; Alam, M. A. *Macromolecules* **1998**, *31* (14), 4574–4580.

(125)   Hassan, M. K.; Tucker, S. J.; Abukmail, A.; Wiggins, J. S.; Mauritz, K. A. *Arab. J. Chem.* **2016**, *9* (2), 305–315.

(126)   Lesser, A. J.; Crawford, E. *J Appl Polym Sci* **1997**, *66* (April), 387–395.

(127)   Monticelli, O.; Fina, A.; Cozza, E. S.; Prato, M.; Bruzzo, V. *J. Mater. Chem* **2011**, *21* (44), 18049–18054.

(128)   Bolln, C.; Tsuchida, A.; Frey, H.; Mu, R. *Chem. Mater.* **1997**, *9* (22), 1475–1479.

(129)   Sinha Ray, S.; Okamoto, M. *Prog. Polym. Sci.* **2003**, *28* (11), 1539–1641.

(130)   Eon, D.; Cartry, G.; Fernandez, V.; Cardinaud, C.; Tegou, E.; Bellas, V.; Argitis, P.; Gogolides, E. *J. Vac. Sci. Technol. B Microelectron. Nanom. Struct.* **2004**, *22* (5), 2526.

(131)   Eon, D.; Raballand, V.; Cartry, G.; Cardinaud, C.; Vourdas, N.; Argitis, P.; Gogolides, E. *J. Vac. Sci. Technol. B Microelectron. Nanom. Struct.* **2006**, *24* (6), 2678.

(132)   Liu, L.; Hu, Y.; Song, L.; Nazare, S.; He, S.; Hull, R. *J. Mater. Sci.* **2007**, *42* (12), 4325–4333.

(133)   Jackson, M.; Kaushik, M.; Nazarenko, S.; Ward, S.; Maskell, R.; Wiggins, J.

Polymer (Guildf). **2011**, *52* (20), 4528–4535.

(134) Lee, W. E. *Ceramic Microstructures*; Chapman & Hall: London, 1994.

(135) Li, G.; Zhang, C.; Wang, Y.; Li, P.; Yu, Y.; Jia, X.; Liu, H.; Yang, X.; Xue, Z.; Ryu, S. *Compos. Sci. Technol.* **2008**, *68* (15–16), 3208–3214.

(136) Cheng, X. Cure kinetics, morphologies, and mechanical properties of thermoplastic/MWCNT modified multifuctional glassy epoxies prepared via continuous reaction method, 2015.

(137) Greenhoe, B. Nanostructured morphologies in glassy polymer networks, 2016.

(138) Misra, R.; Alidedeoglu, A. H.; Jarrett, W. L.; Morgan, S. E. *Polymer (Guildf).* **2009**, *50* (13), 2906–2918.

(139) De Paiva, J. M. F.; Frollini, E. *Macromol. Mater. Eng.* **2006**, *291* (4), 405–417.

(140) Hameed, N.; Sreekumar, P. A.; Francis, B.; Yang, W.; Thomas, S. *Compos. Part A Appl. Sci. Manuf.* **2007**, *38* (12), 2422–2432.

(141) Heitor Luiz Ornaghi, J.; Bolner, A. S.; Fiorio, R.; Zattera, A. J.; Amico, S. C. *J. Appl. Polym. Sci.* **2010**, *118*, 887–896.

(142) Mallarino, S.; Chailan, J. F.; Vernet, J. L. *Eur. Polym. J.* **2005**, *41* (8), 1804–1811.

(143) Pothan, L. A.; Oommen, Z.; Thomas, S. *Compos. Sci. Technol.* **2003**, *63* (2), 283–293.

(144) Pothan, L. A.; Thomas, S.; Groeninckx, G. *Compos. Part A Appl. Sci. Manuf.* **2006**, *37* (9), 1260–1269.

(145) Heinz, S. R. Development and Utilization of Digital Image Correlation Techniques for the Study of Structural Isomerism Effects on Strain development in Epoxy Network Glasses, 2011.

(146) Jumahat, A.; Soutis, C.; Abdullah, S. A.; Kasolang, S. *Procedia Eng.* **2012**, *41*, 1634–1640.

(147) Johnsen, B. B.; Kinloch, A. J.; Mohammed, R. D.; Taylor, A. C.; Sprenger, S. *Polymer (Guildf).* **2007**, *48* (2), 530–541.

(148) Idicula, M.; Malhotra, S. K.; Joseph, K.; Thomas, S. *Compos. Sci. Technol.* **2005**, *65* (7–8), 1077–1087.